Energy transport in saturated porous media

by

Volodymyr Gerasik

A thesis
presented to the University of Waterloo
in fulfillment of the
thesis requirement for the degree of
Doctor of Philosophy
in
Applied Mathematics

Waterloo, Ontario, Canada, 2011

I hereby declare that I am the sole author of this thesis. This is a true copy of the thesis, including any required final revisions, as accepted by my examiners.

I understand that my thesis may be made electronically available to the public.

Abstract

The energy analysis of wave motion in Lamb's problem for a poroelastic half-space in the framework of Biot's theory is presented. The results for the energy velocity and quality factor of poroelastic waves are revisited.

In the case of no dissipation the approach originally established for perfectly elastic media by Miller & Pursey is generalized herein to include poroelastic waves. Special cases of the resonant excitation of the Rayleigh wave and the absence of the Rayleigh wave beyond the cut-off frequency are discussed in detail. Directional diagrams for the volumetric waves are presented. A quantitative picture of the energy partition among the traveling waves is provided for several driving configurations. In the general case of dissipative media the analysis is based on the semi-analytic solution of the Lamb's problem. In the near field, the surface load generates three wavetrains corresponding to the bulk modes. These wavetrains consist of waves which are longer and exhibit greater viscous attenuation than the corresponding volumetric modes, so that, P1, P2 and S modes emerge from the corresponding wavetrains at a certain distance from the source. For the far field, asymptotic expressions have been obtained and clearly indicate that it is only in the far field that the wave motion represents the superposition of the P1, P2, S and Rayleigh waves characterized by their corresponding wavelengths and attenuations. Moreover, these waves also exhibit geometric attenuation $x^{-3/2}$ (similar to the waves in a perfectly elastic half-space). To analyze the energy partition the total input power supplied by the source is decomposed into the contributions associated with the wavetrains and the Rayleigh wave. These results provide the means for controlling the excitation of the various wave modes via changes to the driving configuration.

Biot's theory is a particular example of a non-conservative Lagrangian system with a Rayleigh dissipation function. The group velocities of poroelastic waves are complex and do not provide any information about the velocity of the energy transport. Moreover, in general the precise physical meaning of the complex group velocity is unclear. The analysis based on the detailed study of the coupled system of the damped Klein-Gordon equations (Biot's theory yields such a formalism in the low frequency limit) suggests that both precise and approximate physical interpretations of the complex group velocity are possible. Moreover, these considerations further allow the derivation of exact closed form expressions for the energy velocity and Q factor for both longitudinal and shear poroelastic waves from energy principles. Most notably, the analysis of the resulting expressions reveals that the energy velocity of both longitudinal and shear waves equals (exceeds) the corresponding phase velocity in the case of the low (full) frequency range Biot's theory. The exact expression for the Q factor contains an additive correction due to viscoelastic interphase interaction in the higher frequency range.

Acknowledgements

I am deeply grateful to my supervisor Marek Stastna for his detailed and constructive comments, and for his important support throughout this work. I also wish to thank Arnold Verruijt, emeritus professor of soil mechanics of the Delft University of Technology, and Donald Albert, US Army Cold Regions Research Lab for sharing their expertise.

Table of Contents

List of Tables

List of Figures

Chapter 1

Introduction

Wave propagation in porous materials has many applications in geophysics, acoustics, the energy industry including petrophysics and mining engineering, and medical ultrasound technology. For example, while seismic waves have long been used to map geological formations, the concept of seismicity has been associated with the purely elastic wave propagation and jointed rock masses with interfacial friction. The hydrodynamics of the fluid in the pores was typically ignored. With the development of multiphase continuum theories the focus on the mechanical interaction of solid and fluid has not only refined the science, but also allowed new applications such as the real-time monitoring of oil and gas recovery, geothermal reservoir operations, CO_2 sequestration, and secure deposition of chemical and nuclear wastes. Depending on the major practical application involved, frequency bands may vary greatly. For example, while low-frequency seismic prospecting focuses on frequencies of approximately 50 Hz, medical applications allow for frequencies up to approximately 3 MHz while testing of nanomaterials requires frequencies of approximately 100 MHz.

The early works on porous media are attributed to Fillunger (1913) [48] and Terzhagi (1923) [113]. These two basic works form the foundation for the two approaches used to date [18]. Fillunger was the first to examine a solid-liquid model with the concept of volume fractions combined with surface porosity coefficients, while Terzaghi developed a one-dimensional soil consolidation theory, the descriptive mathematical model of the deformation of the fluid saturated soil under stress. In [113] Terzaghi introduced the effective stress concept (effective in moving soil or causing displacements, it represents the average stress carried by the soil skeleton) and applied Darcy's law to describe the behavior of the saturating fluid. The three-dimensional generalization of the consolidation theory was developed by Biot [10] in 1941, where constitutive relations for the two-phase continuum were proposed. Later, in 1944, Frenkel [51] first considered acoustic wave propagation in a two-phase continuum while studying the seismoelectric effect, and predicted the existence of the longitudinal wave of the second kind, further known as Biot's slow wave, or P2-wave.

Quasi-static consolidation theory for a two-phase continuum was established by Biot in 1941 [10]. Biot's theory of the dynamics of a fluid-saturated solid was formulated in 1956 [11, 12] summarizing all necessary physical concepts related to the acoustic wave propagation. Thereafter Biot developed the theory to include the cases of anisotropic [15] and viscoelastic [14] skeletons. Biot's theory [11, 12] yields the correspondence principle, which states that the equations governing the mechanics of porous media are formally the same for an elastic or viscoelastic system, provided that the elastic coefficients are replaced by the corresponding operators [15]. Nowadays, Biot's theory remains the fundamental theory of acoustical wave propagation in porous media. It is important to stress that Biot's theory not only predicts the existence of three wave types in porous media, two longitudinal waves (fast and slow Biot wave), and one shear wave, but also provides adequate quantitative estimations for the phase velocities, amplitudes and attenuations measured in both natural and synthetic porous materials e.g. [43, 99, 92, 73, 108, 24, 49, 93, 74, 90].

Modern mathematical approaches to acoustic wave propagation in porous media include the classical Biot model, often reformulated for the particular areas of interest [63]: the model for sound-absorbing materials [7]; thermodynamics-based theory with a balance equation for porosity [121]; linearized version of the theory of porous media equations [37, 100] which follow mixture theory fundamental approaches; the Biot-Stoll model [110] with applications to marine sediment acoustics, which considers two loss mechanisms, intergranular friction and viscous friction due to the motion of the frame relative to the fluid, etc. A comprehensive up to date review of the existent theories can be found in [63].

The experimental verification of the theoretically predicted slow P2-wave was first obtained by Plona (1980) [97] and motivated further interest in Biot's theory, and especially in the properties of the P2-wave. Plona's experiments were conducted with an artificial material (water saturated sintered glass spheres) for a wide porosity range (8–28%) on ultrasound frequencies (500 kHz). Johnson's experiments (1980) [71] on the acoustic wave propagation in porous ^{4}He superfluid-filled media and the analysis based on Biot's theory demonstrated that the slow P2-wave is identical to the phenomenon known as fourth sound in superfluids. Moreover, slow wave propagation in air-filled porous materials and natural rocks offers a unique acoustical means to study certain material properties, such as tortuosity and permeability [92]. Because the slow compressional wave is especially sensitive to certain physical properties of the permeable material, the detection of this slow compressional wave has been one of the major issues in the acoustics of fluid-saturated permeable solids [92, 73, 122, 86]. On the other hand in situ measurements of the P2-wave are nearly impossible due to its substantial attenuation [91, 90]. Apart from the substantial attenuation, difficulties measuring P2-waves are also caused by the problem of its specific excitation as well as the possibility of the extraction of the P2-wave data from the general signal (if solely the slow wave was generated, it would be much easier to detect) [92, 90]. The latter essentially motivates the results presented herein, which include the

decomposition of the general signal into the contribution due to the particular wave types as well as the study of the possibility of controlling the excitation of the waves by varying the properties (e.g. shape, frequency) of the driving mechanism. Whether Biot's model may extend the technical possibilities of field measurements remains very much an open question [122].

Throughout the following, commonly used notation will be used without explanation. While all of what is used is standard, some of the main points are collected for the reader's convenience in the following list.

1. Cartesian Tensor notation will be employed for components of vectors and tensors.
2. Einstein's summation convention will be employed, and squared vectors will be assumed to be contracted ($u_i^2 = u_i u_i$).
3. Second order tensors such as the Cauchy strain tensor will be expressed in matrix form when necessary, and rectangular Cartesian coordinates will be used unless otherwise indicated.
4. The Dirac delta generalized function, $\delta(x)$, will be used as if it were a well-defined function, since it will generally be integrated during the Fourier transform operation.
5. Only infinitesimal strain and linear constitutive laws will be considered.
6. Cauchy's theorem will be used to express surface forces (or tractions) in terms of the stress tensor.

1.1 Biot's theory

Consider a porous material which consists of an elastic homogeneous matrix with interconnected pores. The pore space is filled with viscous compressible fluid. By definition, porosity ϕ is the ratio of the pore volume V_p to the total volume V of the porous aggregate,

$$\phi = \frac{V_p}{V}. \tag{1.1}$$

For the unsaturated porous material the volume of the solid frame is $V_s = V - V_p$ and therefore it suffices to measure two of these three parameters to calculate porosity. An overview of measurement methods can be found in [23].

The main assumptions of the theory can be summarized as follows [31, 33, 23, 63]:

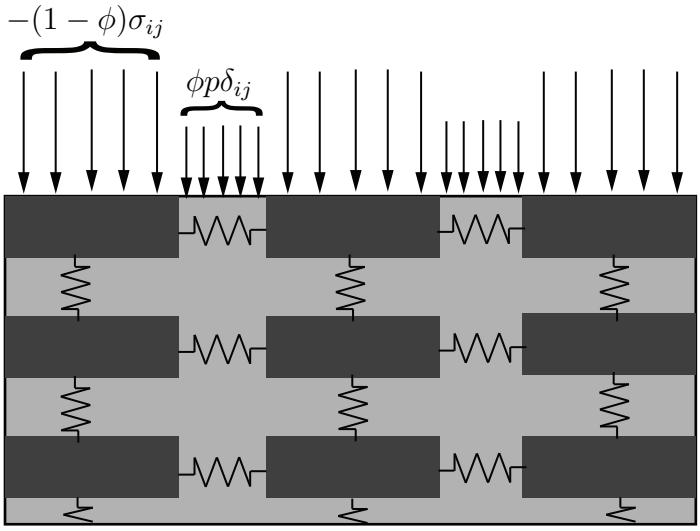

Figure 1.1: Schematic force distribution in porous elementary volume

- Deformations of both solid and fluid phase are assumed to be small (e.g strains in seismic studies are of the order 10^{-6}). Therefore, the Eulerian and Lagrangian description coincide; constitutive equations and dissipation forces are linear; the strain energy, kinetic energy and dissipation potential are quadratic forms in the field variables.

- The principles of continuum mechanics can be applied to measurable macroscopic values, i.e. volume averages of the corresponding microscopic values of the constituents.

- The diameter of pores is assumed to be small compared to the typical wavelength. Thus, the local changes of porosity, permeability and densities are neglected along with the scattering effects.

- Fluid viscosity is only taken into account for the interphase interaction. Otherwise, the fluid phase stress is hydrostatic.

- Thermomechanical coupling and phase transitions are absent

- The material of the solid frame (grains) is assumed to be isotropic. Anisotropy is due to the specific orientation of the pores.

Let $\mathbf{u}$ and $\mathbf{U}$ denote volume average of the displacement of the solid skeleton and saturating fluid respectively. Assuming small deformations the solid strain tensor is the

Cauchy strain tensor

$$e_{ij} = \frac{1}{2}\left(\frac{\partial u_i}{\partial x_j} + \frac{\partial u_j}{\partial x_i}\right), \tag{1.2}$$

while the fluid strain is characterized by the dilatation, and hence expressed as a scalar

$$\varepsilon = \nabla \cdot \mathbf{U}. \tag{1.3}$$

Consider the forces acting on the elementary cubic volume of porous material Figure 1.1. These forces can be separated into two parts:

1. The contact, or surface forces acting on the solid constituent can be represented by the stress tensor

$$\begin{pmatrix} \sigma_{xx} & \sigma_{xy} & \sigma_{xz} \\ \sigma_{yx} & \sigma_{yy} & \sigma_{yz} \\ \sigma_{zx} & \sigma_{zy} & \sigma_{zz} \end{pmatrix}, \tag{1.4}$$

2. The forces acting on the fluid constituent can be represented by the diagonal tensor

$$\begin{pmatrix} s & 0 & 0 \\ 0 & s & 0 \\ 0 & 0 & s \end{pmatrix}, \tag{1.5}$$

   where the scalar s is proportional to the fluid pressure p according to

$$s = -\phi p. \tag{1.6}$$

With the above definitions the kinetic energy can be expressed as (summation over repeated indices is implied here and henceforth)

$$T = \frac{1}{2}\rho_{11}\dot{u}_i\dot{u}_i + \rho_{12}\dot{u}_i\dot{U}_i + \frac{1}{2}\rho_{22}\dot{U}_i\dot{U}_i, \tag{1.7}$$

where the coefficients ρ_{11} and ρ_{22} represent the effective densities of the matrix and fluid respectively, while ρ_{12} serves to describe the added mass effect. According to Biot's theory [11, 12] these are related to the actual solid grain and fluid densities, ρ_s and ρ_f, respectively, by

$$\rho_{11} = (1-\phi)\rho_s + \phi\rho_f(a-1), \tag{1.8}$$
$$\rho_{12} = \phi\rho_f(1-a), \tag{1.9}$$
$$\rho_{22} = a\phi\rho_f, \tag{1.10}$$

where a is the tortuosity parameter related to the the geometry of the pores [23].

The possible values of a are greater or equal to unity indicating that the effective masses always exceed the actual masses. This coefficient takes into account the fact that due to an arbitrary orientation of the pore structure the pore fluid cannot move only in the direction of the filtration velocity $\phi(\dot{\mathbf{U}} - \dot{\mathbf{u}})$, which is also the direction of the macroscopic pressure gradient ∇p according to Darcy's law. Formally, tortuosity can be defined as [33],

$$a = \frac{\langle f_\Omega(\mathbf{x})\rho_f(\mathbf{x})(\mathbf{V} - \dot{\mathbf{u}})^2\rangle}{\phi\rho_f(\dot{\mathbf{U}} - \dot{\mathbf{u}})^2} \geq 1, \tag{1.11}$$

where $\mathbf{V}$ is the microscopic velocity of the fluid particle and f_Ω is the characteristic function of the volume Ω

$$f_\Omega = \begin{cases} 1 & \mathbf{x} \in \Omega, \\ 0 & \mathbf{x} \notin \Omega, \end{cases} \tag{1.12}$$

and $\langle \cdot \rangle$ is the volume average operator.

Note that $a = 1$ if and only if the pore structure is oriented in the direction of the pressure gradient. The value of $a \approx 1.66$ was obtained during experimental measurements in the low frequency range on an ensemble of spheres. The results for different sandstones are found in the range $1.5 < a < 5$, while for the majority of sands $a = 2$ [107]. The frequency dependent character of the tortuosity parameter in the higher frequency range was studied in [70].

Consider the expression for the potential (elastic stored energy) [11]

$$\mathrm{V} = \frac{1}{2}\left(\sigma_{ij}e_{ij} + s\varepsilon\right). \tag{1.13}$$

The differential form of the above equation will represent the deformation work in an infinitesimal deformation

$$\mathrm{dV} = \frac{\partial \mathrm{V}}{\partial e_{ij}}\mathrm{d}e_{ij} + \frac{\partial \mathrm{V}}{\partial \varepsilon}\mathrm{d}\varepsilon. \tag{1.14}$$

The first term corresponds to the elementary deformation work at fixed fluid content, and the second to the work associated with the increase of fluid due to a fixed macroscopic deformation. Hence, the macroscopic stress tensor and pore pressure can be expressed in the form

$$\sigma_{ij} = \frac{\partial \mathrm{V}}{\partial e_{ij}}, \text{ if } i = j; \quad \sigma_{ij} = \frac{1}{2}\frac{\partial \mathrm{V}}{\partial e_{ij}}, \text{ if } i \neq j; \quad s = \frac{\partial \mathrm{V}}{\partial \varepsilon}. \tag{1.15}$$

In the vicinity of any point the deformations and stresses can be characterized by six components of the stress tensor, pore pressure, six components of solid strain and fluid

dilatation. In the very general case the formulation of Hooke's law represents the relations between stresses and strains

$$\begin{aligned}
\sigma_{xx} &= f_1(e_{xx}, e_{yy}, e_{zz}, e_{xy}, e_{xz}, e_{yx}, \varepsilon), \\
\sigma_{yy} &= f_2(e_{xx}, e_{yy}, e_{zz}, e_{xy}, e_{xz}, e_{yx}, \varepsilon), \\
\sigma_{zz} &= f_3(e_{xx}, e_{yy}, e_{zz}, e_{xy}, e_{xz}, e_{yx}, \varepsilon), \\
\sigma_{xy} &= f_4(e_{xx}, e_{yy}, e_{zz}, e_{xy}, e_{xz}, e_{yx}, \varepsilon), \\
\sigma_{xz} &= f_5(e_{xx}, e_{yy}, e_{zz}, e_{xy}, e_{xz}, e_{yx}, \varepsilon), \\
\sigma_{yz} &= f_6(e_{xx}, e_{yy}, e_{zz}, e_{xy}, e_{xz}, e_{yx}, \varepsilon), \\
s &= f_7(e_{xx}, e_{yy}, e_{zz}, e_{xy}, e_{xz}, e_{yx}, \varepsilon).
\end{aligned} \tag{1.16}$$

Expanding these functions in a series to first order we find

$$\begin{aligned}
\sigma_{xx} &= c_{11}e_{xx} + c_{12}e_{yy} + c_{13}e_{zz} + c_{14}e_{xy} + c_{15}e_{xz} + c_{16}e_{yx} + c_{17}\varepsilon, \\
\sigma_{yy} &= c_{21}e_{xx} + c_{22}e_{yy} + c_{23}e_{zz} + c_{24}e_{xy} + c_{25}e_{xz} + c_{26}e_{yx} + c_{27}\varepsilon, \\
&\cdots\cdots\cdots\cdots\cdots \\
\sigma_{yz} &= c_{61}e_{xx} + c_{62}e_{yy} + c_{63}e_{zz} + c_{64}e_{xy} + c_{65}e_{xz} + c_{66}e_{yx} + c_{67}\varepsilon, \\
s &= c_{71}e_{xx} + c_{72}e_{yy} + c_{73}e_{zz} + c_{74}e_{xy} + c_{75}e_{xz} + c_{76}e_{yx} + c_{77}\varepsilon,
\end{aligned} \tag{1.17}$$

where the zero order terms are not included as the undeformed state is assumed to be stress free. Moreover, because V is an exact differential, the above linear relations are obviously symmetric $c_{ij} = c_{ji}$, hence, in the general anisotropic case, 28 poroelastic constants are required to express the constitutive relations.

In the isotropic case, these relations can be simplified further, so that only four independent poromechanical parameters are sought. Indeed, since the stress-strain relations must be independent of a rotation of the coordinate axes, any function of a tensor must be a function of its invariants only. Thus, in the case of an isotropic material, when the material behaviour is independent of the orientation of the axes, the strain potential can be described using the three invariants of the strain tensor only

$$\mathrm{V} = \mathrm{V}(e_{ij}, \varepsilon) = \mathrm{V}(I_1, I_2, I_3, \varepsilon), \tag{1.18}$$

where the symmetric tensor e_{ij} has the following scalar invariants

$$\begin{aligned}
I_1 &= \mathrm{tr}(e_{ij}) = e_{xx} + e_{yy} + e_{zz} = e, \\
I_2 &= 2\left(tr(e_{ij}^2) - I_1^2\right) = e_{xx}e_{yy} + e_{xx}e_{zz} + e_{yy}e_{zz} - e_{xy}^2 - e_{yz}^2 - e_{xz}^2, \\
I_3 &= |e_{ij}|\,.
\end{aligned} \tag{1.19}$$

The expansion of V in the case of a linear material can be limited to the quadratic terms. One may therefore write

$$\mathrm{V} = \frac{1}{2}(\lambda + 2\mu)I_1^2 - 2\mu I_2 + QI_1\varepsilon + \frac{1}{2}\mathcal{R}\varepsilon^2, \tag{1.20}$$

where λ, μ, Q and $\mathcal{R}$ are four constants which completely describe the stress-strain relations in the isotropic case.

According to (1.15) and (1.20) it can be inferred that the stress on solid and the stress on fluid can be expressed by the following constitutive relations

$$\sigma_{ij} = \lambda e \delta_{ij} + 2\mu e_{ij} + Q\varepsilon\delta_{ij}, \tag{1.21}$$

$$s = Qe + \mathcal{R}\varepsilon. \tag{1.22}$$

To determine the values of the four independent coefficients λ, μ, Q and $\mathcal{R}$ in addition to the porosity ϕ, Biot and Willis (1957) [16] introduced the following optimal combination of measurements: the measurement of shear modulus, jacketed and unjacketed compressibility of the porous solid, and an unjacketed coefficient of fluid content. The shear modulus μ of the bulk material can be obtained directly, so that these values measured for the dry or bulk material are equal under the assumption that fluid viscosity is taken into account only in the interphase interaction. In the jacketed compressibility test, a specimen of the material is enclosed in a thin impermeable shell and then subjected to an external fluid pressure (however, the conventional jacketed test is usually performed on a dry specimen). Thus the hydrostatic pressure is transmitted to the frame, and therefore the measured bulk modulus K_b is known as the bulk modulus of the frame, or the drained modulus. In the unjacketed compressibility test, a sample of the material is immersed in a fluid under hydrostatic pressure which now acts on both frame and saturating fluid. Since the solid frame is subjected to the hydrostatic pressure entirely, from inside and outside, the resulting bulk modulus K_s is regarded as the grain bulk modulus.

The four generalized poroelastic parameters λ, μ, Q, $\mathcal{R}$ can be related to the porosity ϕ, the bulk modulus of the solid grains K_s, the bulk modulus of the fluid K_f, the bulk modulus of the porous drained matrix K_b, and the shear modulus μ of the bulk material via Gedanken experiments (Biot & Willis 1957) [16]:

$$\lambda = K_b - 2\mu/3 + K_f \left(1 - \phi - K_b/K_s\right)^2 / \phi_{eff}, \tag{1.23}$$

$$Q = \phi K_f \left(1 - \phi - K_b/K_s\right) / \phi_{eff}, \tag{1.24}$$

$$\mathcal{R} = \phi^2 K_f / \phi_{eff}, \tag{1.25}$$

$$\phi_{eff} = \phi + K_f \left(1 - \phi - K_b/K_s\right) / K_s. \tag{1.26}$$

Determination of physical properties of porous materials is also discussed in number of papers e.g. [53, 110, 52, 81].

Table 1.1: Typical permeabilities of the porous materials [33]

Material	Permeability, κ_{pr} [m^2]
Concrete	10^{-16}–10^{-21}
Clays	10^{-16}–10^{-20}
Bones	10^{-20}
Granites	10^{-16}–10^{-20}
Sandstones	10^{-11}–10^{-17}
Limestone	10^{-12}–10^{-26}
Gravels and sands	10^{-9}–10^{-12}

1.1.1 Darcy's law

In the low frequency range the laminar flow through porous medium obeys the phenomenological Darcy's law [23],

$$\dot{\mathbf{w}} = -\frac{\kappa_{pr}}{\eta}\nabla p, \tag{1.27}$$

where η and κ_{pr} denote the pore fluid viscosity and permeability of porous media respectively, and $\mathbf{w} = \phi(\dot{\mathbf{U}} - \dot{\mathbf{u}})$ is the filtration velocity. The fluid discharge is proportional to the pressure gradient, and thus the permeability parameter is related to the ability of a material to transmit fluids. Permeability has SI units [m^2], while the traditional unit is the Darcy (D), or millidarcy (mD) ($\approx 10^{-15}$m^2), the latter is better adapted to realistic permeability measurements in rocks (see Table 1.1).

Darcy's law is valid only provided the Reynolds number

$$\mathrm{Re} = \frac{|\dot{\mathbf{w}}|l}{\nu}, \tag{1.28}$$

does not exceed a certain critical value, where l denotes characteristic length (pore diameter), ν is kinematic viscosity $\eta = \rho_f \nu$. For instance these critical values for rocks are between 13–14, for sands 3–10 (large grains) and 0.34–0.23 (small grains, diameter less than 0.1mm) [63].

In the framework of Biot's theory fluid viscosity η is taken into account only during interphase interaction. However, the assumption of Poiseuille flow inside the pores breaks down when the frequency exceeds a certain value. In the higher frequency range the boundary layer develops as well as a phase shift between the stress on the wall and the relative fluid flow. The critical frequency for the Darcy's flow is [12]

$$f_t = \frac{\pi\eta}{4d^2}, \tag{1.29}$$

where d is the diameter of the pores. This corresponds to the value for which a quarter wavelength of the boundary layer is of the order of the pore diameter d. For instance, in the case of water at 15°C $f_t = 100$ Hz for $d = 10^{-2}$ cm, and $f_t = 10^4$ Hz for $d = 10^{-3}$ cm. The extension of the Biot's theory beyond the critical frequency f_t requires special consideration (complex viscosity, frequency correction factor). In particular, in the higher frequency range even in the case of zero pressure gradient a fluid discharge can be generated by inertial forces alone. As will be further discussed this results in additional inertial terms in (1.27) (Biot–Darcy law).

Finally, it should be mentioned that Johnson, Koplik & Dashen (1987) [70] developed a theory of dynamic permeability and tortuosity in fluid-saturated porous media, considering the problem of the response of a Newtonian fluid saturating an isotropic porous medium subjected to an infinitesimal oscillatory pressure gradient. The results presented include closed form frequency dependent relations for the tortuosity and permeability valid in the full frequency range.

1.1.2 Governing equations and boundary conditions

Viscous dissipation in Biot's theory depends only on the relative motion between the fluid and solid. It vanishes when there is no relative motion $\dot{u}_i = \dot{U}_i$. The dissipation function, or dissipation pseudo-potential D can be defined as the quadratic form [11, 59, 23]

$$2D = b(\dot{u}_i - \dot{U}_i)^2, \tag{1.30}$$

where the coefficient $b = \eta\phi^2/\kappa_{pr}$ is in agreement with Darcy's law (1.27) in the low frequency range.

Consider the Lagrange's equations [59, 23]

$$\frac{\partial}{\partial t}\frac{\partial \mathcal{L}}{\partial \dot{q}_i} + \frac{\partial}{\partial x_j}\frac{\partial \mathcal{L}}{\partial q_{i,j}} - \frac{\partial \mathcal{L}}{\partial q_i} + \frac{\partial D}{\partial \dot{q}_i} = 0, \tag{1.31}$$

where six generalized coordinates q_i represent solid and fluid displacements u_i and U_i. With the above introduced expressions for the kinetic energy, potential energy and dissipation function,

$$2T = \rho_{11}\dot{u}_i^2 + 2\rho_{12}\dot{u}_i\dot{U}_i + \rho_{22}\dot{U}_i^2, \tag{1.32}$$

$$2V = \sigma_{ij}e_{ij} + s\varepsilon, \tag{1.33}$$

$$2D = b(\dot{u}_i - \dot{U}_i)^2, \tag{1.34}$$

Lagrange's equation simplifies to

$$\frac{\partial}{\partial t}\frac{\partial T}{\partial \dot{q}_i} - \frac{\partial}{\partial x_j}\frac{\partial V}{\partial q_{i,j}} + \frac{\partial D}{\partial \dot{q}_i} = 0. \tag{1.35}$$

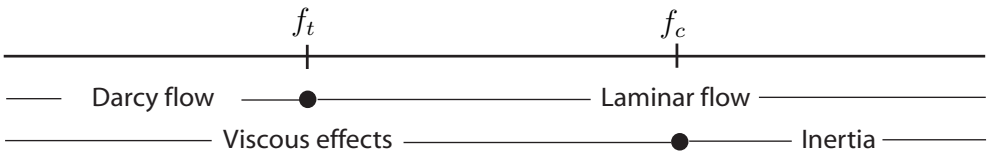

Figure 1.2: Frequency range in Biot's theory, critical frequency f_t and characteristic frequency f_c.

The first term in (1.35) represents the rate of change of momentum, the second term corresponds to the elastic forces and the final term describes the action of viscous friction.

From (1.35) one can derive

$$\frac{\partial^2}{\partial t^2}\left(\rho_{11}u_i + \rho_{12}U_i\right) - \sigma_{ij,j} + b\frac{\partial}{\partial t}\left(u_i - U_i\right) = 0, \tag{1.36}$$

$$\frac{\partial^2}{\partial t^2}\left(\rho_{12}u_i + \rho_{22}U_i\right) - s_{,i} - b\frac{\partial}{\partial t}\left(u_i - U_i\right) = 0, \tag{1.37}$$

or alternatively, in terms of solid and fluid displacements

$$\left(\lambda+\mu\right)\nabla\nabla\cdot\mathbf{u} + \mu\nabla^2\mathbf{u} + Q\nabla\nabla\cdot\mathbf{U} = \rho_{11}\ddot{\mathbf{u}} + \rho_{12}\ddot{\mathbf{U}} + b\left(\dot{\mathbf{u}} - \dot{\mathbf{U}}\right), \tag{1.38}$$

$$Q\nabla\nabla\cdot\mathbf{u} + \mathcal{R}\nabla\nabla\cdot\mathbf{U} = \rho_{12}\ddot{\mathbf{u}} + \rho_{22}\ddot{\mathbf{U}} - b\left(\dot{\mathbf{u}} - \dot{\mathbf{U}}\right). \tag{1.39}$$

Two interphase coupling mechanisms are considered in the model, inertial coupling due to different accelerations of the phases, and the viscous coupling due to interphase interaction. When the frequency approaches a certain characteristic frequency f_c [11]

$$f_c = \frac{b}{2\pi(\rho_{12}+\rho_{22})} = \frac{\eta\phi}{2\pi\kappa_{pr}\rho_f}, \tag{1.40}$$

inertia and viscous forces are of the same order. An alternative definition of the characteristic frequency also commonly used in the literature [70] is

$$f_c = \frac{b}{2\pi a_\infty(\rho_{12}+\rho_{22})} = \frac{\eta\phi}{2\pi a_\infty\kappa_{pr}\rho_f}, \tag{1.41}$$

where a_∞ is the low frequency tortuosity parameter. The introduction of the characteristic frequency f_c in addition to the critical frequency f_t (1.29) allows for the distinction regarding the character of the flow inside the pores as shown in Figure 1.2.

Note that the second momentum equation can be rewritten in terms of pressure p and filtration velocity $\dot{\mathbf{w}}$

$$\dot{\mathbf{w}} = -\frac{\kappa_{pr}}{\eta}\nabla p - \frac{\kappa_{pr}\rho_f}{\eta}\left[(1-a)\ddot{\mathbf{u}} + a\ddot{\mathbf{U}}\right], \tag{1.42}$$

so that in the case of steady flow $\ddot{\mathbf{u}} = \ddot{\mathbf{U}} = 0$ classical Darcy's law (1.27) can be recovered exactly. Unlike the classical Darcy's law in the case of zero pressure gradient inertia driven flow may induce fluid discharge. The governing equations (1.38), (1.39) are only valid in the low frequency range $f < f_t$, when the flow inside the pores is of Poiseuille type and yields Darcy's law.

Consider the limiting cases of unsaturated and totally saturated porous solid. In the case of unsaturated porous solid $\phi = 0$. Consequently $\rho_{11} = \rho_s$, $\rho_{12} = \rho_{22} = 0$, $Q = \mathcal{R} = 0$, $b = 0$, so that (1.39) vanishes, while (1.38) degenerates into the equations for the perfect solid

$$(\lambda + \mu)\,\nabla\nabla\cdot\mathbf{u} + \mu\nabla^2\mathbf{u} = \rho_s\ddot{\mathbf{u}}, \tag{1.43}$$

where $\lambda = K_s - 2\mu/3$.

In the case of the total saturation $\phi = 1$. Setting $a = 1$, so that $\rho_{11} = \rho_{12} = 0$, $\rho_{22} = \rho_f$, and $K_b = \mu = 0$, so that $\lambda = Q = 0$, $\mathcal{R} = K_f$ and now (1.38) vanishes while the equation (1.39) recovers the equation of the perfect fluid

$$K_f\nabla\nabla\cdot\mathbf{U} = \rho_f\ddot{\mathbf{U}}. \tag{1.44}$$

Boundary conditions

The formulation of the boundary conditions for the set of governing equations (1.38), (1.39) includes the following main configurations: the contact of two poroelastic solids, the contact of poroelastic solid and fluid or perfectly elastic solid. External tractions acting on the porous interface can be prescribed as follows from the scheme in Figure 1.3 in the form of a liquid stamp, a permeable stamp, and an impermeable stamp. Finally, two different conditions can be prescribed at the free interface of the poroelastic solid.

In the case of the contact of two porous solids it is necessary to require continuity of the following quantities [41],

$$\sigma_{nn} + s,\ \dot{u}_n,\ \sigma_{n\alpha},\ p,\ \dot{w}_n, \tag{1.45}$$

where σ_{nn}, $\sigma_{n\alpha}$ denote normal and shear components of the stress, and $\dot{u}_n$ and $\dot{w}_n$ denote normal components of the solid phase velocity and relative fluid velocity. This corresponds

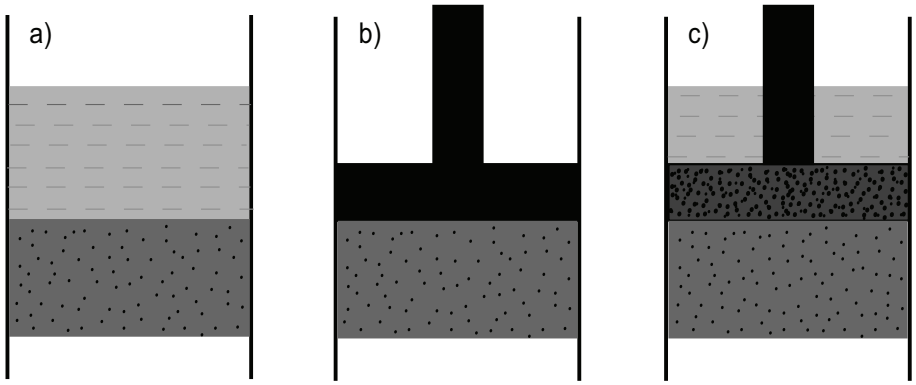

Figure 1.3: Scheme of possible types of boundary conditions; a) liquid stamp, b) impermeable stamp, c) permeable stamp.

to the situation of open pores, so that the pore fluid is free to move through the interface. On the other hand, the alignment of the pores can produce an interfacial flow area which is smaller than that in either medium adjacent to the interface. This effect might be realized physically by inserting a porous membrane between the two media. Flow through such an interface would result in a pressure drop across the interface,

$$p^{(1)} - p^{(2)} = k\dot{w}_n, \tag{1.46}$$

where k is a coefficient of resistance. Thus, in the case of the open pores $k = 0$, in the case of a partially permeable membrane k has to be determined experimentally. The limiting case $k = \infty$ corresponds to the impermeable membrane, so that $\dot{w}_n = 0$ in (1.45). The contact of the two porous solids has been considered e.g. in [53, 34].

The above general conditions reduce to the special cases of contact between a porous medium and an impermeable elastic solid or a liquid. In the case of the contact of perfectly elastic solid and porous media the boundary conditions are

$$\sigma_{nn} + s = \sigma'_{nn},\ \sigma_{n\alpha} = \sigma'_{n\alpha},\ \dot{u}_n = \dot{u}'_n,\ \dot{u}_\alpha = \dot{u}'_\alpha,\ \dot{U}_n - \dot{u}_n = 0. \tag{1.47}$$

where primes denote the characteristics of the perfect solid. These conditions has been used in e.g. [53, 106]. In the case of the contact of a perfect fluid with a porous medium the boundary conditions are

$$\sigma_{nn} + s = -p',\ \sigma_{n\alpha} = 0,\ p = p',\ (1-\phi)\dot{u}_n + \phi\dot{U}_n = \dot{U}'_n, \tag{1.48}$$

where primes denote the characteristics of the fluid. The latter condition implies the continuity of the fluid flow through the interface and stems from the continuity of $\dot{u}_n + \dot{w}_n$

along the interface. The corresponding problems have been considered in [38, 46, 66, 102, 111, 123].

In the case of the free porous interface two different boundary conditions can be prescribed, depending on whether open pores (permeable boundary) or closed pores (impermeable boundary) are considered.

1) open pores

$$\sigma_{nn} = 0,\ \sigma_{n\alpha} = 0,\ s = 0; \tag{1.49}$$

2) closed pores

$$\sigma_{nn} + s = 0,\ \sigma_{n\alpha} = 0,\ \dot{u}_n - \dot{U}_n = 0. \tag{1.50}$$

A comparative study of wave reflection from free boundaries can be found in [40, 61]. In the case of the free boundary of a poroelastic half-space it is only the surface Rayleigh wave that may propagate along the interface (eigen-oscillations).

Finally, in the case of external tractions distributed over a certain area of the porous interface possible boundary conditions include the following cases [94],

1) liquid stamp

$$\sigma_{nn} = -(1-\phi)p',\ \sigma_{n\alpha} = 0,\ s = -\phi p'; \tag{1.51}$$

2) impermeable stamp

$$\sigma_{nn} + s = 0,\ \sigma_{n\alpha} = 0,\ u_n = U_n; \tag{1.52}$$

3) permeable stamp

$$\sigma_{nn} = -p',\ \sigma_{n\alpha} = 0,\ s = 0. \tag{1.53}$$

These are the boundary conditions usually prescribed at the plane boundary of a poroelastic half-space for the solution of the Lamb's problem [75], the classical problem of perfect elasticity theory. This problem is given detailed consideration further in Chapter 3.

Higher frequency range. Viscosity correction factor

In the higher frequency range, beyond the critical frequency f_t, the flow inside the pores is no longer of Poiseuille type. Thin boundary layers develop in the vicinity of the pore wall where the action of the viscous forces is confined, whereas away from the boundary layer the flow is assumed to be potential. As a result there is a phase shift between the relative fluid velocity and the friction force. To elaborate the action of the friction forces in the higher frequency range Biot introduced the complex frequency dependent correction

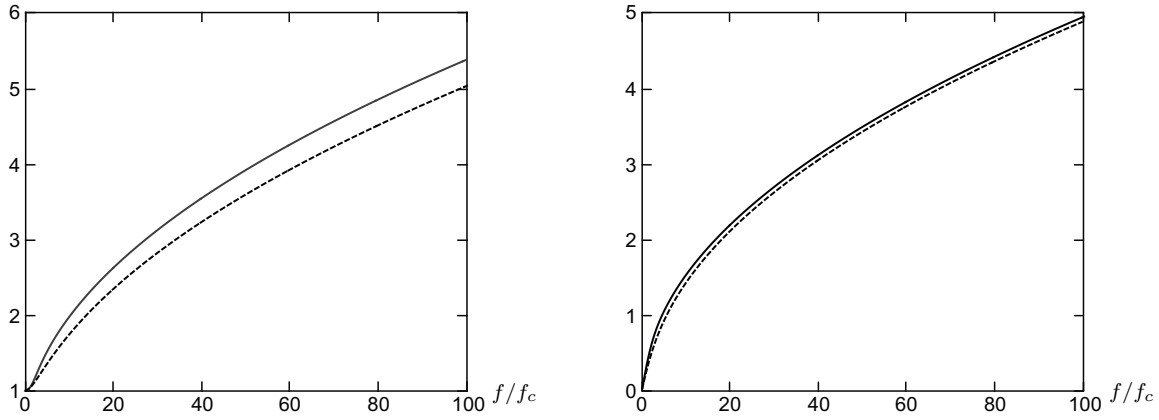

Figure 1.4: Frequency correction factors according to Biot [12] (solid lines) and Johnson *et al.* [70] (dashed lines) for the case of circular pores. Real parts (left), imaginary parts (right).

factor $\mathcal{F}$, so that in the higher frequency range the coefficient b in the governing equations (1.38), (1.39) must be replaced with $b\mathcal{F}$, where [12]

$$\mathcal{F}(\kappa) = \frac{1}{4}\left(\frac{\kappa T(\kappa)}{1 - 2T(\kappa)/i\kappa}\right), \quad T(\kappa) = \frac{\mathrm{ber}'(\kappa) + i\mathrm{bei}'(\kappa)}{\mathrm{ber}(\kappa) + i\mathrm{bei}(\kappa)}, \quad \kappa = \delta\left(\frac{f}{f_c}\right)^{\frac{1}{2}}, \tag{1.54}$$

δ is the structural factor which is related to the pore geometry and thus to be determined from experimental data, bei and ber are zero order Kelvin's functions of the first kind. In other words, the static viscosity η is replaced with the dynamic value $\eta\mathcal{F}(\kappa)$ (complex, or dynamic viscosity). While the pore structure varies greatly, the consideration of all geometric factors is nearly impossible, in derivation of (1.54) Biot assumed that the character of the interphase friction force along the fluid / solid interface is analogous to that in the case of viscous flow in a duct (slit-like pores) and pipe (circular pores) of constant cross-sectional area. For instance, the value of structural factor $\delta = \sqrt{8a}$ corresponds to circular pores. In the low frequency range, the frequency correction factor approaches unity $\mathcal{F} \approx 1$.

Johnson *et al.* [70] suggest the following expression for the frequency correction factor

$$\mathcal{F} = \sqrt{1 + \frac{iM_{js}}{2}\frac{f}{f_c}}, \quad M_{js} = \frac{8a_\infty\kappa_{pr}}{\phi\Lambda^2}, \tag{1.55}$$

where f_c is given by (1.41), Λ is a parameter related to the pore geometry. Apart from (1.54) the frequency dependence in the form (1.55) is widely used in the literature, e.g. [108, 7, 104]. The comparison of the results for the circular pores is provided in Figure 1.4.

Finally, the governing equations valid for the full frequency range can be summarized as follows,

$$(\lambda+\mu)\,\nabla\nabla\cdot\mathbf{u}+\mu\nabla^2\mathbf{u}+Q\nabla\nabla\cdot\mathbf{U} = \rho_{11}\ddot{\mathbf{u}}+\rho_{12}\ddot{\mathbf{U}}+b\mathcal{F}\left(\dot{\mathbf{u}}-\dot{\mathbf{U}}\right), \quad (1.56)$$

$$Q\nabla\nabla\cdot\mathbf{u}+\mathcal{R}\nabla\nabla\cdot\mathbf{U} = \rho_{12}\ddot{\mathbf{u}}+\rho_{22}\ddot{\mathbf{U}}-b\mathcal{F}\left(\dot{\mathbf{u}}-\dot{\mathbf{U}}\right), \quad (1.57)$$

so that the low frequency range theory and the higher frequency range theories can be represented with one set of equations. In his further reformulations of the theory Biot introduced the concept of viscodynamic operator $\bar{Y}$, which is a functional of the differential operator d/dt to incorporate the viscosity correction [14]. In anisotropic media the viscodynamic operator $\bar{Y}_{ij}$ is a symmetric tensor functional of the second rank with complex components, functions of frequency.

1.2 Wave propagation

Analysis of the governing equations (1.56), (1.57) obtained for the full-frequency range allows the study of the wave propagation in a porous solid. Generally speaking, this analysis for the unbounded media reveals the existence of three wave types, two dilatational modes and one shear [11, 12]. In the case of the stress-free plane boundary, one can derive the dispersion relation of the surface Rayleigh wave [39]. The basic properties of the waves propagating in porous solid are briefly outlined in the following.

The frequency dependent character of the phase velocities and attenuations is illustrated based on the following parameter set [44],

$$\begin{gathered}\lambda=0.4026\text{GPa},\ \mu=0.2493\text{GPa},\ R=0.0295\text{GPa},\ Q=0.0672\text{GPa},\\ \rho_{11}=1.9259\cdot10^3\text{kg/m}^3,\ \rho_{22}=0.2151\cdot10^3\text{kg/m}^3,\ \rho_{12}=-0.0019\cdot10^3\text{kg/m}^3,\end{gathered} \quad (1.58)$$

appropriate for sediment acoustics, and adopted throughout the section.

1.2.1 Longitudinal waves

Applying the divergence operator to the governing equations (1.56), (1.57) one can obtain the equations governing the propagation of the dilatational waves

$$\nabla^2\left[(\lambda+2\mu)\,e+Q\varepsilon\right] = \frac{\partial^2}{\partial t^2}\left(\rho_{11}e+\rho_{12}\varepsilon\right)+bF(\kappa)\frac{\partial}{\partial t}\left(e-\varepsilon\right), \quad (1.59)$$

$$\nabla^2\left[Qe+R\varepsilon\right] = \frac{\partial^2}{\partial t^2}\left(\rho_{12}e+\rho_{22}\varepsilon\right)-bF(\kappa)\frac{\partial}{\partial t}\left(e-\varepsilon\right), \quad (1.60)$$

where $e = \nabla \cdot \mathbf{u}$, $\varepsilon = \nabla \cdot \mathbf{U}$.

The following nondimensional parameters are introduced

$$\begin{aligned} \gamma_{11} &= \frac{\rho_{11}}{\rho}, \qquad \gamma_{12} = \frac{\rho_{12}}{\rho}, \quad \gamma_{22} = \frac{\rho_{22}}{\rho}, \\ q_{11} &= \frac{\lambda + 2\mu}{H}, \quad q_{12} = \frac{Q}{H}, \quad q_{22} = \frac{R}{H}, \end{aligned} \tag{1.61}$$

where $\rho = \rho_{11} + \rho_{22} + 2\rho_{12}$, $H = \lambda + 2\mu + R + 2Q$, so that equations (1.59), (1.60) read

$$c^2 \nabla^2 \left(q_{11} e + q_{12} \varepsilon \right) = \frac{\partial^2}{\partial t^2} \left(\gamma_{11} e + \gamma_{12} \varepsilon \right) + F(\kappa) \frac{b}{\rho} \frac{\partial}{\partial t} \left(e - \varepsilon \right), \tag{1.62}$$

$$c^2 \nabla^2 \left(q_{12} e + q_{22} \varepsilon \right) = \frac{\partial^2}{\partial t^2} \left(\gamma_{12} e + \gamma_{22} \varepsilon \right) - F(\kappa) \frac{b}{\rho} \frac{\partial}{\partial t} \left(e - \varepsilon \right), \tag{1.63}$$

where the reference velocity c is defined as $c = \sqrt{H/\rho}$.

A plane wave solution of the form

$$e = C_1 \mathrm{e}^{i(kx + \omega t)}, \quad \varepsilon = C_2 \mathrm{e}^{i(kx + \omega t)}, \tag{1.64}$$

leads to a dispersion relation

$$\left(q_{11} q_{22} - q_{12}^2 \right) z^2 - \left(q_{11} \gamma_{22} + q_{22} \gamma_{11} - 2 q_{12} \gamma_{12} - \frac{ib\mathcal{F}}{\rho \omega} \right) z + \left(\gamma_{11} \gamma_{22} - \gamma_{12}^2 - \frac{ib\mathcal{F}}{\rho \omega} \right) = 0, \tag{1.65}$$

where $z = (ck/\omega)^2$. Two complex roots z_I, z_{II} of the quadratic equation (1.65) are therefore related to the slownesses and attenuations of the two dilatational waves,

$$\sqrt{z_I} = \frac{k_I c}{\omega} = \Re(\sqrt{z_I}) + i \Im(\sqrt{z_I}), \quad \sqrt{z_{II}} = \frac{k_{II} c}{\omega} = \Re(\sqrt{z_{II}}) + i \Im(\sqrt{z_{II}}). \tag{1.66}$$

The roots are conventionally distinguished by the values of the phase velocity at zero frequency as shown in Figure 1.5. Thus, the faster wave, or the wave of the first kind, is referred to as the P1-wave, while the slower wave, or wave of the second kind, is referred to as the P2-wave.

The corresponding phase velocities v_I and v_{II} can be found as

$$\frac{v_I}{c} = \frac{1}{\Re(\sqrt{z_I})}, \quad \frac{v_{II}}{c} = \frac{1}{\Re(\sqrt{z_{II}})}, \tag{1.67}$$

while the attenuation coefficients $\Im(k_I)$ and $\Im(k_{II})$ are given by the following expressions

$$\Im(k_I) L = |\Im(\sqrt{z_I})| \, \frac{f}{f_c}, \quad \Im(k_{II}) L = |\Im(\sqrt{z_{II}})| \, \frac{f}{f_c}, \tag{1.68}$$

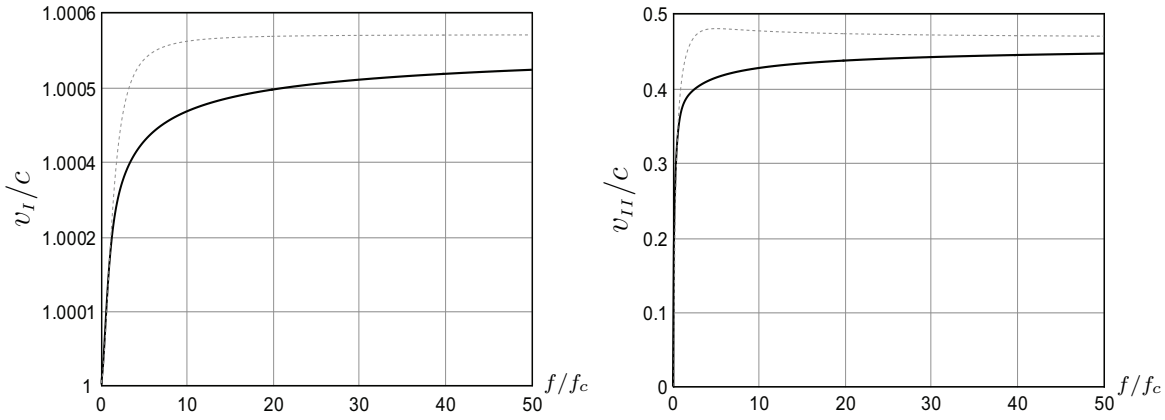

Figure 1.5: Phase velocities of dilatational waves of the first kind (left) and of the second kind (right). Dashed lines indicate the corresponding result when neglecting frequency correction.

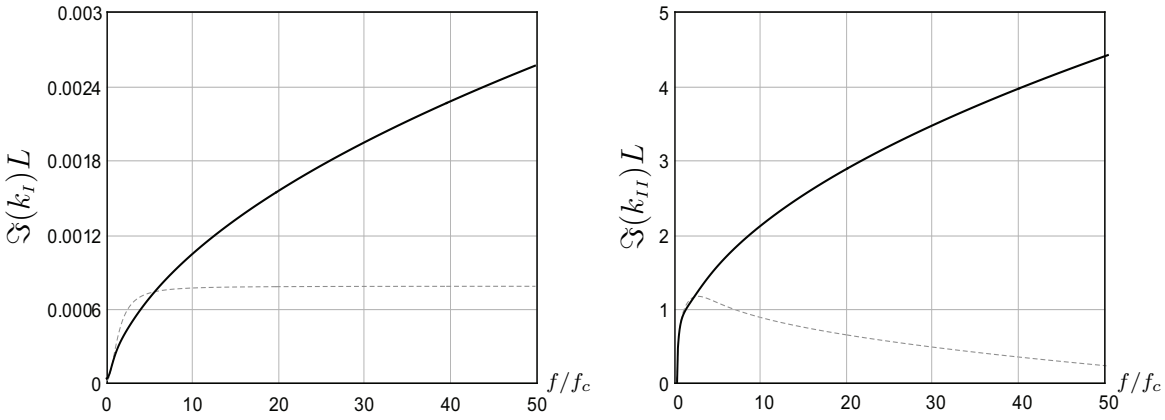

Figure 1.6: Attenuation coefficients of longitudinal waves of the first kind (left) and of the second kind (right). Dashed lines indicate the corresponding result when neglecting frequency correction.

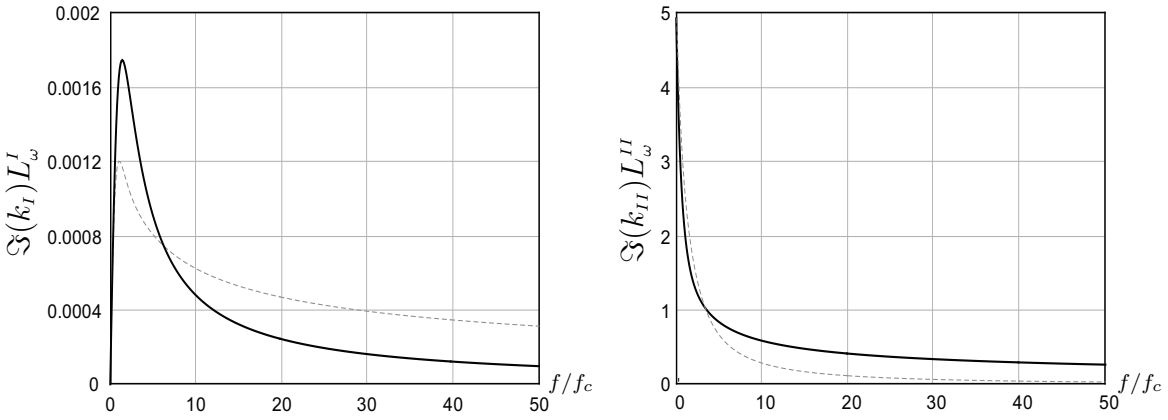

Figure 1.7: Attenuation per cycle of dilatational waves of the first kind (left) and of the second kind (right). Dashed lines indicate the corresponding result when neglecting frequency correction.

where $L = c/2\pi f_c$ is characteristic length.

In addition, it is convenient to introduce a frequency dependent length scales $L^I_\omega = c(\Re\sqrt{z_I})/f$ and $L^{II}_\omega = c\Re(\sqrt{z_{II}})/f$ related to the corresponding wavelengths, so that $k_I L^I_\omega$ and $k_{II} L^{II}_\omega$ represent nondimensional attenuations per cycle,

$$\Im(k_I)L^I_\omega = 2\pi \left| \frac{\Im(\sqrt{z_I})}{\Re(\sqrt{z_I})} \right|, \quad \Im(k_{II})L^{II}_\omega = 2\pi \left| \frac{\Im(\sqrt{z_{II}})}{\Re(\sqrt{z_{II}})} \right|. \tag{1.69}$$

Note that the attenuation per cycle is closely related to the Q factor of a dissipative oscillatory system, as discussed in detail further in Chapter 8. The results for the phase velocity and attenuations of the dilatational waves are provided in Figures 1.5, 1.6, 1.7 respectively.

In the following, the fundamental properties of the dilatational waves are summarized.

- In the case of no dissipation $b = 0$, P1-wave and P2-wave respectively correspond to the in phase and out of phase motion of the solid matrix and pore fluid [11];
- In the low frequency range the phase velocity of the P1-wave approaches the characteristic velocity $c = \sqrt{H/\rho}$, while the phase velocity of the P2-wave tends to zero, $v_{II} \sim c\sqrt{f/f_c}$ [63];
- Attenuation of the P2-wave is significantly (several orders of magnitude) greater than than the attenuation of the P1-wave;

- In the high frequency limit the phase velocities of dilatational waves approach the constant values corresponding to the case of no dissipation $b = 0$ (in which case dilatational waves are not dispersive);
- Attenuation coefficient increases as $\omega^{1/2}$ and attenuations per cycle decreases as $\omega^{-1/2}$ in the high frequency range [12];
- In the limiting case of weak interphase interaction, so that $b \ll 1$, $\gamma_{12} \ll 1$, $q_{12} \ll 1$, $\rho_{12} \ll 1$, P1 and P2 waves phase velocities approach the longitudinal phase velocities of the waves in a corresponding homogeneous solid continuum $c_s = \sqrt{(\lambda + 2\mu)/\rho_{11}}$ and a corresponding compressible fluid $c_f = \sqrt{\mathcal{R}/\rho_{22}}$ [102, 63].

1.2.2 Shear waves

Shear waves can be analyzed in a similar manner where now a starting point is the equations obtained from the governing equations (1.56), (1.57) by the application of curl operator. Hence, denoting vectors $\vec{\psi} = \nabla \times \mathbf{u}$ and $\vec{\Psi} = \nabla \times \mathbf{U}$ one can obtain the following equations

$$\mu \nabla^2 \vec{\psi} = \frac{\partial^2}{\partial t^2}\left(\rho_{11}\vec{\psi} + \rho_{12}\vec{\Psi}\right) + b\mathcal{F}(\kappa)\frac{\partial}{\partial t}\left(\vec{\psi} - \vec{\Psi}\right), \tag{1.70}$$

$$0 = \frac{\partial^2}{\partial t^2}\left(\rho_{12}\vec{\psi} + \rho_{22}\vec{\Psi}\right) - b\mathcal{F}(\kappa)\frac{\partial}{\partial t}\left(\vec{\psi} - \vec{\Psi}\right). \tag{1.71}$$

Consider a rotational plane wave propagating in the x direction, so that

$$\psi = C_1 \mathrm{e}^{i(kx+\omega t)}, \quad \Psi = C_2 \mathrm{e}^{i(kx+\omega t)}. \tag{1.72}$$

With these definitions (1.70) and (1.71) yields

$$q_\mu^2 z C_1 = \gamma_{11} C_1 + \gamma_{12} C_2 - \Xi(C_1 - C_2), \tag{1.73}$$

$$0 = \gamma_{12} C_1 + \gamma_{22} C_2 + \Xi(C_1 - C_2), \tag{1.74}$$

where Ξ and q_μ are defined as

$$\Xi = \frac{ib\mathcal{F}}{\rho\omega}, \quad q_\mu = \sqrt{\frac{\mu}{H}}. \tag{1.75}$$

Note that shear wave amplitudes in the solid and in the fluid are linearly dependent. Indeed, the second equation (1.74) reads

$$C_2 = \frac{\gamma_{12} + \Xi}{\Xi - \gamma_{22}} C_1 = M_s C_1, \quad M_s = \frac{\gamma_{12} + \Xi}{\Xi - \gamma_{22}}. \tag{1.76}$$

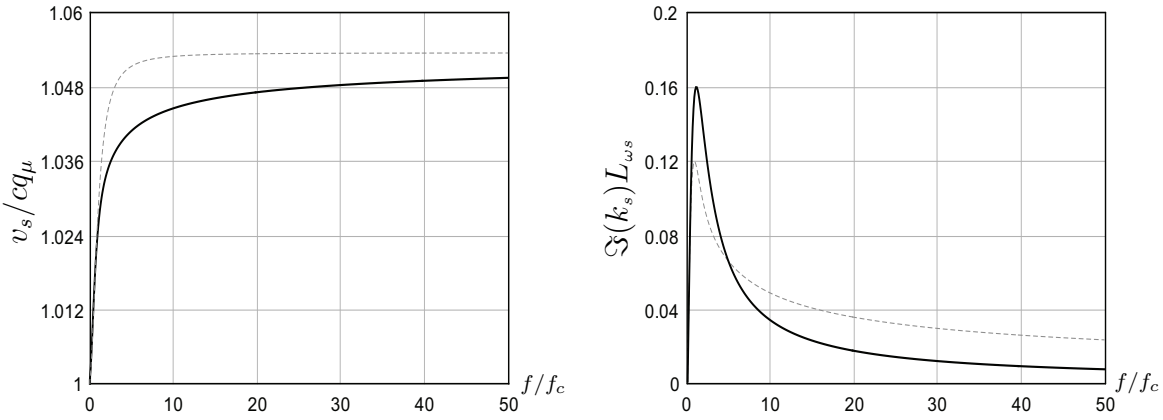

Figure 1.8: Phase velocity (left) and attenuation per cycle (right) of rotational waves. Dashed lines indicate the corresponding result when neglecting frequency correction.

Elimination of C_1 and C_2 in the equations (1.73), (1.74) gives the expression for the shear waves phase velocity v_s

$$\frac{v_s}{cq_\mu} = \frac{1}{\Re(\sqrt{z})}, \quad z = \gamma_{11} + \gamma_{12}M_3 - \Xi(1 - M_3), \tag{1.77}$$

where $cq_\mu = \sqrt{\mu/\rho}$ is the reference velocity of the rotational waves. In the high frequency limit $\omega \to \infty$

$$v_s \to v_s^\infty = \sqrt{\frac{\mu}{\rho_{11} - \frac{\rho_{12}^2}{\rho_{22}}}}, \tag{1.78}$$

what corresponds to the phase velocity of the rotational waves in the case of no dissipation [11].

Introducing the characteristic lengths $L_s = cq_\mu/2\pi f_c$ and $L_{\omega s} = cq_\mu \Re(z)/f$ the attenuation coefficients and attenuations per cycle of rotational waves can be evaluated as follows

$$\Im(k_s)L_s = \left|\Im(\sqrt{z})\right| \frac{f}{f_c}, \quad \Im(k_s)L_{\omega s} = 2\pi \left|\frac{\Im(\sqrt{z})}{\Re(\sqrt{z})}\right|, \tag{1.79}$$

The results for the phase velocity and attenuation per cycle are plotted in Figure 1.8. The fundamental properties of the shear waves can be summarized as follows.

- The phase velocity of the rotational waves is always smaller than the velocity of the fast compressional wave for a physically meaningful mechanical parameter set;

- Shear waves in pore fluid exist in both dissipative and non-dissipative media. In the latter case the vorticity in the inviscid fluid is non-zero due to inertial coupling as long as in the co-occupied continuum Biot's theory the velocity field $\mathbf{U}$ does not represent the actual microscopic flow but the average volume flow [11];

- In the low frequency range the phase velocity of the rotational waves approaches the reference velocity $v_s \to cq_\mu = \sqrt{\mu/\rho}$, while in the high frequency limit it tends to $v_s \to \sqrt{\mu}/\sqrt{(\rho_{11} - \rho_{12}/\rho_{22})}$ what corresponds to the case of no dissipation $b = 0$ (in which case shear waves are not dispersive) [11];

- The attenuation coefficient increases as $\omega^{\frac{1}{2}}$ and attenuation per cycle decreases as $\omega^{-\frac{1}{2}}$ at the high frequency range [12];

- In the case of weak interphase interaction, dispersion relation (1.77) provides $v_s = \sqrt{\mu/\rho_{11}}$, the shear wave phase velocity in the corresponding solid continuum.

1.2.3 Surface waves

Surface waves are waves which propagate along the interface between media with different mechanical properties. In solid mechanics and poromechanics surface waves are the only possible wave motion with no forcing and a free boundary (i.e. normal modes). Maximum amplitudes of the surface waves are found at the boundary, and appreciable amplitudes are only found in the neighborhood of this boundary. Surface waves commonly exhibit relatively low attenuation when propagating along the interface and exponential decay away from the interface.

Various problems of surface wave propagation along the interface of porous media have been considered in a series of papers by Deresiewicz and his coworkers (1960–1967), e.g. [39, 40, 41]. The effect of the boundary conditions as well as the problem of reflection and refraction at the plane porous interface has been investigated for a number of configurations including porous half-space with the free plane boundary (Rayleigh waves), porous layer (Love waves), two porous media with different properties having a common plane boundary (Lamb waves), and a liquid layer supported by the porous half-space (Stoneley waves). The study of Rayleigh waves [4, 6, 39, 40, 61, 69, 88, 102, 112, 123] is mostly motivated by the problems of quantitative seismology [2], while the study of Stoneley waves [32, 45, 46, 66, 105, 119] is mainly of interest in the fields of borehole acoustics and sediment acoustics [67].

The existence of the Rayleigh wave propagating along the plane boundary separating porous media and a vacuum was first reported in the works of Deresiewicz and (independently) Johnson [39, 40, 69]. In particular, a numerical analysis of the secular equation

(pertaining to a kerosene-saturated sandstone) revealed a high frequency cut-off for the surface wave for certain values of the dynamical coefficients [39]. Thus, unlike the Rayleigh wave in a perfectly elastic solid, in a poroelastic solid saturated with an inviscid fluid the Rayleigh wave may not exist [39, 88]. It is important to distinguish between the Rayleigh wave propagating along the impermeable and permeable interface in accordance with the choice of the boundary conditions (1.49) or (1.50). Thus, while in the case of a permeable boundary there exists only one surface wave, in the case of an impermeable boundary two different surface modes can be observed [61]. The first wave propagates with the phase velocity close to that of the surface wave in the half-space with a permeable boundary, and exhibits relatively low attenuation. The second wave attenuates more rapidly, with the phase velocity approaching the velocity of the slow longitudinal wave in the high frequency limit. The greater part of energy transferred by the first wave is concentrated in the elastic skeleton. Most of energy of the significantly attenuating wave is concentrated in the liquid.

Using Biot theory in a high-frequency approximation, Feng & Johnson [45] performed a detailed study of surface waves propagating along the interface between a porous solid and a fluid. It has been found that, in the high-frequency range, one, two or three surface modes can propagate, depending on the elastic parameters of the skeleton and fluid and the conditions on the interface. Feng & Johnson distinguished a true mode, whose velocity is lower than the velocities of all body waves in both contacting media, and Rayleigh and Stoneley leaky modes (pseudo interfatial waves). While the true mode propagates along the interface without attenuation, the leaky modes [2] are substantially attenuated due to energy radiation into the depth of the porous medium and the fluid (or only the porous medium). Dispersion characteristics of these waves in the general dissipative formulation were obtained e.g. in [32, 66]. Recently, it has been demonstrated that the pseudo modes may have physical significance for the transient problem [119].

Finally, consider a dispersion relation of the Rayleigh wave propagating along the plane permeable interface between the porous half-space and vacuum (a detailed derivation is provided in Chapter 3)

$$\left(2p^2 - p_s^2\right)\left[n_1(p^2 - m_2) - n_2\left(p^2 - m_1\right)\right] + 2p^2\xi_s\left(n_2\xi_1 - n_1\xi_2\right) = 0, \tag{1.80}$$

where p_i, $i = 1, 2, s$ represent the complex slownesses (per unit characteristic slowness $1/c$) of the P1, P2 and S-waves respectively, $\xi_{1,2} = \left(p^2 - p_{1,2}^2\right)^{\frac{1}{2}}$, $\xi_s = \left(p^2 - p_s^2\right)^{\frac{1}{2}}$, and

$$m_{1,2} = \frac{\lambda + 2\mu + QM_{1,2}}{2\mu}p_{1,2}^2, \quad n_{1,2} = \frac{Q + \mathcal{R}M_{1,2}}{2\mu}p_{1,2}^2, \tag{1.81}$$

$$M_{1,2} = \frac{q_{22}\gamma_{11} - q_{12}\gamma_{12} - (q_{11}q_{22} - q_{12}^2)\bar{z}_{1,2} - (q_{22} + q_{12})ib\mathcal{F}/\omega\rho}{q_{12}\gamma_{22} - q_{22}\gamma_{12} - (q_{22} + q_{12})ib\mathcal{F}/\omega\rho}. \tag{1.82}$$

The results for the phase velocity v_r and attenuation per cycle $k_r L_{\omega r}$ are provided in Figure 1.9. The results for the low and high frequency limits for all four waves is summarized in Table 1.2.

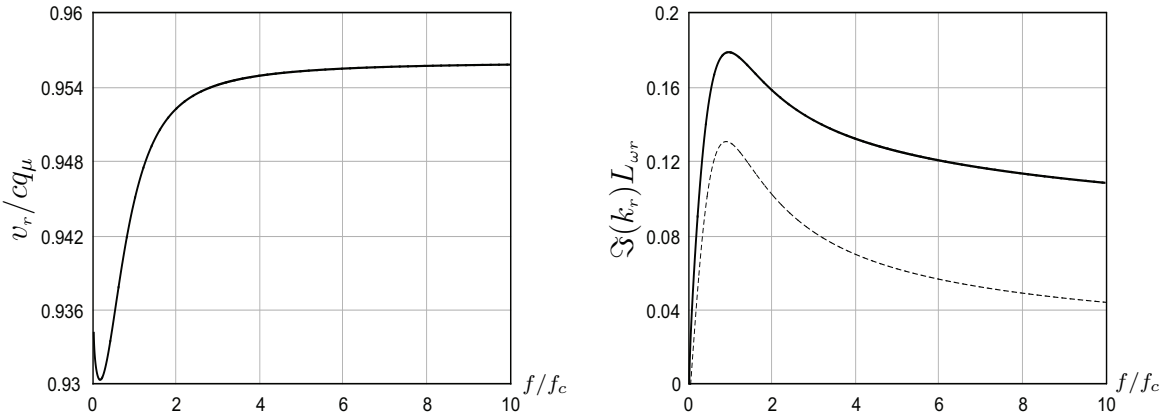

Figure 1.9: Phase velocity (left) and attenuation per cycle (right) of the Rayleigh wave. Dashed line indicates attenuation per cycle of rotational wave for comparison.

The main fundamental properties of the poroelastic Rayleigh wave in the case of a permeable boundary can be summarized as follows.

- The particle motion in this wave is elliptic (prograde and retrograde) as can be verified by the analysis of the displacement fields [3];
- Depending on the values of poroelastic parameters the Rayleigh wave either propagate in the whole frequency range, or may have an upper cut-off frequency [39, 87];
- The phase velocity of the Rayleigh wave is slightly non-monotonic in the low frequency range [3, 39]. Attenuation of the Rayleigh wave is higher than attenuation of the shear wave [39];
- In the high frequency limit the phase velocity approaches the constant value corresponding to the case of no dissipation $b = 0$ (in which case the Rayleigh wave is not dispersive);
- Transcendental nature of the dispersion relation prevents qualitative analysis for the attenuations at high frequency range;
- In the limiting case of an unsaturated medium, such that $\gamma_{12} = \gamma_{22} = 0$, $q_{12} = q_{22} = 0$, $\phi = 0$, $b = 0$ dispersion relation recovers the dispersion relation of the Rayleigh waves in perfectly elastic solid [102]

$$\left(2p^2 - 1\right)^2 - 4p^2 \left(p^2 - p_1^2\right)^{\frac{1}{2}} \left(p^2 - 1\right)^{\frac{1}{2}} = 0. \tag{1.83}$$

Table 1.2: Low and high frequency limiting values of the phase velocities for parameter set (1.58).

	P1-wave	P2-wave	S-wave	Rayleigh wave
Low frequency limit, [m/s]	705.95	0	341.54	319.20
High frequency limit, [m/s]	706.346	326.77	359.79	326.26

1.3 Summary of the Introductory Chapter

The main subject matter of the thesis is the energy analysis of wave motion in a poroelastic half-space under the action of distributed loads. Despite the large number of topics covered in the literature on poroelastic wave propagation, the energy partition analysis of wave motion in porous media has not been considered. Most notably, the qualitative energy partition analysis presented in the following indicates the possibility of controlling the excitation of the various wave types through the driving configuration, which in turn may have broad practical implications (e.g. geophysics, non-destructive testing, acoustoelectronics and medical ultrasound devices). Apart from these main results, energy transport characteristics of poroelastic waves such as group velocity, energy velocity and quality factor are investigated. An energetic interpretation of the complex group velocity is obtained. Fundamental relations for the energy velocity and quality factor are revisited. The content of the thesis is organized as follows.

Introductory Chapters 2, 3 include the derivation of the energy balance equation and the formal solution of the Lamb's problem for a poroelastic half-space (permeable stamp version), respectively, thus providing the necessary foundation for further analysis. Previously known energy balance equations, i.e. Carcione (2007) [31] and Dazel *et al.* (2008) [36] stem from the complex Poynting theorem (complex power flow) [8] and the theorem of kinetic energy [33], respectively (the latter implies that for any material subdomain and for any velocity field whether actual or virtual, the sum of the powers of external, inertia, and internal forces is zero). The alternative derivation of the energy balance equations presented herein follows the Poynting theorem methodology as described in [8] and can be thought of as a generalization of the low frequency energy balance equation derived by Deresiewicz [41]. In the higher frequency range interphase interaction is viscoelastic, so that it is characterized by an elastic energy storage as well as viscous dissipation. This mechanism is reflected by the presence of an additional term in the energy balance equation which quantitatively represents the rate of change of the elastic stored energy. The formal solution of the Lamb's problem provided for the case of open boundary implies two possibilities for the surface wave. Depending on the choice of mechanical parameters the Rayleigh wave either exists over the whole frequency range, or may have a high-frequency

cut-off beyond which the wave vanishes [39, 87].

The energy analysis of poroelastic waves in the case of non-dissipative porous medium is provided in Chapter 4. The energy budget is quantitatively analyzed in the framework of the classical Miller & Pursey approach to elastodynamics problems [84, 85, 64]. Generalization of this well-known approach to the case of a multiphase continuum allows for the decomposition of the total input power entering the poroelastic half-space into the contributions due to particular poroelastic waves. Special cases such as resonant excitation and possible absence of the surface wave are given detailed consideration from an energetic point of view.

Chapter 5 is dedicated to the analysis of the structure of the wave field at the surface of a poroelastic half-space subjected to the action of line traction. Using complex analysis methods it is shown that the contributions of the body waves can be represented in the form of corresponding branch-cut integrals, while the contribution of the surface Rayleigh wave can be taken into account in the form of the residual term. The analysis of the resulting expressions reveals the following: in the near field a line traction generates three wavetrains corresponding to the body waves which represent the superposition of the spectrum components characterized by certain velocity and attenuation bands. Asymptotic results indicate that P1, P2 and S waves emerge from corresponding wavetrains at a certain distance from the source, moreover, these body waves propagating along the plane boundary are subjected to geometric attenuation, which is found quantitavely to be $x^{-3/2}$, similar to the classical results in perfect elasticity theory.

The properties of the poroelastic wavetrains are further investigated in Chapter 6. It is demonstrated that in the case of a distributed source, the waves beneath the contact area represent the superposition of standing waves. In turn, this allows for decomposition of the total power supplied by the source into the constituent powers due to particular wave types. Unlike the case of no dissipation, some of these contributing powers can possibly be negative as long as the corresponding displacements are essentially in phase with the external stress (e.g. this is especially vivid in the case of resonant excitation of the Rayleigh wave). Energy analysis reveals the possibilities of controlling the generation of poroelastic waves. The special case of the absence of the Rayleigh wave is considered in detail. Power redistribution between the surface Rayleigh wave and P2-wave, also previously encountered in the case of no dissipation, is explained by the presence of an additional leaky Raleigh mode (the root of the dispersion relation situated on the "unphysical" Riemann sheet).

Chapters 7 and 8 represent the second logical part of the thesis. The scope of Chapter 7 is the energy analysis of the complex group velocity, while the Chapter 8 is dedicated to such fundamental energy transport characteristics of poroelastic waves as energy velocity and Q factor. The considerations provided in Chapter 7 are intended to expound the complex group velocity from energy principles for a class of hyperbolic, dissipative dynamical systems. It is demonstrated that the complex group velocity can possibly be

related to such energetic characteristics of dissipative media as energy flux, energy losses, and kinetic energy. The remarkable examples of exact interpretations of the complex group velocity from energy principles are outlined, including electromagnetic waves in partially conducting media, and waves governed by the Klein-Gordon equation with dissipation. Approximate energetic interpretations of complex group velocities are obtained for both longitudinal poroelastic waves. The expressions for the energy velocity and Q factor of poroelastic longitudinal and shear waves are rigorously derived from energy considerations in Chapter 8. Most notably, the analysis of the resulting expressions reveals that the energy velocity of both longitudinal and shear waves equals (exceeds) the corresponding phase velocity in the case of the low (full) frequency range Biot's theory. The exact expression for the Q factor contains an additive correction due to viscoelastic interphase interaction in the higher frequency range. The comparison with previously known results on the topic, namely these summarized in Carcione 2007 [31], is given detailed consideration.

Several parts of this thesis have appeared in the literature. The results of Chapters 3 and 5 appeared in [55, 54], the results of Chapters 7 in [56], the results of Chapter 8 (also briefly introduced in Chapter 2) appeared in [58]. The results of Chapter 4 are presently being revised, [57].

Finally, the general conclusions are summarized in Chapter 9.

Chapter 2

Poroelastic Poynting theorem

According to Biot's theory [11] the kinetic energy density T, potential energy density V (strain energy), and dissipation function D (Rayleigh dissipation pseudopotential), are respectively,

$$\begin{aligned} 2T &= \rho_{11}\dot{u}_i^2 + 2\rho_{12}\dot{u}_i\dot{U}_i + \rho_{22}\dot{U}_i^2, && (2.1)\\ 2V &= \sigma_{ij}e_{ij} + s\varepsilon, && (2.2)\\ 2D &= b(\dot{u}_i - \dot{U}_i)^2, && (2.3) \end{aligned}$$

where u and U are the displacements of the solid and fluid phases respectively, ρ_{ij} is the mass matrix whose diagonal (off-diagonal) components represent reference phase densities (added mass effects); $b = \phi^2\eta_f/K$, where ϕ, η_f and K denote porosity, viscosity and permeability, respectively. The solid stress σ_{ij}, and the stress on fluid s, are related to the solid strain tensor e_{ij}, and fluid strain ε,

$$e_{ij} = \frac{1}{2}\left(u_{i,j} + u_{j,i}\right), \quad \varepsilon = U_{i,i}, \tag{2.4}$$

via constitutive equations

$$\begin{aligned} \sigma_{ij} &= \lambda e_{kk}\delta_{ij} + 2\mu e_{ij} + Q\varepsilon\delta_{ij}, && (2.5)\\ s &= Qe_{kk} + \mathcal{R}\varepsilon. && (2.6) \end{aligned}$$

The generalized poroelastic parameters λ, μ, Q and $\mathcal{R}$ are related to porosity, bulk modulus of the solid, bulk modulus of the fluid, bulk modulus of the porous drained matrix, and shear modulus of both the matrix and of the composite [16].

2.1 Low frequency range

Consider the rate of change of the total mechanical energy per unit volume Σ,

$$\frac{d}{dt}\iiint_{\Sigma}(T+V)\,d\Sigma = \tag{2.7}$$
$$= \iiint_{\Sigma}\left[\left(\rho_{11}\ddot{u}_i+\rho_{12}\ddot{U}_i\right)\dot{u}_i+\left(\rho_{22}\ddot{U}_i+\rho_{12}\ddot{u}_i\right)\dot{U}_i+\sigma_{ij}\dot{u}_{i,j}+s\dot{U}_{i,i}\right]d\Sigma,$$

which, with the application of Gauss' theorem, reads ($S=\partial\Sigma$),

$$\frac{d}{dt}\iiint_{\Sigma}(T+V)\,d\Sigma = -\iint_{S}\left(-\sigma_{ij}\dot{u}_i-s\dot{U}_i\delta_{ij}\right)n_j dS- \tag{2.8}$$
$$-\iiint_{\Sigma}\left[\left(\sigma_{ij,j}-\rho_{11}\ddot{u}_i-\rho_{12}\ddot{U}_i\right)\dot{u}_i+\left(s_{,i}-\rho_{22}\ddot{U}_i-\rho_{12}\ddot{u}_i\right)\dot{U}_i\right]d\Sigma.$$

The coefficients in front of $\dot{u}_i$ and $\dot{U}_i$ in the volume integral represent the difference between the rate of change of the linear momentum and surface forces acting on the solid and fluid phases respectively. According to the low frequency Biot's theory these are frictional forces, proportional to the filtration velocity $b(\dot{u}_i-\dot{U}_i)$. Including possible external volumetric forces acting on the solid skeleton, F_i^s, and on the pore fluid, F_i^f, one recovers the governing equations from energy principles,

$$\rho_{11}\ddot{u}_i+\rho_{12}\ddot{U}_i = \sigma_{ij,j}+F_i^s-b\left(\dot{u}_i-\dot{U}_i\right), \tag{2.9}$$
$$\rho_{22}\ddot{U}_i+\rho_{12}\ddot{u}_i = s_{,i}+F_i^f+b\left(\dot{u}_i-\dot{U}_i\right). \tag{2.10}$$

Consequently, according to (2.8), (2.9) and (2.10) the energy balance equation reads,

$$W_{vol} = \frac{d}{dt}\iiint_{\Sigma}(T+V)\,d\Sigma+\iint_{S}\vec{P}\cdot\hat{\mathbf{n}}\,dS+2\iiint_{\Sigma}D\,d\Sigma, \tag{2.11}$$

where W_{vol} denotes the source power of the volumetric forces,

$$W_{vol} = \iiint_{\Sigma}\left(F_i^s\dot{u}_i+F_i^f\dot{U}_i\right)d\Sigma, \tag{2.12}$$

and the poroacoustic Poynting vector is defined as

$$P_j = -\sigma_{ij}\dot{u}_i-s\dot{U}_i\delta_{ij}, \tag{2.13}$$

so that the expression $P_j n_j$ can be interpreted as the energy flux per unit area in the direction of the outward surface normal vector $\hat{\mathbf{n}}$. The terms on the right hand side of (2.11) represent the rate of change of the total mechanical energy, energy flux and power dissipation, respectively.

2.1.1 Poroacoustic Poynting vector

In the case of harmonic motion, the value of the period-average flux density is often important. For example in the 2D case, for the time dependence $e^{i\omega t}$, one derives the following expressions for the period-averaged components of the Poynting vector

$$\langle P_x \rangle = \frac{i\omega}{4} \left(\sigma_{xx} u_x^* - \sigma_{xx}^* u_x + \sigma_{xz} u_z^* - \sigma_{xz}^* u_z + s U_x^* - s^* U_x \right), \tag{2.14}$$

$$\langle P_z \rangle = \frac{i\omega}{4} \left(\sigma_{zz} u_z^* - \sigma_{zz}^* u_z + \sigma_{xz} u_x^* - \sigma_{xz}^* u_x + s U_z^* - s^* U_z \right), \tag{2.15}$$

where a superscript star denotes the complex conjugate (expressions with an opposite sign correspond to a time dependence of the form $e^{-i\omega t}$).

2.2 Full frequency range

In the higher frequency range the derivation of the energy balance equation requires special care. So far, the damping factor b was assumed to be purely real, as is the case for purely viscous interphase interaction and hence is restricted to the low frequency range. In the higher frequency range it is necessary to include viscoelastic effects and thus introduce the complex viscosity $\mathcal{F}\eta_f$ (by means of the frequency dependent complex correction factor $\mathcal{F}$) to describe the lag between the filtration velocity and the shear stress exerted on the pore wall [12]. As a result, in the general form, governing equations (2.9)–(2.10) contain a complex, frequency dependent coefficient $b\mathcal{F} = b\mathcal{F}_R + ib\mathcal{F}_I$, and thus can only be satisfied exactly with complex form solutions.

Assuming the solutions to be of the form $u_i = \hat{u}_i + i\tilde{u}_i$, $U_i = \hat{U}_i + i\tilde{U}_i$, the real parts of the governing equations can be written as follows ($\hat{\sigma}_{ij,j}$ and $\hat{s}_{,i}$ denote the real parts of the corresponding quantities)

$$\rho_{11}\ddot{\hat{u}}_i + \rho_{12}\ddot{\hat{U}}_i = \hat{\sigma}_{ij,j} + F_{si} - b\mathcal{F}_R \left(\dot{\hat{u}}_i - \dot{\hat{U}}_i \right) + b\mathcal{F}_I \left(\dot{\tilde{u}}_i - \dot{\tilde{U}}_i \right), \tag{2.16}$$

$$\rho_{22}\ddot{\hat{U}}_i + \rho_{12}\ddot{\hat{u}}_i = \hat{s}_{,i} + F_{fi} + b\mathcal{F}_R \left(\dot{\hat{u}}_i - \dot{\hat{U}}_i \right) - b\mathcal{F}_I \left(\dot{\tilde{u}}_i - \dot{\tilde{U}}_i \right). \tag{2.17}$$

Multiplying the above equations by $\hat{\dot{u}}_i$ and $\hat{\dot{U}}_i$ respectively and then adding the two one obtains the following expression

$$\frac{d}{dt}\left(\frac{1}{2}\rho_{11}\hat{\dot{u}}_i^2+\rho_{12}\hat{\dot{u}}_i\hat{\dot{U}}_i+\frac{1}{2}\rho_{22}\hat{\dot{U}}_i^2\right)= \tag{2.18}$$
$$=\hat{\sigma}_{ij,j}\hat{\dot{u}}_i+\hat{s}_{,i}\hat{\dot{U}}_i+F_{si}\hat{\dot{u}}_i+F_{fi}\hat{\dot{U}}_i-b\mathcal{F}_{R}\left(\hat{\dot{u}}_i-\hat{\dot{U}}_i\right)^2+b\mathcal{F}_{I}\left(\tilde{\dot{u}}_i-\tilde{\dot{U}}_i\right)\left(\hat{\dot{u}}_i-\hat{\dot{U}}_i\right),$$

which after integration over the volume and application of Gauss theorem can be written in the form of an energy balance,

$$W_{vol}=\frac{d}{dt}\iiint\limits_{\Sigma}(T+V)\,d\Sigma+\iint\limits_{S}\vec{P}\cdot\hat{\mathbf{n}}\,dS+2\iiint\limits_{\Sigma}D\,d\Sigma-2\iiint\limits_{\Sigma}\Omega\,d\Sigma, \tag{2.19}$$

where

$$D=\frac{1}{2}b\mathcal{F}_{R}\left(\hat{\dot{u}}_i-\hat{\dot{U}}_i\right)^2,\quad \Omega=\frac{1}{2}b\mathcal{F}_{I}\left(\tilde{\dot{u}}_i-\tilde{\dot{U}}_i\right)\left(\hat{\dot{u}}_i-\hat{\dot{U}}_i\right). \tag{2.20}$$

The energy balance equation (2.19) is valid in the full frequency range, and the result (2.11) can be recovered from (2.19) for the low frequency range by taking $\mathcal{F}\approx 1$. Unlike (2.11) the dissipation function D in (2.19) is defined in a more general form, moreover, (2.19) contains an additional term Ω to account for the rate of change of the total elastic stored energy.

2.2.1 Elastic energy stored

During the deformation of a viscoelastic body, part of the total work of deformation is dissipated as heat through viscous losses but the reminder of the deformation energy is stored as elastic energy. Elastic stored energy is potential energy [115]. In a porous solid in the higher frequency range the interphase interaction is viscoelastic. Consequently, similarly to viscoelastic materials the rate of change of the total mechanical energy per unit volume $E=T+V$ [as it follows from (2.19) in the absence of volumetric forces] is characterized by the power dissipation $2D$ and the rate of change of the elastic stored energy 2Ω,

$$\dot{E}=-2D+2\Omega. \tag{2.21}$$

It is frequently of interest to determine the amount of energy dissipated as well as the amount of energy stored. According to (2.16) the forces acting on the solid phase exerted by the fluid

$$-b\mathcal{F}_{R}\left(\hat{\dot{u}}_i-\hat{\dot{U}}_i\right)+b\mathcal{F}_{I}\left(\tilde{\dot{u}}_i-\tilde{\dot{U}}_i\right). \tag{2.22}$$

While the first term represents the component of the force which is out of phase with the relative solid velocity $\left(\hat{\dot{u}}_i - \hat{\dot{U}}_i\right)$, and thus corresponds to viscous frictional force, the second term is $\pi/2$ phase-shifted compared to the relative solid velocity and in phase with the relative solid displacement $\left(\hat{u}_i - \hat{U}_i\right)$. Therefore, the latter component corresponds to the elastic deformation.

Consequently, the elastic energy stored can be quantified as follows,

$$\mathcal{E} = \frac{1}{2} b \mathcal{F}_I \left(\tilde{u}_i - \tilde{U}_i\right) \left(\hat{u}_i - \hat{U}_i\right), \tag{2.23}$$

so that the following obvious identity holds

$$\frac{d\mathcal{E}}{dt} = 2\Omega. \tag{2.24}$$

The elastic energy stored $\mathcal{E}$ builds to a maximum followed by recovery over each cycle, as a result the rate of change of the energy stored in one cycle is necessarily zero, $\langle \Omega \rangle = 0$. The time-averaged value of the elastic energy stored per unit volume $\langle \mathcal{E} \rangle$ can be quantified in terms of complex solutions u_i, U_i as follows,

$$\langle \mathcal{E} \rangle = \frac{1}{4} \omega b \mathcal{F}_I \left(u_i - U_i\right) \left(u_i - U_i\right)^* = \frac{1}{4} \omega b \mathcal{F}_I \left|u_i - U_i\right|^2, \tag{2.25}$$

in which case the maximum energy stored is given by $2 \langle \mathcal{E} \rangle$.

2.3 Average energy balance equations

In the case of harmonic motion of angular frequency ω, averaging (2.19) over one cycle one finds

$$\langle W_{vol} \rangle = \iint\limits_S \langle \vec{P} \rangle \cdot \hat{\mathbf{n}} \, dS + 2 \iiint\limits_\Sigma \langle D \rangle \, d\Sigma, \tag{2.26}$$

so that the part of the power supplied by the source is lost due to viscous dissipation while the remaining part is transported through the boundary. This is the very general form of the average energy balance equation suitable for both low and full frequency range.

Semi-infinite solid

Consider the particular case of a semi-infinite solid under the action of a surface distributed source in the absence of volumetric forces. Let the surface traction be applied over the

finite area S_0, $S_0 \subset S$,

$$\iint\limits_{S_0} \langle \vec{P} \rangle \cdot \hat{\mathbf{n}}\, dS + \iint\limits_{S/S_0} \langle \vec{P} \rangle \cdot \hat{\mathbf{n}}\, dS + 2 \iiint\limits_{\Sigma} \langle D \rangle\, d\Sigma = 0. \tag{2.27}$$

While the contribution from the second term in (2.27) vanishes, the power of the surface traction $\langle W \rangle$ is given by the first term of (2.27),

$$\langle W \rangle = - \iint\limits_{S_0} \langle \vec{P} \rangle \cdot \hat{\mathbf{n}}\, dS. \tag{2.28}$$

Consequently, the average power supplied by the source is dissipated as in the case of damped harmonic oscillator,

$$\langle W \rangle = -2 \iiint\limits_{\Sigma} \langle D \rangle\, d\Sigma. \tag{2.29}$$

Assuming no dissipation $\langle D \rangle = 0$ the average energy balance equation (2.27) can be recast as follows

$$\langle W \rangle = \iint\limits_{S/S_0} \langle \vec{P} \rangle \cdot \hat{\mathbf{n}}\, dS, \tag{2.30}$$

in which case the energy supplied by the source is radiated away at infinity as in the case of a semi-infinite perfect elastic solid.

Chapter 3

Lamb's problem. Formal solution

Consider the equations governing the propagation of poroelastic waves (Biot 1956*b*),

$$(\lambda+\mu)\,\nabla\nabla\cdot\mathbf{u}+\mu\nabla^2\mathbf{u}+Q\nabla\nabla\cdot\mathbf{U}=\rho_{11}\ddot{\mathbf{u}}+\rho_{12}\ddot{\mathbf{U}}+b\mathcal{F}\left(\dot{\mathbf{u}}-\dot{\mathbf{U}}\right), \tag{3.1}$$

$$Q\nabla\nabla\cdot\mathbf{u}+\mathcal{R}\nabla\nabla\cdot\mathbf{U}=\rho_{12}\ddot{\mathbf{u}}+\rho_{22}\ddot{\mathbf{U}}-b\mathcal{F}\left(\dot{\mathbf{u}}-\dot{\mathbf{U}}\right), \tag{3.2}$$

on a two-dimensional poroelastic half-space that occupies the region $z>0$ and is subjected to the action of an external harmonic traction $Pf(x)e^{i\omega t}$, so that the forces are applied normally at the boundary $z=0$ and act exclusively on the solid matrix. We recover a line source if $f(x)=\delta(x)$ and distributed source if $f(x)\equiv 0$, $|x|>a$ and $f(x)\neq 0$, $|x|\leq a$. In this formulation of the Lamb's problem the boundary conditions at the surface $z=0$ can be represented in the form

$$\sigma_{zz}(x,0,t)=Pf(x)\mathrm{e}^{i\omega t},\ \sigma_{xz}(x,0,t)=s(x,0,t)=0. \tag{3.3}$$

A standard Helmholtz decomposition allows for the expansion of the displacement fields into irrotational and solenoidal components by means of only three scalar functions Φ_1, Φ_2 and Ψ_s as follows,

$$\mathbf{u}=\nabla\Phi_1+\nabla\times\mathbf{j}\Psi_s,\mathbf{U}=\nabla\Phi_2+M_s\nabla\times\mathbf{j}\Psi_s,\ \nabla\cdot\mathbf{j}\Psi_s=0, \tag{3.4}$$

where M_s is some quantity to be determined hereafter. This leads to the following set of equations in the frequency domain,

$$\mathbf{A}\vec{\nabla}^2\vec{\Phi}+\omega^2\mathbf{N}\vec{\Phi}=0,\quad \nabla^2\Psi_s+\omega^2\chi\Psi_s=0, \tag{3.5}$$

where $\vec{\Phi}=(\Phi_1,\Phi_2)$,

$$\begin{gathered}\mathbf{A}=\begin{pmatrix}\lambda+2\mu & Q\\ Q & R\end{pmatrix},\quad \mathbf{N}=\begin{pmatrix}\rho_{11}-ib\mathcal{F}/\omega & \rho_{12}+ib\mathcal{F}/\omega\\ \rho_{12}+ib\mathcal{F}/\omega & \rho_{22}-ib\mathcal{F}/\omega\end{pmatrix},\\ \chi=\frac{1}{\mu}\left[\rho_{11}+M_s\rho_{12}-(1-M_s)\,ib\mathcal{F}/\omega\right],\quad M_s=-\frac{\rho_{12}+ib\mathcal{F}/\omega}{\rho_{22}-ib\mathcal{F}/\omega}.\end{gathered} \tag{3.6}$$

In terms of nondimensional parameters $\bar{x} = \omega x/c$, $\bar{z} = \omega z/c$ (henceforth bars over spatial coordinates are omitted, all spatial variables are implied nondimensional, per unit length c/ω, unless otherwise specified),

$$\begin{array}{lll} \gamma_{11} = \rho_{11}/\rho, & q_{11} = (\lambda + 2\mu)/H, & c = \sqrt{H/\rho}, \\ \gamma_{12} = \rho_{12}/\rho, & q_{12} = Q/H, & \rho = \rho_{11} + 2\rho_{12} + \rho_{22}, \\ \gamma_{22} = \rho_{22}/\rho, & q_{22} = \mathcal{R}/H, & H = \lambda + 2\mu + R + 2Q, \end{array} \tag{3.7}$$

(3.5) and (3.6) read respectively,

$$\bar{\mathbf{A}}\vec{\nabla}^2\vec{\Phi} + \bar{\mathbf{N}}\vec{\Phi} = 0, \quad \nabla^2\Psi_s + \bar{\chi}\Psi_s = 0, \tag{3.8}$$

where

$$\begin{aligned} \bar{\mathbf{A}} = \begin{pmatrix} q_{11} & q_{12} \\ q_{12} & q_{22} \end{pmatrix}, \quad \bar{\mathbf{N}} = \begin{pmatrix} \gamma_{11} - ib\mathcal{F}/\rho\omega & \gamma_{12} + ib\mathcal{F}/\rho\omega \\ \gamma_{12} + ib\mathcal{F}/\rho\omega & \gamma_{22} - ib\mathcal{F}/\rho\omega \end{pmatrix}, \\ \bar{\chi} = \frac{H}{\mu}\left[\gamma_{11} + \gamma_{12}M_s - (1 - M_s)\, ib\mathcal{F}/\rho\omega\right], \quad M_s = -\frac{\gamma_{12} + ib\mathcal{F}/\rho\omega}{\gamma_{22} - ib\mathcal{F}/\rho\omega}. \end{aligned} \tag{3.9}$$

With a similarity transformation $\bar{\mathbf{A}}^{-1}\bar{\mathbf{N}} = \mathbf{S}\mathbf{\Lambda}\mathbf{S}^{-1}$, $\mathbf{\Lambda} = \mathrm{diag}\,(z_1,\ z_2)$ the first equation (3.8) decouples into two wave equations in an eigenvector reference system. Here $z_{1,2}$ denotes the distinct roots of the characteristic polynomial of the similarity transformation,

$$\begin{aligned} (q_{11}q_{22} - q_{12}^2)z^2 - (q_{11}\gamma_{22} - 2q_{12}\gamma_{12} + q_{22}\gamma_{11} - ib\mathcal{F}/\omega\rho)z + \\ +(\gamma_{11}\gamma_{22} - \gamma_{12}^2 - ib\mathcal{F}/\omega\rho) = 0, \end{aligned} \tag{3.10}$$

which provides the dispersion relation for the two compressional waves (Biot 1956*b*). The connection between the reference systems is given by the eigenvector matrix $\mathbf{S}$, normalized as follows,

$$\begin{pmatrix} \Phi_1 \\ \Phi_2 \end{pmatrix} = \mathbf{S}\begin{pmatrix} \Phi_1^* \\ \Phi_2^* \end{pmatrix}, \quad \mathbf{S} = \begin{pmatrix} 1 & 1 \\ M_1 & M_2 \end{pmatrix}. \tag{3.11}$$

Consequently, one arrives at the following set of Helmholtz equations,

$$\nabla^2\Phi_1^* + \bar{z}_1\Phi_1^* = 0, \ \ \nabla^2\Phi_2^* + \bar{z}_2\Phi_2^* = 0, \ \ \nabla^2\Psi_s + \bar{\chi}\Psi_s = 0, \tag{3.12}$$

where

$$\Phi_1 = \Phi_1^* + \Phi_2^*, \ \ \Phi_2 = M_1\Phi_1^* + M_2\Phi_2^*, \tag{3.13}$$

$$M_{1,2} = \frac{q_{22}\gamma_{11} - q_{12}\gamma_{12} - (q_{11}q_{22} - q_{12}^2)\bar{z}_{1,2} - (q_{22} + q_{12})ib\mathcal{F}/\omega\rho}{q_{12}\gamma_{22} - q_{22}\gamma_{12} - (q_{22} + q_{12})ib\mathcal{F}/\omega\rho}. \tag{3.14}$$

The solutions of the above Helmholtz equations (3.12) in Fourier space (transformed solutions will be indicated by the arguments),

$$f(p) = \int_{-\infty}^{+\infty} f(x)\mathrm{e}^{-ipx}dx, \quad f(x) = \frac{1}{2\pi}\int_{-\infty}^{+\infty} f(p)\mathrm{e}^{ipx}dp, \tag{3.15}$$

can be written as follows,

$$\Phi^*_{1,2} = A_{1,2}\exp\left(-\xi_{1,2}z\right), \ \Psi_s = A_s\exp\left(-\xi_s z\right); \tag{3.16}$$

$$\xi_{1,2} = \left(p^2 - p^2_{1,2}\right)^{\frac{1}{2}}, \ \ \xi_s = \left(p^2 - p^2_s\right)^{\frac{1}{2}}, \ \ p_{1,2} = \sqrt{z_{1,2}}, \ \ p_s = \sqrt{\overline{\chi}}, \tag{3.17}$$

where $A_{1,2}$ and A_s remain to be determined from the boundary conditions. In this notation, the corresponding phase velocities of the P1-, P2- and S-waves are the expressions $c_i = c/p_i, \ i = 1, 2, s$ respectively, and thus the parameters $p_i, \ i = 1, 2, s$ represent corresponding nondimensional slownesses.

It now remains to satisfy the boundary conditions. According to (2.5), (2.6) and representation (3.4),

$$\begin{gathered}
\sigma_{zz} = \lambda\nabla^2\Phi_1 + Q\nabla^2\Phi_2 + 2\mu\left(\frac{d^2\Phi_1}{dz^2} + \frac{d^2\Psi_s}{dxdz}\right), \\
\sigma_{xz} = \mu\left(2\frac{d^2\Phi_1}{dxdz} + \frac{d^2\Psi_s}{dx^2} - \frac{d^2\Psi_s}{dz^2}\right), \\
s = Q\nabla^2\Phi_1 + \mathcal{R}\nabla^2\Phi_2.
\end{gathered} \tag{3.18}$$

Taking into account the solutions (3.17) and the boundary conditions (3.3), one arrives at the following algebraic system in slowness–frequency space,

$$\begin{cases}
A_1\left(m_1 - p^2\right) + A_2\left(m_2 - p^2\right) + A_s ip\xi_s = -\dfrac{Pf(p)}{2\mu}, \\
2A_1 ip\xi_1 + 2A_2 ip\xi_2 + A_s\left(2p^2 - p^2_s\right) = 0, \\
A_1 n_1 + A_2 n_2 = 0,
\end{cases} \tag{3.19}$$

where

$$m_{1,2} = \frac{\lambda + 2\mu + QM_{1,2}}{2\mu}p^2_{1,2}, \ \ n_{1,2} = \frac{Q + \mathcal{R}M_{1,2}}{2\mu}p^2_{1,2}. \tag{3.20}$$

The application of the boundary conditions uniquely determines the values of the unknown coefficients $A_{1,2}$, A_s:

$$A_1 = -Pf(p)\frac{n_2\left(2p^2 - p^2_s\right)}{2\mu F(p,\omega)}, \ A_2 = Pf(p)\frac{n_1\left(2p^2 - p^2_s\right)}{2\mu F(p,\omega)}, \tag{3.21}$$

$$A_s = -Pf(p)\frac{2ip\left(n_1\xi_2 - n_2\xi_1\right)}{2\mu F(p,\omega)}, \tag{3.22}$$

$$F(p) = \left(2p^2 - p^2_s\right)\left[n_1(p^2 - m_2) - n_2\left(p^2 - m_1\right)\right] + 2p^2\xi_s\left(n_2\xi_1 - n_1\xi_2\right). \tag{3.23}$$

The equation $F(p) = 0$ is the dispersion relation of the surface Rayleigh waves. The root of this equation, if one exists, is denoted by p_r and the corresponding phase velocity is $c_r = c/p_r$.

The results for the displacement fields in nondimensional slowness space can be summarized as follows,

$$\begin{pmatrix} u_x \\ u_z \\ U_x \\ U_z \end{pmatrix} = \begin{pmatrix} ip & ip & \xi_s \\ -\xi_1 & -\xi_2 & ip \\ ipM_1 & ipM_2 & \xi_s M_s \\ -\xi_1 M_1 & -\xi_2 M_2 & ipM_s \end{pmatrix} \begin{pmatrix} A_1 \mathrm{e}^{-z\xi_1} \\ A_2 \mathrm{e}^{-z\xi_2} \\ A_s \mathrm{e}^{-z\xi_s} \end{pmatrix}. \tag{3.24}$$

Three typical driving configurations

$$\begin{aligned} &\text{(i)} && f(x) = \delta(x), && f(p) = 1; \\ &\text{(ii)} && f(x) = 1, && f(p) = \frac{2a\sin(ap)}{ap}; \\ &\text{(iii)} && f(x) = \cos(p_0 x), && f(p) = a\left[\frac{\sin a(p+p_0)}{a(p+p_0)} + \frac{\sin a(p-p_0)}{a(p-p_0)}\right]; \end{aligned} \tag{3.25}$$

a line source (i), and two distributed sources ($f(x) \equiv 0,\ |x| > a$), (ii) and (iii), are considered in the following. Solutions (3.24) and relations (3.25) constitute the foundation for further analysis.

Chapter 4

Energy partition and resonant excitation in the case of no dissipation

Two-dimensional motion of non-dissipative poroelastic half-space under the action of normal harmonic driving forces is considered in the context of Biot's theory of poroelasticity. The classical approach to the energy analysis of the wave motion in the Lamb's problem, originally established for elastic waves by Miller & Pursey (1954, 1955) [84, 85], is applied to poroelastic non-dissipative waves. The total power radiated by the source is represented as a superposition of the powers transported by poroelastic waves viz. P1, P2, S and surface Rayleigh waves. Two possible situations are considered, one in which the Rayleigh mode does and one in which it does not exist in the poroelastic half-space. The energy partition results are presented for several driving configurations to investigate the possibilities of controlling the excitation of particular wave types. The results are compared with, and recover in the limiting case, those known from classical elasticity theory.

The energy partition among longitudinal, shear and surface Rayleigh waves in the Lamb's problem [75] has been a subject of intense research in the classical elasticity theory [64] ever since the pioneering work of Miller & Pursey. In the context of Biot's theory [11, 12] the mathematical complexity has prevented any quantitative energy analysis of the wave motion. Nevertheless, the classical approach originally established by Miller & Pursey for elastic waves can also be applied to an idealized case of non-dissipative poroelastic waves. Such idealization implies either the assumption of inviscid interphase interaction, or the high frequency limit of the dynamical system (since in this limit the dissipation terms in the governing equations become asymptotically smaller compared to the inertia terms). In the absence of dissipation the far-field interior solution for a poroelastic half-space under the action of harmonic surface loads can be obtained by use of the asymptotic

results suggested by Miller & Pursey [84, 64]. The expression for the poroelastic Poynting vector [102, 123, 104] takes a more complicated form in a two-phase continuum as it now contains the information about the energy transported by the two longitudinal waves (i.e. the P1 and P2-waves) propagating in both the solid and fluid phases, as well as the shear wave (i.e. the S-wave) in the solid phase. The surface Rayleigh wave in a porous solid and its relative contribution to the energy budget can be analyzed similarly to the case of a perfectly elastic solid [64] with evaluation of the corresponding residues. Moreover, the governing equations of elasticity theory represent an appropriate limiting case of Biot's theory [23, 102]. Consequently, the energy partition results known from elasticity, in particular these obtained for the two-dimensional problem by Meleshko [82], can be recovered from the solutions obtained herein.

The energy budget considered consists of the energy transported by the P1 and P2-waves in both fluid and solid phases, and by the S-wave and Rayleigh wave in the solid phase (the absolute values of these average powers are often referred to as wave intensities). As will subsequently be discussed, the shear wave in the fluid phase, although excited, does not carry any energy as long as there is no energy flux associated with this wave; the contribution of the Rayleigh wave in the fluid phase is minuscule due to the particular choice of boundary conditions. It is important to stress that unlike the case of perfectly elastic solid in the fluid saturated porous solid the Rayleigh wave does not always exist [87]. The comparison of the energy partition results for the two different cases reveals that when the Rayleigh wave is absent, the P2-wave contribution to the energy budget becomes notably more significant, and even predominant.

4.1 Far-field interior solution in the absence of dissipation

Neglecting b in the governing equations, consider the idealized case of no dissipation. When viscous dissipation effects due to interphase interaction are ignored, phase velocities are purely real and the wave fields are undamped and non-dispersive.

Introducing polar coordinates

$$x = R\sin\theta,\ z = R\cos\theta,\ R = \sqrt{x^2 + z^2}, \tag{4.1}$$

the displacement fields can be expressed as follows,

$$u_{_R} = u_x \sin\theta + u_z \cos\theta, \quad u_\theta = u_x \cos\theta - u_z \sin\theta; \tag{4.2}$$

$$U_{_R} = U_x \sin\theta + U_z \cos\theta, \quad U_\theta = U_x \cos\theta - U_z \sin\theta; \tag{4.3}$$

in which case the inversion of the Fourier transform in (3.24) provides the solution for the above displacement fields in terms of 12 integrals of the type

$$I = \int_{-\infty}^{+\infty} \chi(p) \mathrm{e}^{Rq(p)} dp, \tag{4.4}$$

where $q(p) = ip \sin\theta - (p^2 - p_i^2)^{\frac{1}{2}} \cos\theta,\ i = 1, 2, s.$

Estimation of the above integral does not pose any mathematical difficulty owing to the classical asymptotic result by Miller & Pursey (1954),

$$I \sim \sqrt{\frac{2\pi p_i}{R}} \chi(-p_i \sin\theta) \exp\left[i\left(\frac{\pi}{4} - p_i R\right)\right] \cos\theta + O(R^{-\frac{3}{2}}),\ \ 0 \leq \theta < \frac{\pi}{2}, \tag{4.5}$$

as $R \to \infty$, see also Graff (1991).

Application of the steepest descent approximation (4.5) to (3.24) in polar coordinates provides the following expressions in the far-field,

$$\begin{aligned}
u_{_R}(R,\theta) &= \frac{Pc}{2\mu\omega}\sqrt{\frac{1}{2\pi R}}\left[p_1^{3/2}\mathcal{A}_{p1}(\theta)\exp\left(-ip_1R + i\frac{3\pi}{4}\right) + \right. \\
&\qquad \left. + p_2^{3/2}\mathcal{A}_{p2}(\theta)\exp\left(-ip_2R + i\frac{3\pi}{4}\right)\right] + O(R^{-\frac{3}{2}}), \\
u_\theta(R,\theta) &= \frac{Pc}{2\mu\omega}\sqrt{\frac{1}{2\pi R}}p_s^{5/2}\mathcal{A}_{sh}(\theta)\exp\left(-ip_sR + i\frac{\pi}{4}\right) + O(R^{-\frac{3}{2}}), \\
U_{_R}(R,\theta) &= \frac{Pc}{2\mu\omega}\sqrt{\frac{1}{2\pi R}}\left[p_1^{3/2}M_1\mathcal{A}_{p1}(\theta)\exp\left(-ip_1R + i\frac{3\pi}{4}\right) + \right. \\
&\qquad \left. + p_2^{3/2}M_2\mathcal{A}_{p2}(\theta)\exp\left(-ip_2R + i\frac{3\pi}{4}\right)\right] + O(R^{-\frac{3}{2}}), \\
U_\theta(R,\theta) &= \frac{Pc}{2\mu\omega}\sqrt{\frac{1}{2\pi R}}p_s^{5/2}M_s\mathcal{A}_{sh}(\theta)\exp\left(-ip_sR + i\frac{\pi}{4}\right) + O(R^{-\frac{3}{2}}),
\end{aligned} \tag{4.6}$$

where

$$\begin{aligned}
\mathcal{A}_{p1}(\theta) &= f(p_1\sin\theta)\frac{n_2\left(2p_1^2\sin^2\theta - p_s^2\right)\cos\theta}{F(p_1\sin\theta)}, \\
\mathcal{A}_{p2}(\theta) &= -f(p_2\sin\theta)\frac{n_1\left(2p_2^2\sin^2\theta - p_s^2\right)\cos\theta}{F(p_2\sin\theta)}, \\
\mathcal{A}_{sh}(\theta) &= -f(p_s\sin\theta)\frac{n_1\xi_2(p_s\sin\theta) - n_2\xi_1(p_s\sin\theta)}{F(p_s\sin\theta)}\sin(2\theta).
\end{aligned} \tag{4.7}$$

The direct substitution of expressions (4.6) into the constitutive relations in polar coordinates (see Appendix A) yields

$$\begin{aligned}
\sigma_{_R} &= -iP\sqrt{\frac{1}{2\pi R}}\left[m_1 p_1^{1/2}\mathcal{A}_{p1}(\theta)\exp\left(-ip_1R+i\frac{3\pi}{4}\right)+\right.\\
&\qquad\left.+\, m_2 p_2^{1/2}\mathcal{A}_{p2}(\theta)\exp\left(-ip_2R+i\frac{3\pi}{4}\right)\right]+O(R^{-\frac{3}{2}}),\\
\sigma_{R\theta} &= -\frac{iP}{2}\sqrt{\frac{1}{2\pi R}}p_s^{7/2}\mathcal{A}_{sh}(\theta)\exp\left(-ip_sR+i\frac{\pi}{4}\right)+O(R^{-\frac{3}{2}}),\\
s &= -iP\sqrt{\frac{1}{2\pi R}}\left[n_1 p_1^{1/2}\mathcal{A}_{p1}(\theta)\exp\left(-ip_1R+i\frac{3\pi}{4}\right)+\right.\\
&\qquad\left.+\, n_2 p_2^{1/2}\mathcal{A}_{p2}(\theta)\exp\left(-ip_2R+i\frac{3\pi}{4}\right)\right]+O(R^{-\frac{3}{2}}).
\end{aligned}\tag{4.8}$$

The asymptotic results (4.6) and (4.8) allow for the separation of P1, P2 and S motions along a cylindrical surface of sufficiently large radius R, i.e. the expressions u_θ, U_θ and $\sigma_{R\theta}$ represent the displacements of, and the stresses on, the solid in the shear wave, while $u_{_R}$, $U_{_R}$, $\sigma_{_R}$ and s represent a superposition of the longitudinal waves,

$$\begin{aligned}
u_{_R} &= u_{_R}^{p1}+u_{_R}^{p2}, \quad U_{_R} = U_{_R}^{p1}+U_{_R}^{p2};\\
\sigma_{_R} &= \sigma_{_R}^{p1}+\sigma_{_R}^{p2}, \qquad s = s^{p1}+s^{p2}.
\end{aligned}\tag{4.9}$$

It can be noted that the only difference between the expressions for the solid and fluid phases is the presence of the amplitude factors M_1, M_2 and M_s. Thus for example, for parameter set I, provided in table 4.1, these values are $M_1 = 1.091$, $M_2 = -8.262$, $M_s = -\gamma_{12}/\gamma_{22} = -0.009$. Unlike P1 motion, the P2-wave in the fluid exhibits amplitudes approximately eight times larger compared to those in the solid phase. Moreover, these two waves are out of phase in accord with predictions in (Biot 1956*a*). In this example the amplitude of the shear wave in the fluid phase is approximately two orders of magnitude smaller compared to that in the solid phase. In general $M_s < 0$, and thus these two waves are also out of phase in the far-field.

The absolute values of the functions $\mathcal{A}_{p1}(\theta)$, $\mathcal{A}_{p2}(\theta)$, $\mathcal{A}_{sh}(\theta)$ with $f(p) \equiv 1$ plotted versus polar angle $-\pi/2 < \theta < \pi/2$ are shown in Figure 4.1 (parameter set I, table 4.1). The radiation pattern of poroelastic P1 and S-waves appears very similar to that of purely elastic P and S-waves (Miller & Pursey 1954, Graff 1991).

4.2 Energy partition

As was mentioned above, the energy budget consists of the power transported by the P1 and P2-waves in both the fluid and solid phases, and by the S-wave and Rayleigh wave in

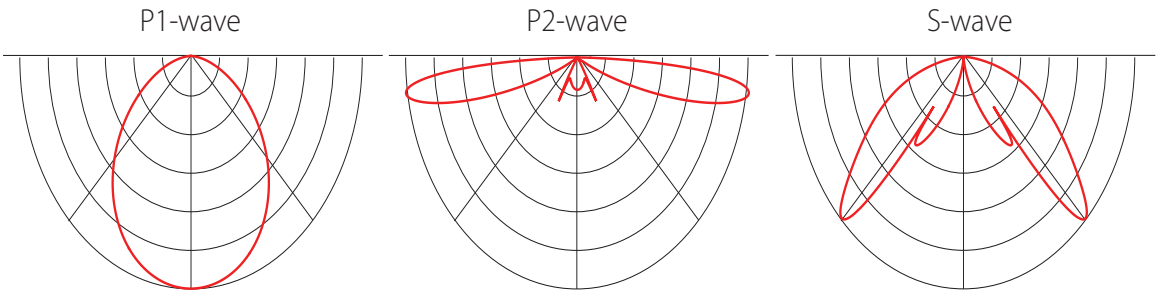

Figure 4.1: Directional diagrams (polar plots) of the far-field displacements $-\frac{\pi}{2} < \theta < \frac{\pi}{2}$.

the solid phase. The energy spent in generating the Rayleigh wave can be derived from the expression for the total power radiated by the source. In turn, the power flow through the cylindrical surface of large radius R can be represented as a superposition of power contributions due to the longitudinal and transverse waves. Consequently, the total power is represented in terms of power contributions due to longitudinal, transverse and Rayleigh waves.

4.2.1 Total power and Rayleigh wave contribution

For driving forces normal to the surface $z = 0$, the input source power W can be expressed as follows,

$$\langle P_z \rangle = \begin{cases} 0, & |x| > a; \\ \frac{1}{2}\omega P f(x) \mathrm{Im} u_z(x,0), & |x| \le a; \end{cases} \tag{4.10}$$

$$\langle W \rangle = \frac{c}{\omega} \int_{-a}^{a} \langle P_z \rangle \, dx = cP \int_{0}^{a} f(x) \mathrm{Im} u_z(x,0) dx, \tag{4.11}$$

where a is a nondimensional parameter related to c/ω, and according to (3.24) the expression for $u_z(x,0)$ is

$$u_z(x,0) = -\frac{cp_s^2 P}{4\pi\mu\omega} \int_{-\infty}^{+\infty} f(p) \frac{n_2\xi_1(p) - n_1\xi_2(p)}{F(p)} e^{ipx} dp. \tag{4.12}$$

Assuming the existence of the root of the Rayleigh equation, $F(p_r) = 0$, the imaginary

part of the principal value of the integral (4.12) can be represented as follows

$$\begin{aligned}\mathrm{Im}u_z(x,0) = -\frac{cp_s^2P}{2\pi\mu\omega}\int\limits_0^{\max(p_2,p_s)} f(p)\mathrm{Im}\left[\frac{n_2\xi_1(p)-n_1\xi_2(p)}{F(p)}\right]\cos(px)dp+ \\ +\frac{cp_s^2P}{2\pi\mu\omega}f(p_r)\mathrm{Im}\left[\pi i\frac{n_2\xi_1(p_r)-n_1\xi_2(p_r)}{F'(p_r)}\right]\cos(p_rx),\end{aligned} \tag{4.13}$$

where the latter residual term corresponds to the Rayleigh wave displacement. This allows the explicit separation of the power spent in the generation of the surface wave $\langle W_r^s\rangle$. The equations (4.11) and (4.13) yield

$$\langle W_r^s\rangle = \frac{c^2P^2p_s^2}{4\pi\mu\omega}\left[f(p_r)\right]^2\mathrm{Im}\left[\pi i\frac{n_2\xi_1(p_r)-n_1\xi_2(p_r)}{F'(p_r)}\right]. \tag{4.14}$$

Alternatively, in the absence of the Rayleigh pole, the residual term in (4.13) vanishes and $\langle W_r^s\rangle = 0$.

4.2.2 Longitudinal and shear waves contribution

In order to separate out the power spent in generation longitudinal and shear waves the total power flow through a cylindrical surface of sufficiently large radius R is considered,

$$\langle W_{cyl}\rangle = 2\int\limits_0^{\pi/2}\langle P_R\rangle\, Rd\theta, \tag{4.15}$$

$$\langle P_R\rangle = \frac{i\omega}{4}\left(\sigma_R u_R^* - \sigma_R^* u_R + \sigma_{R\theta}u_\theta^* - \sigma_{R\theta}^*u_\theta^* + sU_R^* - s^*U_R\right). \tag{4.16}$$

Taking into account (4.9) the radial component of the Poynting vector reads,

$$\begin{aligned}P_R &= -\sigma_R\dot{u}_R - \sigma_R\dot{u}_R - \sigma_{R\theta}\dot{u}_\theta - s\dot{U}_R = \\ &= -\left(\sigma_R^{p1}+\sigma_R^{p2}\right)\left(\dot{u}_R^{p1}+\dot{u}_R^{p2}\right) - \sigma_{R\theta}^s\dot{u}_\theta^s - \left(s^{p1}+s^{p2}\right)\left(\dot{U}_R^{p1}+\dot{U}_R^{p2}\right) = \\ &= -\sigma_R^{p1}\dot{u}_R^{p1} - \sigma_R^{p2}\dot{u}_R^{p2} - \sigma_{R\theta}^s\dot{u}_\theta^s - s^{p1}\dot{U}_R^{p1} - s^{p2}\dot{U}_R^{p2},\end{aligned} \tag{4.17}$$

where the upper index is introduced to denote the type of body wave. Fortunately, the remaining terms obtained by cross multiplication in (4.17) vanish,

$$-\sigma_R^{p1}\dot{u}_R^{p2} - \sigma_R^{p2}\dot{u}_R^{p1} - s^{p1}\dot{U}_R^{p2} - s^{p2}\dot{U}_R^{p1} = 0. \tag{4.18}$$

The above statement is based on the application of the following identities:

$$M_1 = -\frac{m_2}{n_2}, \quad M_2 = -\frac{m_1}{n_1}, \tag{4.19}$$

whose proof is more cumbersome than complicated (4.4). In particular, these identities give rise to the following relations for the longitudinal stresses and displacements in the far-field:

$$\sigma_R^{p1} u_R^{p2} + s^{p1} U_R^{p2} = 0, \quad \sigma_R^{p2} u_R^{p1} + s^{p2} U_R^{p1} = 0. \tag{4.20}$$

According to (4.17), the total average power flow in the interior consists of the power contributions spent in the generation of P1, P2 and S-waves in the solid phase, and power contributions spent in the generation of P1 and P2-waves in the fluid phase.

Finally, taking into account the power spent in the generation of the Rayleigh wave (4.14) one arrives at (upper index denotes either fluid or solid phase)

$$\langle W \rangle = \langle W_{cyl} \rangle + \langle W_r^s \rangle = \langle W_{p1}^s \rangle + \langle W_{p2}^s \rangle + \langle W_{p1}^f \rangle + \langle W_{p2}^f \rangle + \langle W_{sh}^s \rangle + \langle W_r^s \rangle, \tag{4.21}$$

where $\langle W_r^s \rangle$ is given by (4.14), and as follows from (4.6), (4.8) and (4.15)–(4.17),

$$\langle W_{p1}^s \rangle = \frac{c^2 P^2}{4\pi\mu\omega} p_1^2 m_1 \int_0^{\pi/2} \mathcal{A}_{p1}(p_1 \sin\theta) \mathcal{A}_{p1}^*(p_1 \sin\theta) d\theta, \tag{4.22}$$

$$\langle W_{p1}^f \rangle = \frac{c^2 P^2}{4\pi\mu\omega} p_1^2 n_1 M_1 \int_0^{\pi/2} \mathcal{A}_{p1}(p_1 \sin\theta) \mathcal{A}_{p1}^*(p_1 \sin\theta) d\theta, \tag{4.23}$$

$$\langle W_{p2}^s \rangle = \frac{c^2 P^2}{4\pi\mu\omega} p_2^2 m_2 \int_0^{\pi/2} \mathcal{A}_{p2}(p_2 \sin\theta) \mathcal{A}_{p2}^*(p_2 \sin\theta) d\theta, \tag{4.24}$$

$$\langle W_{p2}^f \rangle = \frac{c^2 P^2}{4\pi\mu\omega} p_2^2 n_2 M_2 \int_0^{\pi/2} \mathcal{A}_{p2}(p_2 \sin\theta) \mathcal{A}_{p2}^*(p_2 \sin\theta) d\theta, \tag{4.25}$$

$$\langle W_{sh}^s \rangle = \frac{c^2 P^2}{8\pi\mu\omega} p_s^6 \int_0^{\pi/2} \mathcal{A}_{sh}(p_s \sin\theta) \mathcal{A}_{sh}^*(p_s \sin\theta) d\theta. \tag{4.26}$$

In particular, the following identities hold for the average powers transported by longitudinal waves in terms of coefficients M_1 and M_2,

$$\frac{W_{p1}^s}{W_{p1}^f} = -\frac{M_2}{M_1}, \quad \frac{W_{p2}^s}{W_{p2}^f} = -\frac{M_1}{M_2}. \tag{4.27}$$

Table 4.1: Poromechanical parameters (GPa), reference phase densities ($\mathrm{kg\,m^{-3}}$); nondimensional slownesses and velocities ($\mathrm{m\,s^{-1}}$)

	λ	μ	Q	R	ρ_{11}	ρ_{12}	ρ_{22}
I	0.2493	0.2493	0.0672	0.0295	$1.9259{\cdot}10^3$	$-0.0019{\cdot}10^3$	$0.2151{\cdot}10^3$
II	0.2493	0.2493	0.0672	0.0295	$1.9259{\cdot}10^3$	$-0.1500{\cdot}10^3$	$0.2151{\cdot}10^3$
III	0.2493	0.2493	0	0	$1.9259{\cdot}10^3$	0	0

	p_1	p_2	p_s	p_r	c_1	c_2	c_s	c_r
I	1	2.074	1.815	2.081	653.358	315.005	359.788	313.918
II	0.975	2.401	1.902	–	721.930	293.156	369.974	–
III	1	–	1.732	1.884	623.168	–	359.786	330.788

Table 4.2: Energy partition results for load (i) (units $\omega Q^2/2\pi\mu$ and percentage)

	$\langle W^s_{p1}\rangle$	$\langle W^f_{p1}\rangle$	$\langle W^s_{p2}\rangle$	$\langle W^f_{p2}\rangle$	$\langle W^s_{sh}\rangle$	$\langle W^s_r\rangle$	$\langle W\rangle$
I	0.176	0.023	0.044	0.334	0.341	0.439	1.356
	13.0%	1.7%	3.3%	24.6%	25.1%	32.3%	100%
II	0.142	0.034	0.163	0.673	0.339	–	1.351
	10.5%	2.5%	12.1%	49.8%	25.1%	–	100%
III	0.258	–	–	–	0.334	0.576	1.169
	22.1%	–	–	–	28.6%	49.3%	100%

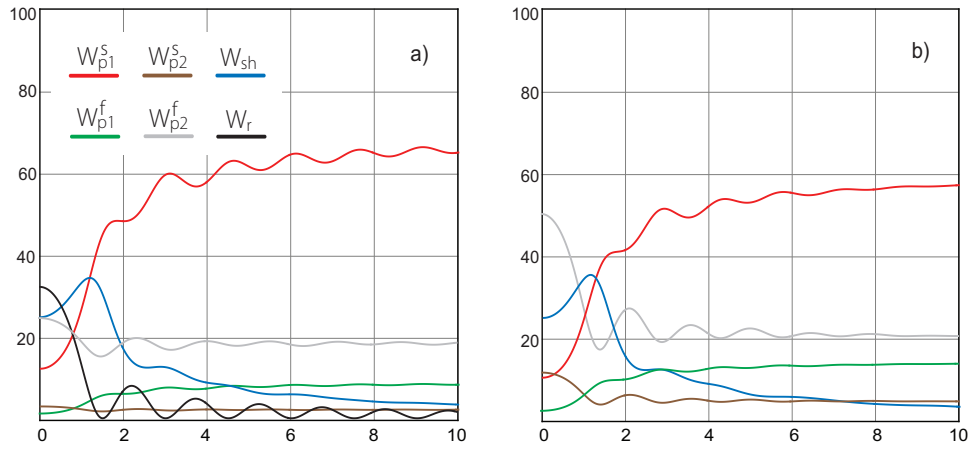

Figure 4.2: Energy partition results for load (ii) (percentage) versus distribution radius a; a) parameter set I; b) parameter set II.

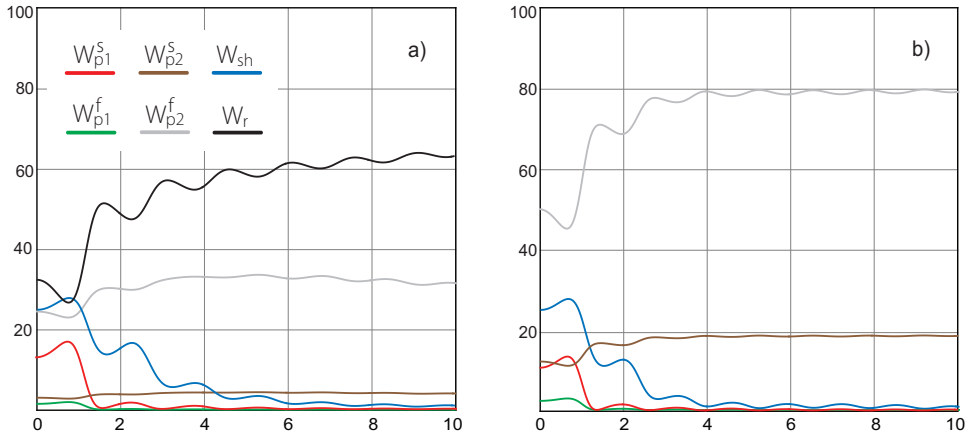

Figure 4.3: Energy partition results for load (iii) (percentage) versus distribution radius a; a) parameter set I, load (iii) with $p_0 = p_r$; b) parameter set II, load (iii) with $p_0 = p_2$.

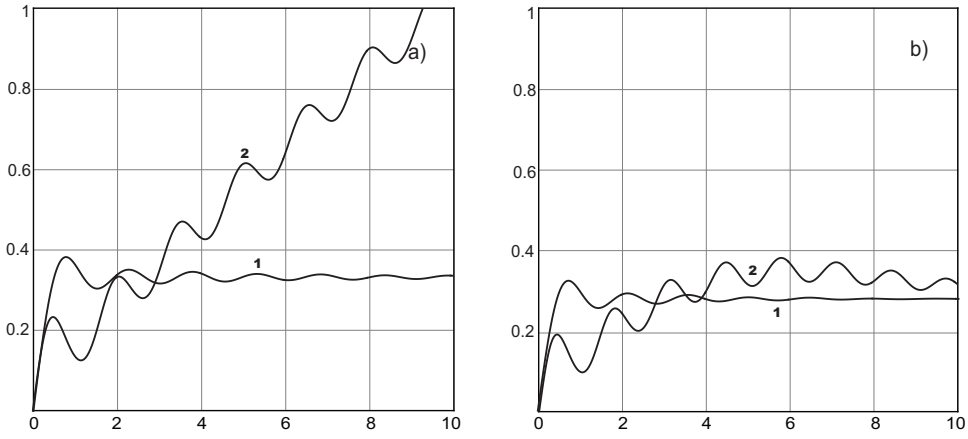

Figure 4.4: Specific source powers $\langle W \rangle / 2a$ (units $cp_s^2 P^2 / 2\pi\mu$) versus distribution radius a; a) parameter set I; b) parameter set II; curves 1 and 2 correspond to loads (ii) and (iii).

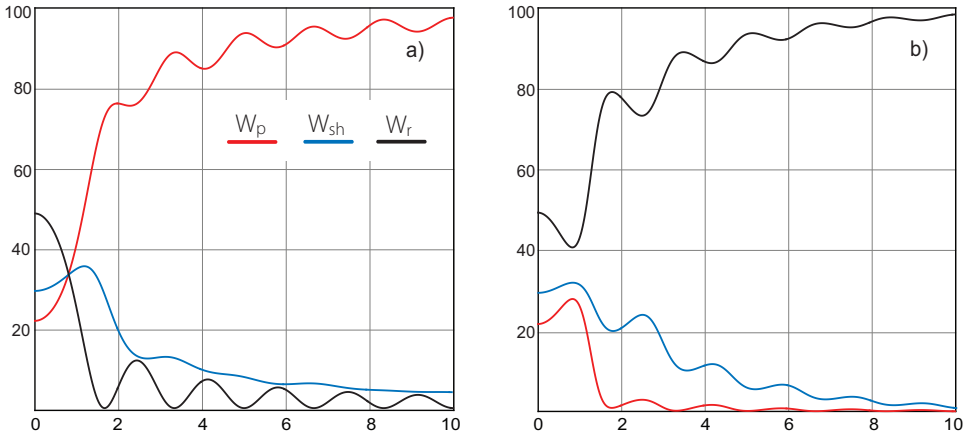

Figure 4.5: Energy partition results in the limiting case of perfectly elastic solid (percentage) versus distribution radius a; a) parameter set III, load (ii); b) parameter set III, load (iii) with $p_0 = p_r$.

4.2.3 Numerical examples

The energy partition results are presented for the three different parameter sets provided in table 4.1 and driving configurations (3.25). The choice of poromechanical parameters is mainly dictated by theoretical reasoning. This exemplifies the possible absence of the surface Rayleigh wave and allows the recovery of previously known results for purely elastic waves (Meleshko 1981) in the limiting case. Thus, parameter sets I and II cover the two possible situations in which the Rayleigh wave exists (I) or does not exist (II), while parameter set III corresponds to the limiting case of perfectly elastic media characterized by Poisson coefficient $\nu = 0.25$. In the latter case the P2 motion is not present and the energy is transported by means of longitudinal, shear and Rayleigh waves in which case (4.21) degenerates to

$$\langle W \rangle = \langle W_p \rangle + \langle W_{sh} \rangle + \langle W_r \rangle. \tag{4.28}$$

The action of the line source (load i) represents the limiting case of a uniform load (load ii). As $a \to 0$, $2acP/\omega \to Q$, where Q represents the force per unit length. The results for the energy partition according to (4.22)–(4.26) and (4.14) are summarized in table 4.2. The results for case I indicate that approximately 43% of the total power is transported by the longitudinal waves, 15% by the P1-wave and 28% by the P2-wave, 25% by the shear wave and 32% by the Rayleigh wave. The corresponding results for parameter set II suggest that approximately 75% of the source power is transported by longitudinal waves, 13% by the P1-wave and 62% by the P2-wave, and 25% by the shear wave. In the absence

of the Rayleigh wave the most significant fraction of the total energy, approximately 50%, is transported by the P2-wave in the fluid phase. The results for parameter set III recover the energy partition results for the perfectly elastic half-space, and these are in agreement with Meleshko (1981).

The energy partition results for parameter sets I and II in the case of distributed loads (ii) and (iii) are provided in figures 4.2 and 4.3 respectively. Note that in the case of load (iii) two different configurations are used, $p_0 = p_r$ for parameter set I (resonant excitation), and $p_0 = p_2$ for parameter set II. Figure 4.4 contains the corresponding specific powers, $\langle W \rangle / 2a$ (dimensional a). Finally, the results for distributed loads in the limit of a perfectly elastic medium (parameter set III) are provided in Figure 4.5, and again these are in agreement with Meleshko (1981).

4.3 Chapter Summary

The energy analysis of the wave motion in the two-dimensional Lamb's problem for non-dissipative poroelastic half-space is presented. These results obtained for both line and distributed surface loads cover two possible situations depending on whether the surface Rayleigh wave exists in the poroelastic half-space or not. The energy budget considered consists of the average powers transported by the longitudinal P1 and P2-waves in both fluid and solid phases, and by the S-wave and Rayleigh wave in solid phase. The shear wave and the Rayleigh wave although excited in the fluid phase do not contribute to the energy budget. The shear wave in the fluid phase has no corresponding energy flux and thus does not transfer energy as indicated by the expression for the radial component of the Poynting vector. The situation when the propagating wave carries no energy may seem somewhat paradoxical, however, this is only a consequence of the generally accepted idealization in macroscopic theories: each point in space is assumed to be co-occupied by both solid and fluid particles. Unlike the case of the shear wave, the Rayleigh wave in the fluid does transfer energy, however, the corresponding contribution into the energy budget is negligible. Indeed, since the amplitudes of the Rayleigh waves (in both fluid and solid phases) reach their maximum values at the surface $z = 0$ and exhibit exponential decay with depth, the corresponding energy fluxes through the cylindrical surface of sufficiently large radius R in the interior $z > 0$ provide only exponentially small contributions. While a significant portion of energy is only transfered along the surface, the free-pressure boundary condition (prescribed herein for simplicity) prevents the Rayleigh wave in the fluid from contributing to the energy budget.

The solution of the problem is based on the remarkable property of the Poynting vector that allows for the explicit separation of the energy fluxes due to contributing wave modes in the far-field. The validity of this result is not limited to the case of no dissipation and

can be proven to hold in the very general case of full frequency Biot's theory. Nevertheless, the approach to the energy partition originally established for elastic waves, and developed herein for poroelastic non-dissipative waves, can not be directly applied to the general case of Biot's theory. When viscoelastic interphase interaction is taken into account the energy fluxes through the cylindrical surface of large radius are minuscule, in which case the average energy balance equation merely states the equality between the energy entering the medium and the energy dissipated in the medium.

Most notably, the results for the energy partition indicate the following. The results for the line source (table 4.2) suggest that the most significant fraction of the energy is transported by the Rayleigh wave when it exists, and otherwise by the P2-wave in the fluid phase. On the other hand, both the relative intensities of the wave modes as well as the total power delivered by the source (Figure 4.4) change with the dimensions of the driving area. Thus, in the case of the uniform load (Figure 4.2), it is neither the Rayleigh wave nor the P2-wave in the fluid phase that is predominant as the radius a increases. As $a \to \infty$ the fraction of energy transported by the shear and the Rayleigh waves vanishes as long as this limiting case recovers the one-dimensional problem, in which case only longitudinal modes propagate. The distribution of the energy among the P1 and P2-waves is approximately 79% and 21% in case I, and 75% and 25% in case II. In the case of resonant excitation of the Rayleigh wave (Figure 4.3*a*) the results are similar to those for the perfectly elastic solid (Figure 4.5*b*). As a increases the fraction of energy transported by the Rayleigh wave tends to unity while the specific power grows unbounded (Figure 4.4*a*).

In the special case when the Rayleigh wave does not exist and the driving forces are in the form of a standing wave of P2 wavelength (Figure 4.3*b*) the P2-wave propagating in the fluid phase exhibits predominant behaviour, i.e. propagates with the greatest relative intensity for all possible radii a. Moreover, as the radius a increases, the sum of the fractions of the energy transported by the P2-waves in both fluid and solid phases approaches unity. At the same time, unlike the case of resonant excitation, the corresponding specific power has a tendency to decay (Figure 4.4*b*). This property has been observed with other numerical examples using different parameter sets.

Finally, the validity of the results has been verified in two different ways. First of all, the total average power radiated by the source (calculated independently) has been compared with the average powers transported by the corresponding wave modes, and secondly, the results have been shown to reproduce corresponding results for a perfectly elastic medium, in the appropriate asymptotic limit.

4.4 The proof of identities $M_1 = -m_2/n_2$ and $M_2 = -m_1/n_1$

With the above introduced definitions it is easy to see that each identity is equivalent to

$$q_{22}M_1M_2 + q_{12}\left(M_1 + M_2\right) + q_{11} = 0. \tag{4.29}$$

From the dispersion relation (3.10) according to Vieta's formula

$$z_1 + z_2 = \frac{q_{11}\gamma_{22} - 2q_{12}\gamma_{12} + q_{22}\gamma_{11} - ib\mathcal{F}/\omega\rho}{q_{11}q_{22} - q_{12}^2}, \tag{4.30}$$

$$z_1 z_2 = \frac{\gamma_{11}\gamma_{22} - \gamma_{12}^2 - ib\mathcal{F}/\omega\rho}{q_{11}q_{22} - q_{12}^2}, \tag{4.31}$$

and consequently (also noting $q_{11} + 2q_{12} + q_{22} = 1$),

$$M_1 + M_2 = \frac{1}{\Delta}\left[q_{22}\gamma_{11} - q_{11}\gamma_{22} + (q_{11} - q_{22})\theta\right], \tag{4.32}$$

$$\begin{aligned} M_1M_2 = \frac{1}{\Delta^2}\Big\{&\left[q_{22}\gamma_{11} - q_{12}\gamma_{12} - (q_{22} + q_{12})\theta\right]^2 \\ &- \left[q_{22}\gamma_{11} - q_{12}\gamma_{12} - (q_{22} + q_{12})\theta\right]\left(q_{11}\gamma_{22} - 2q_{12}\gamma_{12} + q_{22}\gamma_{11} - \theta\right) \\ &+ (q_{11}q_{22} - q_{12}^2)(\gamma_{11}\gamma_{22} - \gamma_{12}^2 - \theta)\Big\}, \end{aligned} \tag{4.33}$$

where

$$\Delta = q_{12}\gamma_{22} - q_{22}\gamma_{12} - (q_{22} + q_{12})\theta, \quad \theta = ib\mathcal{F}/\omega\rho. \tag{4.34}$$

Substitution of (4.32) and (4.33) into (4.29) leads to the required relation after a lengthy, though straightforward, calculation involving the use of identities $q_{11} + 2q_{12} + q_{22} = 1$ and $\gamma_{11} + 2\gamma_{12} + \gamma_{22} = 1$. The resulting relation finally simplifies to the obvious identity

$$(q_{11} + 2q_{12} + q_{22} - 1)\left[(q_{12} + q_{22})\theta + q_{12}\gamma_{12}\right] = 0. \tag{4.35}$$

Chapter 5

Poroelastic acoustic wavetrains

Realistic physical problems imply the existence of energy sources. Once this initial energy is supplied, mechanical waves travel through the medium transferring the provided energy away from the source. These mechanical waves are typically characterized by their wavelength, phase and group velocities. However, in linear dissipative media this description may not offer clear physical insight (e.g. complex group velocity commonly encountered in dissipative media is a quantity with no apparent physical meaning as further discussed in detail in Chapter 7). The common distinction between the near and the far field zones is somewhat artificial in the case of exponentially decaying waves since these waves cannot transfer energy over arbitrarily long distances. As will be discussed further in Chapter 8, the distance over which the energy transferred by the wave falls off significantly can be characterized by the energy damping length. Therefore, in dissipative media it is often the wave processes in the near field that provide physically meaningful information. However, the wave processes in the near field are not completely understood, due to obvious mathematical difficulties in contrast to the far field solutions where asymptotic approximations can commonly be established (e.g. in the case of perfectly elastic media there is no qualitative description of the waves in the near field, while the far field solutions has been known for more than a century [75]). In the following the structure of the wave field is analyzed in detail. Most notably it is demonstrated that poroelastic mechanical waves observed in the near field cannot be described by their fixed wavelengths and phase velocities but rather propagate in the form of wavetrains which represent the superposition of spectrum components within certain wavelength and attenuation bands.

A two-dimensional boundary value problem for a porous half-space with an open boundary in the context of Biot's theory of poroelasticity is considered. Using complex analysis techniques, a general solution is represented as a superposition of contributions from the four different types of motion corresponding to P1, P2, S and Rayleigh waves. Far field asymptotic solutions for the bulk modes, as well as near field numerical results are investi-

gated. Most notably, this analysis reveals the following: (i) a line traction generates three wavetrains corresponding to the bulk modes, so that P1, P2 and S modes emerge from corresponding wavetrains at a certain distance from the source; (ii) bulk modes propagating along the plane boundary are subjected to geometric attenuation, which is found quantitavely to be $x^{-3/2}$, similar to the classical results in perfect elasticity theory; (iii) the Rayleigh wave is found to be predominant at the surface in both the near (due to the negation of the P1 and S wavetrains) and the far field (due to geometric attenuation of the bulk modes); (iv) the recovery of the transition to the classical perfect elasticity asymptotic results validates the asymptotics established herein.

Boundary value problems for a poroelastic half-space in the framework of Biot's theory have been studied extensively. In particular, the poroelastic Lamb's problem, the counterpart of the Lamb's problem in perfect elasticity (Lamb 1904 [75]), was considered in [102, 118, 96, 42, 68, 95, 46, 87, 88]. The solutions for the case of axial symmetry was discussed in the works of Halpern & Christiano [68], Seimov *et al.* [102] and Molotkov [87, 88]. A closed form Cagniard solution [2] was derived for the transient response problems in the high frequency limit in the work of Paul [95] and, for the case of fluid/porous solid interface, by Feng & Johnson [46]. Surface, or poroelastic Rayleigh waves were studied extensively in a series of works by Deresiewicz, e.g. [39]; results for the fluid–porous interface can be found in the works of Feng & Johnson [46] (high frequency limit) and Gubaidullin *et al.* [66] (general case). Purely numerical results can be found, for example, in the works of Mesgouez *et al.* [83] (finite element formulation) and Schanz & Struckmeier [101] (boundary element formulation). Asymptotic results for the contact stresses can be found in the work of Gomilko *et al.* [60]. It is important to distinguish between viscous attenuation due to the viscous interphase interaction and geometric attenuation along a plane boundary. Physically, waves propagating along the plane boundary of the porous half-space consist of superimposed bulk modes (P1, P2 and S-waves) and a surface mode, or poroelastic Rayleigh wave (Deresiewicz & Rice 1962, Seimov *et al.* 1990). While in the presence of dissipation all the waves in porous media exhibit viscous attenuation, it is logical to assume that, similarly to the perfectly elastic case (Lamb 1904 [75]), porous bulk modes will also exhibit geometric attenuation. Unlike the previous studies, the primary aim of the present work is to carry out an in-depth analysis of the comparative contribution of each of the four wave types to general response. Consequently, analysis of the resulting expressions will allow the characterization of the geometric attenuation of the bulk modes in a quantitative manner.

In the present work a two-dimensional boundary value problem for a porous half-space, described by the widely recognized Biot's equations of poroelasticity is considered. In this poroelastic version of Lamb's problem, the surface of a porous half-space is subjected to a prescribed line traction. A formal analytical solution of the problem is obtained in Chapter 3 by the application of Helmholtz potential decomposition. Analysis of the formal solution

based on branch cut integration in the complex slowness plane allows the representation of the response at the surface as a superposition of three wavetrains, each containing P1, P2, S-wave, and Rayleigh wave. While the Rayleigh wave contribution is found in the closed form of a residue, the solution for the three bulk wavetrains is given in the form of well behaved integrals for which far field asymptotic results are obtained. The properties of the bulk and surface modes propagating along the surface are subsequently discussed in detail.

5.1 Harmonic line traction. Formal solution

Consider a poroelastic half-space with an open boundary occupying the region $z > 0$ under the action of the harmonic line source. The boundary conditions can thus be represented as follows,

$$\sigma_{zz}(x,0,t) = -P\delta(x)e^{i\omega t},\ \sigma_{xz}(x,0,t) = s(x,0,t) = 0, \tag{5.1}$$

where P now has dimensions N/m unlike the case of distributed source, where P [N/m^2].

In this case Fourier solutions for the displacement fields are provided in Chapter 3, see (3.24) with $f(x) = \delta(x)$. In particular, consider in detail the expressions for the vertical displacements u_z, U_z at the surface $z = 0$, and the pore pressure $p_f = -s/\phi$ in the interior of the domain $z > 0$,

$$u_z(x,0,\omega) = \frac{P}{2\pi\mu}\int_0^\infty p_s^2 \frac{n_2\xi_1(p) - n_1\xi_2(p)}{F(p,\omega)}\cos(px)dp, \tag{5.2}$$

$$\begin{aligned} U_z(x,0,\omega) = &-\frac{P}{2\pi\mu}\int_0^\infty \frac{1}{F(p,\omega)}\{\, n_2\xi_1(p)\left[2p^2(M_1+M_3) - M_1p_s^2\right] - \\ &-n_1\xi_2(p)\left[2p^2(M_2+M_3) - M_2p_s^2\right]\,\}\cos(px)dp, \end{aligned} \tag{5.3}$$

$$p_f(x,z,\omega) = -\frac{P}{2\pi\phi\mu}\int_0^\infty \frac{2p^2 - p_s^2}{F(p,\omega)} n_1n_2\left[e^{-z\xi_1(p)} - e^{-z\xi_2(p)}\right]\cos(px)dp, \tag{5.4}$$

where $\xi_i(p) = (p^2 - p_i^2)^{1/2}$, $i = 1, 2, s$ and $F(p,\omega)$ is the Rayleigh equation (3.23). Without loss of generality, the time dependence factor $\exp(i\omega t)$ is omitted in (5.2)–(5.4) and this allows the representation of the solutions in the form of a cosine Fourier transform.

The above multivalued integrals represent the formal solution of the problem. The evaluation must be carried out taking into account far field conditions $\mathrm{Re}\,\xi_1 > 0$, $\mathrm{Re}\,\xi_2 > 0$, $\mathrm{Re}\,\xi_3 > 0$, in order to define the values of the integral unambiguously. The radiation condition also implies that the line source is the only source of energy in the system. In

other words these requirements can be satisfied if every wave in set (5.2)–(5.4) is either inhomogeneous (exponentially decaying with depth), or is a traveling wave propagating away from the source. Hence, it is inferred that

$$\xi_i(p) = \sqrt{p^2 - p_i^2},\ |\xi| > p_i; \quad \xi_i(p) = i\sqrt{p_i^2 - p^2},\ |\xi| < p_i. \tag{5.5}$$

Moreover, as was pointed out by Lamb [75] for an analogous problem in elasticity theory, the treatment of the integrals of the type (5.2)–(5.4) in the principal value sense may appear inconsistent with the physics of the problem. This is because an arbitrary standing Rayleigh wave satisfying the null-stress boundary conditions can be added to the solution. These standing waves do not carry energy and therefore must be excluded by the radiation condition.

While straightforward numerical evaluation of the integral (5.4) does not encounter any computational difficulty as the integrand decays exponentially for large values of p, evaluation of the expressions (5.2) and (5.3) requires special care for sufficiently large values of x, as these results are represented in the form of slowly decaying and highly oscillating, though convergent integrals when $x \neq 0$. At the point $x = 0$, where the traction is applied, an integrable singularity is present, which disappears, for example, in the case of the uniformly distributed stripe load. The asymptotic behavior of the integrands in (5.2), (5.3) is of the form $\cos(px)/\mathrm{p}$ as $p \to \infty$, and therefore, the convergence of the above integrals follows from the convergence of the integral cosine function $Ci(x)$ (e.g. Abramovich & Stegun [1]).

Alternatively, the numerical evaluation of the above integrals can be conducted using branch cut integration considered further in Section 5.3.1, in which case, the resulting integrals along the hyperbolic branch cuts pose no computational difficulties. On the other hand, the results of the numerical integration obtained for moderate values of x (where the convergence is still satisfactory) may serve as a test for the branch cut integration. Despite of the above mentioned disadvantages of the numerical approach, including slow convergence and the error introduced while bounding an improper integral, both approaches have been confirmed to yield matching results for the x values employed herein.

5.2 Numerical example

Numerical results for the vertical solid and fluid displacements according to (5.2)–(5.4) are presented in Figures 5.1–5.3 for the case of water saturated Berea sandstone (Table 5.1). The following dimensional frequencies are used in calculations: $f = f_c,\ 10f_c,\ 100f_c$, where characteristic frequency f_c is defined following [12]

$$f_c = \frac{b}{2\pi\rho(\gamma_{12} + \gamma_{22})}. \tag{5.6}$$

Table 5.1: Physical properties of the porous material (Berea sandstone) and saturating fluid (water).

Porosity	ϕ	0.20
Permeability (mD)	K	360.00
Tortuosity	a	2.40
Structural factor[1]	δ	2.83
Frame bulk modulus (GPa)	K_b	10.37
Shear modulus (GPa)	μ	7.02
Grain bulk modulus (GPa)	K_s	36.50
Liquid bulk modulus (GPa)	K_f	2.25
Solid density (kg/m^3)	ρ_s	2644.00
Liquid density (kg/m^3)	ρ_f	1000.00
Liquid viscosity (mPa·s)	η_f	1.00
P1-wave phase velocity (m/s)	V_{p1}^{∞}	3268.37
P2-wave phase velocity (m/s)	V_{p2}^{∞}	793.10
S-wave phase velocity (m/s)	V_s^{∞}	1772.27
Characteristic frequency (kHz)	f_c	6.07
Characteristic velocity (m/s)	c	3260.40

Biot parameters (GPa)				Phase densities (kg/m^3)		
λ	μ	Q	R	ρ_{11}	ρ_{12}	ρ_{22}
8.224	7.020	0.982	0.380	2415.2	-300	500

Table 5.2: Nondimensional slownesses p_i, $i = 1, 2, s, R$ at different typical frequencies f (Rayleigh wave cut-off frequency $f \approx 2450 f_c$).

	p_1	p_2	p_s	p_R
$f = f_c$	0.998–7.444i$\times 10^{-4}$	4.449–0.823i	1.847–9.52i$\times 10^{-3}$	2.001–0.024i
$f = 10 f_c$	0.998–1.861i$\times 10^{-4}$	4.241–0.164i	1.842–2.314i$\times 10^{-3}$	1.995–0.019i
$f = 100 f_c$	0.998–5.521i$\times 10^{-5}$	4.152–0.045i	1.840–6.814i$\times 10^{-4}$	1.993–0.018i
$f = 2449 f_c$	0.998–1.089i$\times 10^{-5}$	4.118–8.670i$\times 10^{-3}$	1.840–1.340i$\times 10^{-4}$	1.993–0.018i
$f = 2450 f_c$	0.998–1.089i$\times 10^{-5}$	4.118–8.668i$\times 10^{-3}$	1.840–1.340i$\times 10^{-4}$	–

Table 5.3: Wavelengths λ_i, $i = 1, 2, s, R$ at different typical frequencies f.

	λ_1 [m]	λ_2 [m]	λ_s [m]	λ_R [m]
$f = f_c$	5.38×10^{-1}	1.21×10^{-1}	2.91×10^{-1}	2.68×10^{-1}
$f = 10f_c$	5.38×10^{-2}	1.27×10^{-2}	2.92×10^{-2}	2.69×10^{-2}
$f = 100f_c$	5.38×10^{-3}	1.29×10^{-3}	2.92×10^{-3}	2.70×10^{-3}
$f = 2449f_c$	2.20×10^{-4}	5.33×10^{-5}	1.19×10^{-4}	1.10×10^{-4}
$f = 2450f_c$	2.20×10^{-4}	5.32×10^{-5}	1.19×10^{-4}	–

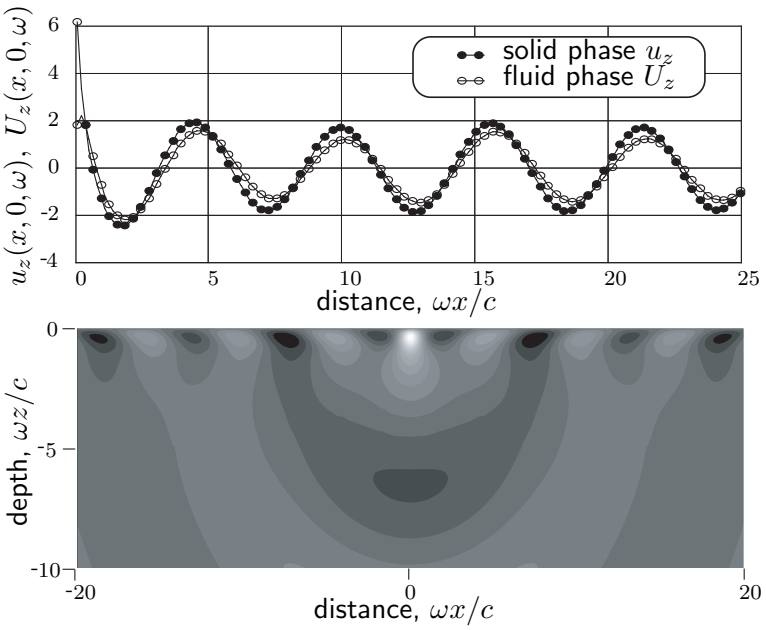

Figure 5.1: Normalized fluid and solid displacements at the surface and pressure contour plots in the interior. Source frequency $f = f_c$.

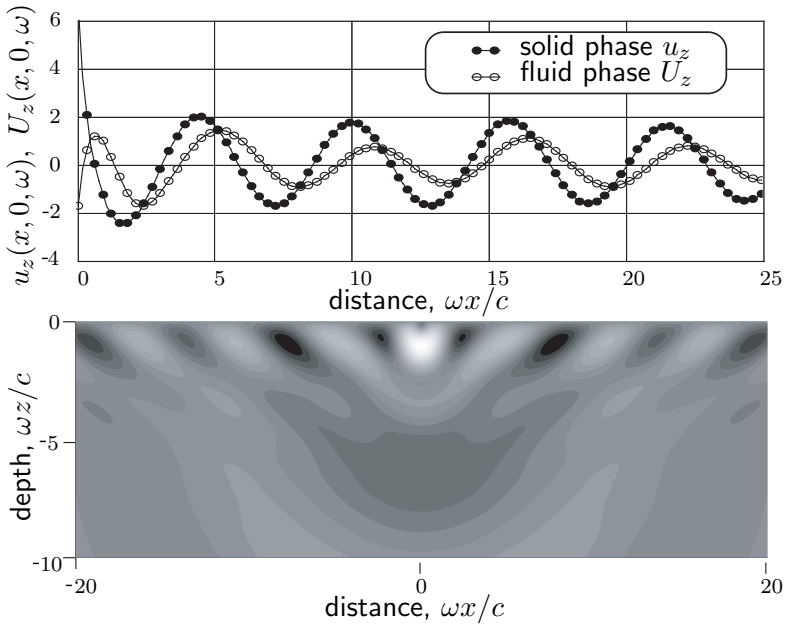

Figure 5.2: Normalized fluid and solid displacements at the surface and pore pressure contour plots in the interior. Source frequency $f = 10f_c$.

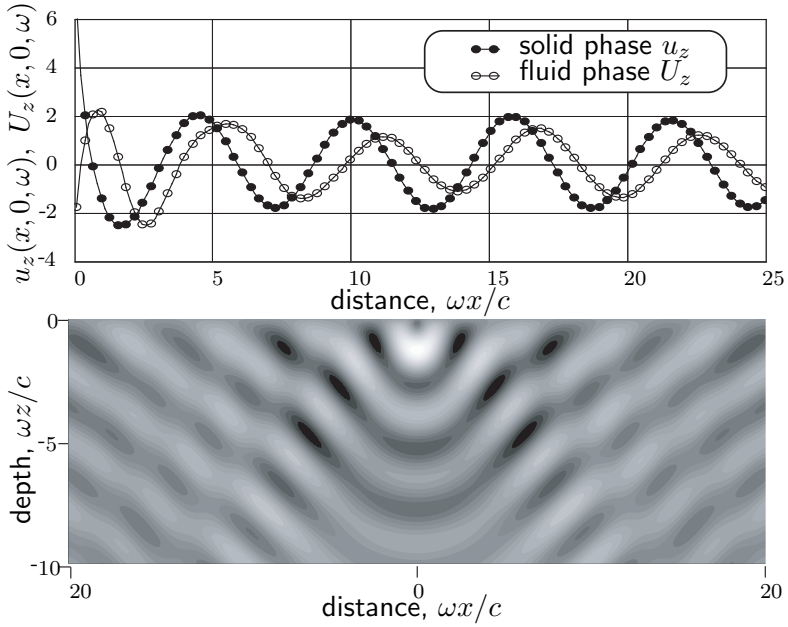

Figure 5.3: Normalized fluid and solid displacements at the surface and pressure contour plots in the interior. Source frequency $f = 100f_c$.

Further decrease or increase of the source frequency gives results similar to Figure 5.1 and Figure 5.3 respectively.

Numerical results shown in Figures 5.1–5.3 illustrate the influence of the source frequency on the character of the spatial oscillations in both displacements and pore pressure. For relatively low frequencies displacements are observed to be almost in phase, with approximately the same amplitudes (see Figure 5.1), while an increase of the source frequency leads to a weakening of the viscous coupling effect and, as a consequence, solid and fluid displacements can be of different amplitude and phase (Figures 5.1 and 5.3), or in fact nearly out of phase in the high frequency range for certain materials. Indeed, as follows from the governing equations, in the case when the characteristic frequency lies near unity, the inertia and viscous terms are approximately of the same order [12], so that an increase of the source frequency makes inertia terms dominant over viscous terms.

These numerical results results are only the first step and included to illustrate the response at different frequencies. A more intriguing task is to decompose the obtained general solution into components related to the four different waves types. This can be achieved by means of contour integration in the upper complex slowness half-plane, in which case the numerical results obtained for moderate values of x and presented in Figures 5.1–5.3 serve as a benchmark solution.

5.3 Wavetrains excited by harmonic tractions

5.3.1 Branch cut integration

The integrands in (5.2), (5.3), (5.4) contain six branch points located at $p = \pm\beta_1$, $\pm\beta_2$, $\pm\beta_3$, such that $\mathrm{Im}(\beta_i) \neq 0$, when $\omega \neq 0$; and two poles at $p = \pm p_R$, $\mathrm{Re}(p_R) > 0$, satisfying $F(p_R, \omega) = 0$, which correspond to the Rayleigh wave contribution. The necessary hyperbolic branch cuts (see figure 5.4) in the complex p-plane ($p = \zeta + i\eta$) can be selected according to

$$\zeta^2 - \eta^2 - \alpha_i^2 + \lambda_i^2 \leq 0,\ \zeta\eta + \alpha_i\lambda_i = 0,\ i = 1, 2, s, \tag{5.7}$$

where $\alpha_i = \mathrm{Re}(\beta_i)$, $\lambda_i = -\mathrm{Im}(\beta_i) > 0$ (discussion of hyperbolic branch cuts can be found e.g. in [64, 65]).

Consider in detail, for example, the integral expression for the solid phase vertical displacement component u_z (5.2),

$$u_z(x, 0, t, \omega) = \frac{Pce^{i\omega t}}{4\pi\mu\omega} p_s^2 \int_{-\infty}^{+\infty} \frac{n_2\xi_1(p) - n_1\xi_2(p)}{F(p, \omega)} e^{ipx} dp \tag{5.8}$$

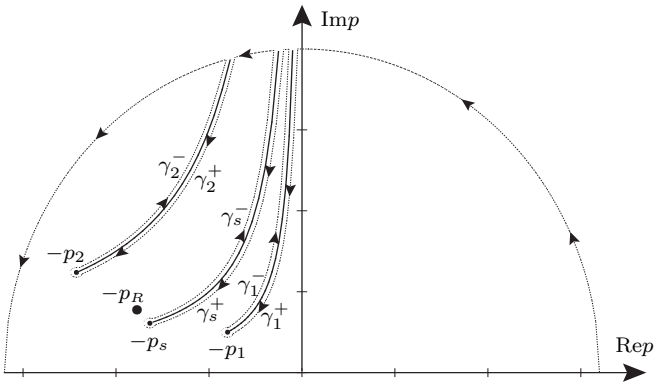

Figure 5.4: Hyperbolic branch cuts, branch points $p = \pm p_i$ $(i = 1, 2, s)$, Rayleigh pole $p = -p_R$ in the complex p-plane (upper half-plane closure for $x > 0$)

Conducting contour integration according to the scheme shown in figure 5.4 we note that for $x > 0$ the contour is closed in the upper half-plane, while for $x < 0$ one should consider the lower half-plane. Because the contribution of the integral along the semicircle of infinite radius vanishes according to Jordan's lemma, the above integral can be represented symbolically as follows,

$$\int_{-\infty}^{+\infty} = 2\pi i \text{Res} - \oint_{\gamma_1^+} - \oint_{\gamma_1^-} - \oint_{\gamma_2^+} - \oint_{\gamma_2^-} - \oint_{\gamma_3^+} - \oint_{\gamma_3^-}, \tag{5.9}$$

where the Rayleigh pole, $p = -p_R$, always has a positive imaginary part when $\omega \neq 0$, and the values of the radicals along $\gamma_1^{\pm}$, $\gamma_2^{\pm}$, $\gamma_3^{\pm}$ are prescribed uniquely according to the far field conditions as follows: $\xi_i(p) = \sqrt{p^2 - \beta_i^2}$ along γ_i^+ and $\xi_i(p) = -\sqrt{p^2 - \beta_i^2}$ along γ_i^-.

Introducing the parameterization

$$\begin{aligned} p_1(\tau) &= \tau - i\alpha_1\lambda_1/\tau, \\ p_2(\tau) &= \tau - i\alpha_2\lambda_2/\tau, \\ p_s(\tau) &= \tau - i\alpha_s\lambda_s/\tau \end{aligned} \tag{5.10}$$

one arrives at $(\gamma_i = \gamma_i^- + \gamma_i^+)$

$$\int_{-\infty}^{+\infty} = 2\pi i \text{Res} - \oint_{\gamma_1} - \oint_{\gamma_2} - \oint_{\gamma_s}, \tag{5.11}$$

where the residue and three contour integrals can be found as

$$\mathrm{Res} = \frac{n_2\xi_1(p_R) - n_1\xi_2(p_R)}{F'(p_R,\omega)} e^{-ip_R x}, \tag{5.12}$$

$$\oint_{\gamma_1} = \int_0^{-\alpha_1} \left[\frac{n_2\xi_1(p_1) - n_1\xi_2(p_1)}{F(p_1,\omega)} + \frac{n_2\xi_1(p_1) + n_1\xi_2(p_1)}{F_1(p_1,\omega)} \right] \frac{dp_1}{d\tau}\ e^{ip_1 x} d\tau, \tag{5.13}$$

$$\oint_{\gamma_2} = \int_0^{-\alpha_2} \left[\frac{n_2\xi_1(p_2) - n_1\xi_2(p_2)}{F(p_2,\omega)} - \frac{n_2\xi_1(p_2) + n_1\xi_2(p_2)}{F_2(p_2,\omega)} \right] \frac{dp_2}{d\tau}\ e^{ip_2 x} d\tau, \tag{5.14}$$

$$\oint_{\gamma_s} = \int_0^{-\alpha_s} \left[\frac{n_2\xi_1(p_s) - n_1\xi_2(p_s)}{F(p_s,\omega)} - \frac{n_2\xi_1(p_1) - n_1\xi_2(p_3)}{F_s(p_s,\omega)} \right] \frac{dp_3}{d\tau}\ e^{ip_3 x} d\tau, \tag{5.15}$$

where

$$\begin{aligned} F_1(p,\omega) &= \left(2p^2 - p_s^2\right)\left[n_1\left(p^2 - m_2\right) - n_2(p^2 - m_1)\right] - 2p^2\xi_s\left(n_1\xi_2 + n_2\xi_1\right), \\ F_2(p,\omega) &= \left(2p^2 - p_s^2\right)\left[n_1\left(p^2 - m_2\right) - n_2(p^2 - m_1)\right] + 2p^2\xi_s\left(n_1\xi_2 + n_2\xi_1\right), \\ F_s(p,\omega) &= \left(2p^2 - p_s^2\right)\left[n_1\left(p^2 - m_2\right) - n_2(p^2 - m_1)\right] + 2p^2\xi_s\left(n_1\xi_2 - n_2\xi_1\right). \end{aligned} \tag{5.16}$$

Now the solution for u_z (5.2) is represented in the form of a sum of contributions of three wavetrains (5.13)–(5.15), and the contribution of the Rayleigh wave (5.12). The location of the pole (p_R) should be first found numerically to evaluate an expression for the residue. Summarizing the results obtained with the branch cut integration one can write the following decomposition for the displacement field:

$$\int_{-\infty}^{+\infty} f(p) \frac{n_2\xi_1(p) - n_1\xi_2(p)}{F(p,\omega)} e^{ipx} dp = \Lambda_1 + \Lambda_2 + \Lambda_s + 2\pi i \mathrm{Res}, \tag{5.17}$$

where Λ_1, Λ_2 and Λ_s are the expressions of the type (5.13)–(5.15) taken with opposite sign, and the residual term $2\pi i$Res corresponds to the contribution of the Rayleigh wave (5.12).

Similarly, representations in the form (5.17) can be derived for the rest of the components (though these cumbersome expressions are not provided explicitly, the results for the fluid phase U_z will be used further for numerical evaluation). Integrals of the type (5.13)–(5.15) pose no computational difficulties for numerical evaluation as their integrands do not contain any singularities, the integration path is limited, and the integrands take zero

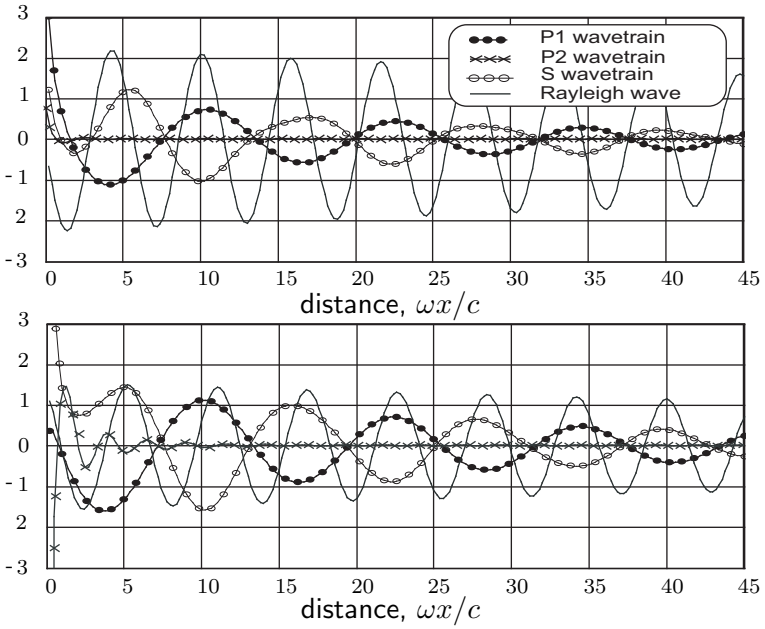

Figure 5.5: Contributions from different wave types. Solid phase displacement decomposition (upper panel), fluid phase displacement decomposition (lower panel). Source frequency $f = 100 f_c$ deliberately high to emphasize P2-wave contribution.

values at the endpoints. Numerical results illustrating the above introduced decomposition are presented in Figure 5.5 for dimensional frequency $f = 100 f_c$.

Each wavetrain (5.13)–(5.15) represents the waves propagating with the phase slownesses and attenuations in the range $[-\alpha_i, 0]$, $[\lambda_i, \infty)$, respectively. Thus, each wavetrain contains P1, P2 and S-waves as well as the waves which propagate faster and attenuate at a faster rate than corresponding modes. Consequently, at a certain distance from the source one can expect solely P1, P2 and S modes along with the Rayleigh wave.

While detailed discussion of the above results will follow in Section 5.4, we will next pursue the asymptotic analysis of integrals of the type (5.13)–(5.15). The evolution of the wavetrains in the far field, and the emergence of the P1, P2 and S-waves will be subsequently discussed in the following section, where asymptotic results for each wavetrain are sought.

5.3.2 Asymptotic solutions

Integrals of the type (5.13)–(5.15)

$$\Lambda_i = -\int_0^{-\alpha_i} F(\tau)\, e^{ip_i x} d\tau = -\int_0^{-\alpha_i} F(\tau)\, e^{i\tau x} e^{\alpha_i \lambda_i x/\tau} d\tau, \tag{5.18}$$

with an appropriate change of variable $\hat{\tau} = -\lambda_i - \alpha_i \lambda_i / \tau$, can be approximated by the following model integral for sufficiently large x:

$$\Lambda_i \approx \alpha_i \lambda_i e^{-i\alpha_i x} e^{-\lambda_i x} \int_0^{\infty} \frac{\hat{F}(\hat{\tau})}{(\hat{\tau} + \lambda_i)^2} e^{i\frac{\alpha_i}{\lambda_i} x\hat{\tau}} e^{-x\hat{\tau}} d\hat{\tau}, \tag{5.19}$$

where the oscillatory term in (5.19) is approximated by the first two terms in the expansion of the expression $\alpha_i \lambda_i / (\hat{\tau} + \alpha_i) \approx \alpha_i - \alpha_i \hat{\tau} / \lambda_i + O(\hat{\tau}^2)$ around $\hat{\tau} = 0$.

The integral in the expression (5.19) is an oscillating Laplace-type integral of the form (5.33), discussed in detail further in Section 5.5 [equation (5.35)], and satisfies the conditions of Watson's lemma reformulated for this particular type of integral. An expression for the leading order term follows the general asymptotic expansion (5.35) for sufficiently large x,

$$I_i(x) \sim a_{0,i} \frac{\Gamma(\gamma+1)}{x^{\gamma+1}} \exp\left[i(\gamma+1) \arctan\left(\frac{\alpha_i}{\lambda_i}\right)\right] \left(1 + \frac{\alpha_i^2}{\lambda_i^2}\right)^{-\frac{\gamma+1}{2}}, \tag{5.20}$$

where in order to determine the unknowns γ and a_0 it is necessary to investigate the asymptotic behavior of the function $\hat{F}(\hat{\tau})$ as $\hat{\tau} \to 0^+$, or in other words, the behavior of the integrands (5.13)–(5.15) as $\tau \to -\alpha_i$.

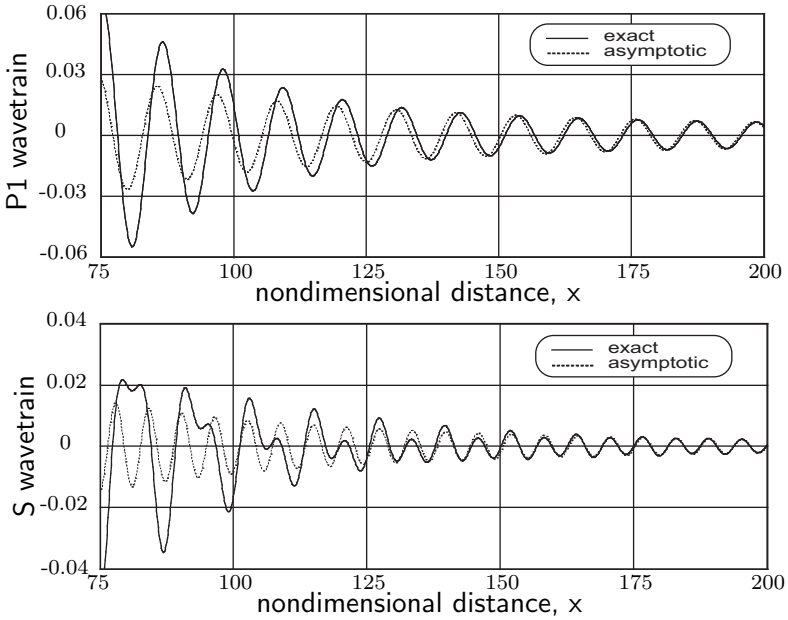

Figure 5.6: P1 and S wavetrains at certain distance from the source (P1 and S-waves emerging from corresponding wavetrains). Exact and asymptotic solutions for the vertical solid displacement field. Source frequency $f = f_c$.

It is easy to see that simple manipulations with the integrands allow the factoring out of the terms $\xi_i(p_i)$ which completely determine the asymptotic behaviour as $\tau \to -\alpha_i$. For example, in (5.13), the expression in the square brackets equals

$$\frac{2n_2\xi_1(p_1)\left(2p_1^2-\beta_3^2\right)\left[n_1\left(p_1^2-m_2\right)-n_2(p_1^2-m_1)\right]}{F(p_1,\omega)F_1(p_1,\omega)}. \tag{5.21}$$

The factor $\xi_i(p_i)$ in some vicinity of $\tau = -\alpha_i$ can be approximated by

$$\begin{aligned}\xi_i(p_i) &= \frac{i}{|\tau|}\sqrt{(\alpha_i-\tau)(\lambda_i^2+\tau^2)}\sqrt{\tau+\alpha_i} \\ &\approx i\sqrt{2\alpha_i\left(1+\frac{\lambda_i^2}{\alpha_i^2}\right)}\sqrt{\tau+\alpha_i},\end{aligned} \tag{5.22}$$

or in terms of $\hat{\tau}$ as

$$\xi_i(p_i) \approx i\sqrt{2\alpha_i\left(1+\frac{\lambda_i^2}{\alpha_i^2}\right)}\sqrt{\frac{\alpha_i\hat{\tau}}{\lambda_i}}. \tag{5.23}$$

Taking into account the above considerations according to (5.19) and (5.20) the asymptotic results for all three integrals (5.13)–(5.15) can be summarized as follows,

$$\Lambda_i \sim i\mathcal{A}_i\sqrt{2\alpha_i}\left(\frac{\alpha_i^2}{\alpha_i^2+\lambda_i^2}\right)^{\frac{1}{4}}\frac{\Gamma(3/2)}{x^{3/2}}\exp\left[ip_i(-\alpha_i)x\right]\exp\left[\frac{3i}{2}\arctan\left(\frac{\alpha_i^2}{\lambda_i^2}\right)\right]\left(1+i\frac{\lambda_i}{\alpha_i}\right). \tag{5.24}$$

It is convenient to introduce an upper index to denote the phase, while lower index corresponds to the wave type. Thus $\mathcal{A}_i^F$ and $\mathcal{A}_i^S$ will denote the value of coefficient $\mathcal{A}_i$ for the fluid and solid phase, respectively. For example, these coefficients for the solid phase displacements are

$$\mathcal{A}_1^S = \frac{2n_2\mathcal{L}(p_1)}{F(p_1,\omega)F_1(p_1,\omega)}, \tag{5.25}$$

$$\mathcal{A}_2^S = -\frac{2n_1\mathcal{L}(p_2)}{F(p_2,\omega)F_2(p_2,\omega)}, \tag{5.26}$$

$$\mathcal{A}_s^S = -\frac{4p_s^2\left(n_1\sqrt{p_s^2-\beta_2^2}-n_2\sqrt{p_s^2-p_1^2}\right)^2}{F(p_s,\omega)F_3(p_s,\omega)}, \tag{5.27}$$

where

$$\mathcal{L}(p) = p_3^2\left(2p^2-p_s^2\right)\left[n_1\left(p^2-m_2\right)-n_2(p^2-m_1)\right]. \tag{5.28}$$

Figure 5.6 shows the comparison of the exact and asymptotic solutions for the P1 and S wavetrains for the vertical solid phase displacement, $\Lambda_{P_1}^S$ and Λ_S^S, respectively. The

asymptotic solution appears to be quantitatively accurate. The figure also provides a vivid illustration of the process of emergence of a particular wave from its corresponding wavetrain and allows an estimate of the distance over which this occurs.

Benchmark solution

It should be mentioned that the far field solution of the form (5.17), (5.24) in the appropriate limiting case, exactly recovers classical asymptotic results, first derived by Lamb [75], for the analogous elasticity problem.

Indeed, the transition to perfect elasticity (see e.g. Bourbie *et al.* 1987) follows from the vanishing of the poroelastic parameters: $Q \to 0$, $R \to 0$, $\phi \to 0$, so that $\rho_{11} \to \rho_s$, $\rho_{12} \to 0$, $\rho_{22} \to 0$, $n_{1,2} \to 0$, $m_{1,2} \to 1/2$, $p_1 = p_2$, $p_s = 1$, $\lambda_i \to 0$.

The solution for the far field bulk modes for the vertical component of the solid phase displacement u_z, in dimensional form in accordance with (5.17), (5.24) is given by (tildes are reintroduced to indicate nondimensional quantities)

$$u_z = \frac{P}{4\pi\mu}\left(\Lambda_{P_1}^S + \Lambda_{P_2}^S + \Lambda_S^S\right) e^{i\omega t}. \tag{5.29}$$

Using $\Gamma(3/2) = \sqrt{\pi}/2$ and the values of the coefficients $\mathcal{A}_i^S$ provided in (5.25)–(5.28) one gets

$$\Lambda_i \to -\mathcal{A}_i^S \frac{\sqrt{\pi}}{2}\sqrt{2\tilde{\beta}_i}\frac{ie^{i(-\tilde{\beta}_i\tilde{x}-\pi/4)}}{\tilde{x}^{3/2}}, \quad \text{as } \lambda_i \to 0,$$

where $\tilde{\beta}_{1,2} = c_s/c_p$, and c_p, c_s are longitudinal and transverse phase velocities, respectively. Introducing $h = \omega/c_p$ and $k = \omega/c_s$, so that $\tilde{\beta}_{1,2} = h/k$, $\tilde{x} = kx$, one arrives at the following expression:

$$u_z = -\frac{P}{8\mu}\sqrt{\frac{2}{\pi}}\left[\left(\mathcal{A}_{P_1}^S + \mathcal{A}_{P_2}^S\right)\sqrt{\frac{h}{k}}\frac{ie^{i(\omega t-hx-\pi/4)}}{(kx)^{3/2}} + \mathcal{A}_S^S\frac{ie^{i(\omega t-kx-\pi/4)}}{(kx)^{3/2}}\right]. \tag{5.30}$$

The values of the coefficients $\mathcal{A}_i^S$ in the limiting case can be found to be

$$\mathcal{A}_{P_1}^S + \mathcal{A}_{P_2}^S \to -\frac{4}{\left(2h^2/k^2-1\right)^2}, \quad \mathcal{A}_S^S \to -16\left(1-h^2/k^2\right), \tag{5.31}$$

so that finally, using Lamb's original notation one arrives at the classical result [75]

$$u_z = \frac{P}{2\mu}\sqrt{\frac{2}{\pi}}\frac{h^2k^2}{(2h^2-k^2)^2}\frac{ie^{i(\omega t-hx-\pi/4)}}{(hx)^{3/2}} + \frac{2P}{\mu}\sqrt{\frac{2}{\pi}}\left(1-\frac{h^2}{k^2}\right)\frac{ie^{i(\omega t-kx-\pi/4)}}{(kx)^{3/2}}. \tag{5.32}$$

5.4 Chapter Summary

The present chapter is dedicated to the detailed investigation of the wave processes at the boundary of a porous half-space subjected to a harmonic line traction in the framework of Biot's theory. Formal analytical and closed form far field asymptotic solutions have been established herein, and these allow analysis of the response at different source frequencies, as well as an investigation of the fundamental properties of the four wave types, the combination of which makes up a disturbance traveling along the plane boundary.

Examples of numerical results have been shown (Figures 5.1–5.3) and these illustrate the influence of the source frequency on the character of the spatial oscillations in both displacements and pore pressure. These may be summarized as showing a weakening of the viscous coupling between phases as frequency is increased, with higher frequency regimes leading to oscillations that are of differing amplitude and phase in the fluid and solid. As has been pointed out by Biot [12], this follows from the governing equations. Indeed, in the case when the characteristic frequency lies near unity, the inertia and viscous terms are approximately of the same order, so that a further increase of the source frequency makes inertial terms dominant over viscous terms.

An oscillating line source generates three bulk wavetrains, containing P1, P2 and S-waves, respectively, and a surface poroelastic Rayleigh wave. Decomposition of the formal general solution into contributions of the four wave types reveals the following: bulk modes propagating along the surface exhibit $x^{-3/2}$ attenuation in addition to attenuation due to viscous interphase interactions (terms of the form $e^{-\lambda_i x}$ in expression (5.24)). Results for the spatial attenuation are found to be similar to those known from the classical elastic wave theory (Lamb 1904). Moreover, the classical elastic wave theory asymptotic results can be exactly recovered in the appropriate limiting case from the asymptotic solution obtained herein for the poroelastic waves. Analysis of the formal solution shows that the wavetrains consist of waves which propagate faster and also exhibit greater viscous attenuation than the corresponding bulk modes. Thus, at a certain distance from the source one can observe solely P1, P2 and S modes, or, in other words, the emergence of these modes from the corresponding wavetrains (Figure 5.6).

It is known that the P2 effect is difficult to measure at low frequencies (Nagy 1999). Indeed, due to the rapid viscous attenuation of the slow P2 wave, high frequency oscillations are necessary to capture this effect. In the present work, relatively high dimensional frequency $f = 100 f_c$ was used to emphasize the P2 wave contribution. In this particular case, the P2 effect is only observed in the vicinity of the source, and is found to be more pronounced in the fluid phase (Figure 5.5).

Poroelastic Rayleigh waves are found to be predominant at the surface in both the near field, due to the negation of the P1 and S wavetrains, and in the far field, due to

the geometric attenuation of the bulk modes. Thus, the frequency dependent character of spatial oscillations and relative vertical fluid/solid motion, or flux, at the surface will mostly be determined by the properties of the poroelastic Rayleigh waves in both the solid and fluid phases.

5.5 Watson's lemma for oscillatory Laplace-type integrals

Consider the following oscillatory Laplace-type integral:

$$I(x) = \int_0^\infty f(t)\mathrm{e}^{i\eta xt}\mathrm{e}^{-xt}\mathrm{d}t,\ \mathrm{Im}(\eta) = 0, \tag{5.33}$$

where $f(t)$ is continuous on $[0, \infty)$ and has the asymptotic expansion as $t \to 0^+$

$$f(t) \sim t^\gamma \sum_{n=0}^{\infty} a_n t^{\beta n}. \tag{5.34}$$

Assume that the integral is convergent, so that $\gamma > -1$, $\beta > 0$ and $f(t) = o(e^{ct})$ for some c as $t \to \infty$. Then, as $x \to \infty$,

$$I(x) \sim \sum_{n=0}^{\infty} a_n \frac{\Gamma(\nu_n)}{x^{\nu_n}} \left(\frac{\mathrm{e}^{i \arctan(\eta)}}{\sqrt{1+\eta^2}} \right)^{\nu_n},\ \nu_n = \gamma + \beta n + 1. \tag{5.35}$$

□ Replacing $I(x)$ with $I(x;\epsilon)$,

$$I(x;\epsilon) = \int_0^\epsilon f(t)\mathrm{e}^{i\eta xt}\mathrm{e}^{-xt}\mathrm{d}t, \tag{5.36}$$

introduces exponentially small errors for any $\epsilon > 0$. To show this rigorously, integration by parts can be applied.

Assume $\epsilon > 0$ is small enough so that the first N terms in the asymptotic series for $f(t)$ are a good approximation to $f(t)$, i.e.

$$\left| f(t) - t^\gamma \sum_{n=0}^{N} a_n t^{\beta n} \right| \leq K t^{\gamma + \beta(N+1)}, \tag{5.37}$$

for $0 \leq t \leq \epsilon$ and some constant $K > 0$.

Thus, the following estimate holds:

$$\left| I(x;\epsilon) - \sum_{n=0}^{N} a_n \int_0^{\epsilon} t^{\gamma+\beta n} \mathrm{e}^{i\eta x t} \mathrm{e}^{-xt} \mathrm{d}t \right| = \left| \int_0^{\epsilon} \left(f(t) - t^{\gamma} \sum_{n=0}^{N} a_n t^{\beta n} \right) \mathrm{e}^{i\eta x t} \mathrm{e}^{-xt} \mathrm{d}t \right|$$

$$\leq \int_0^{\epsilon} \left| f(t) - t^{\gamma} \sum_{n=0}^{N} a_n t^{\beta n} \right| \mathrm{e}^{-xt} \mathrm{d}t \leq K \int_0^{\epsilon} t^{\gamma+\beta(N+1)} \mathrm{e}^{-xt} \mathrm{d}t \qquad (5.38)$$

$$\leq K \int_0^{\infty} t^{\gamma+\beta(N+1)} \mathrm{e}^{-xt} \mathrm{d}t = K \frac{\Gamma(\gamma+\beta(N+1)+1)}{x^{\gamma+\beta(N+1)+1}}.$$

Extending the range of integration in the above established inequality (5.38) to $[0, \infty)$, and using (5.40), one gets

$$\begin{aligned} I(x) &= \sum_{n=0}^{N} a_n \int_0^{\infty} t^{\gamma+\beta n} \mathrm{e}^{i\eta x t} \mathrm{e}^{-xt} \mathrm{d}t + \mathrm{o}\left(\frac{1}{x^{\gamma+\beta N+1}} \right) \\ &= \sum_{n=0}^{N} a_n \frac{\Gamma(\gamma+\beta n+1)}{x^{\gamma+\beta n+1}} \left(\frac{\mathrm{e}^{i \arctan(\eta)}}{\sqrt{1+\eta^2}} \right)^{\gamma+\beta n+1} + \mathrm{o}\left(\frac{1}{x^{\gamma+\beta N+1}} \right), \qquad (5.39) \end{aligned}$$

as $x \to \infty$. Since this is true for every N, (5.35) is proved and thus the Lemma follows. ■

The proof of the above proposition, in general, repeats the proof of the classical Watson's lemma (e.g. Bender & Orszag 1978), where the following model integral (Prudnikov *et al.* 1986) must be applied instead of a Gamma function integral:

$$\int_0^{\infty} x^{\nu-1} \mathrm{e}^{-(p+iq)t} \mathrm{d}t = \Gamma(\nu) \left(p^2+q^2 \right)^{-\frac{\nu}{2}} \mathrm{e}^{-i\nu \arctan\left(\frac{q}{p}\right)}, \qquad (5.40)$$

where $p > 0$, $\mathrm{Re}(\nu) > 0$ or $p = 0$, $0 < \mathrm{Re}(\nu) < 1$. Setting $\eta = 0$ one can recover the classical Watson's lemma results.

Chapter 6

Energy partition and resonant excitation in the general case

Energy partition of poroelastic waves in the idealized case of no dissipation has been considered in detail in Chapter 4. In the general case it is necessary to take into account viscous (low frequency range) or viscoelastic (high frequency range) interphase interaction, so that all wave fields are characterized with exponential spatial decay. The method established by Miller & Pursey and developed herein for poroelastic waves in Chapter 4 cannot be adopted in the general case. The fixed proportion of the energy fraction transfered by the propagating waves in the far field is only relevant for non-dissipative media. Although analogous far field solutions can be obtained in the general case (e.g. following the method outlined in Section 5.3.2), these results cannot be used in a practical analysis of the energy partition. The energy analysis in Lamb's problem in the more general dissipative case must be conducted in a different manner. In order to obtain qualitative results for the energy partition, the problem can be reformulated as follows: what fraction of the total energy supplied by the source is directed into particular wavetrains corresponding to certain wave types. Another important question is whether and to what extent one can control the excitation of particular wave types by means of driving technique.

As was discussed above in Section 2.3, unlike the case of no dissipation (2.30) in the general dissipative case the total energy supplied by the source located at the surface is absorbed by viscous dissipation (2.29), so that

$$\langle W \rangle = 2 \iiint\limits_{\Sigma} \langle D \rangle \, d\Sigma, \tag{6.1}$$

or in other words, the input power equals power dissipation.

Assuming distributed normal driving forces $\sigma_{zz}(x,0,t) = Pf(x)e^{i\omega t},\ |x| < a$, the expression for the total power supplied by the source W [following current notation (4.10), (4.11)] is

$$\langle W \rangle = \frac{c}{\omega} \int_{-a}^{a} \langle P_z \rangle \, dx = cP \int_{0}^{a} f(x) \mathrm{Im} u_z(x,0) dx, \tag{6.2}$$

where $f(x)$ describes the driving configuration (3.25). According to (6.2) the source power can be decomposed into the contributions due to particular wavetrains provided the wavetrain solution of the type (5.17) for the surface vertical displacement $\mathrm{Im} u_z(x,0)$ is obtained. Consequently, it is possible to analyze the relative power distribution among the wavetrains, as well as to investigate whether the relative energy partition can be controlled by changing the configuration of the driving forces (e.g. resonant excitation).

6.1 Distributed source. Wavetrain solution

Consider the very general expression for the vertical component of solid displacement at the surface (3.24),

$$u_z(x,0,\omega) = -\frac{Pc}{4\pi\mu\omega} p_s^2 \int_{-\infty}^{+\infty} f(p) \frac{n_2\xi_1(p) - n_1\xi_2(p)}{F(p,\omega)} e^{ipx} dp, \tag{6.3}$$

where $f(p)$ represents the driving configuration in Fourier space (3.25). It can be noted that the distributed source (3.25, ii) represents a limiting case of the distributed source (3.25, iii) as $p_0 \to 0$, and in turn, the line source (3.25, i) can be recovered in the limiting case of the distributed source (3.25, ii) as $a \to 0$ and $\lim_{a\to 0} f(x)/2a = \delta(x)$.

The wavetrain solution for (6.3) can be recovered in a similar manner as described in Chapter 5 for the line source. However, it is important to take into account some additional difficulties when conducting branch cut integration related to distributed sources. In the latter case the function $f(p)$ can be represented in the form

$$f(p) = g_1(p)e^{ipa} + g_2(p)e^{-ipa}, \tag{6.4}$$

and therefore in the calculation of $u_z(x,0)$ the contour must be closed in the upper part of the complex p-plane for the first term in (6.4), and in the lower plane for the second term, to satisfy the conditions of Jordan's lemma (Figure 6.1). For instance, in the case of distributed source (3.25, iii)

$$f(x) = \cos(p_0 x),\ |x| < a; \qquad f(p) = a\left[\frac{\sin a(p+p_0)}{a(p+p_0)} + \frac{\sin a(p-p_0)}{a(p-p_0)}\right], \tag{6.5}$$

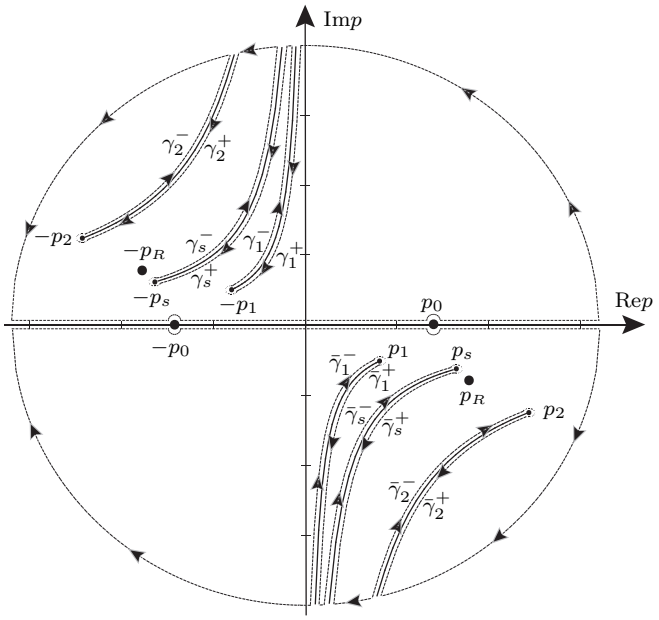

Figure 6.1: Hyperbolic branch cuts, branch points $p = \pm p_i$ $(i = 1, 2, s)$, Rayleigh poles $p = \pm p_R$, additional poles $p = \pm p_0$ in the complex p-plane (upper half-plane closure for $x + a > 0$, lower half-plane closure for $x + a < 0$).

functions $g_1(p)$ and $g_2(p)$ are

$$g_1(p) = \frac{1}{2ia}\left(\frac{e^{iap_0}}{p+p_0} + \frac{e^{-iap_0}}{p-p_0}\right), \quad g_2(p) = -\frac{1}{2ia}\left(\frac{e^{-iap_0}}{p+p_0} + \frac{e^{iap_0}}{p-p_0}\right). \tag{6.6}$$

Introducing parameterization (5.10) the wavetrain decomposition for the integral in (6.3) according to Figure 6.1 can be schematically summarized in the form

$$\int_{-\infty}^{+\infty} f(p)\frac{n_2\xi_1(p) - n_1\xi_2(p)}{F(p,\omega)}e^{ipx}dp = \Lambda_1 + \Lambda_2 + \Lambda_s + \mathrm{Res}_1 + \mathrm{Res}_2, \tag{6.7}$$

where the integral components Λ_i represent the integral expressions along the corresponding branch cuts in both the upper and lower half-space, while the residual terms Res_1 and Res_2 contain the contributions of the residues at Rayleigh poles $p = \pm p_R$ and the poles $p = \pm p_0$ respectively. Omitting the cumbersome details, one arrives at the following final result for

the integral and residual components in (6.7) [sgn(x) denotes the sign function]

$$\Lambda_1 = \int_0^{-\alpha_1} \left\{ g_1(p_1) e^{ip_1(x+a)} + g_2[\mathrm{sgn}(x-a)p_1] e^{ip_1|x-a|} \right\} \times \left[\frac{n_2\xi_1(p_1) - n_1\xi_2(p_1)}{F(p_1,\omega)} + \frac{n_2\xi_1(p_1) + n_1\xi_2(p_1)}{F_1(p_1,\omega)} \right] \frac{dp_1}{d\tau}\, d\tau, \tag{6.8}$$

$$\Lambda_2 = \int_0^{-\alpha_2} \left\{ g_1(p_1) e^{ip_2(x+a)} + g_2[\mathrm{sgn}(x-a)p_2] e^{ip_2|x-a|} \right\} \times \left[\frac{n_2\xi_1(p_2) - n_1\xi_2(p_2)}{F(p_2,\omega)} - \frac{n_2\xi_1(p_2) + n_1\xi_2(p_2)}{F_2(p_2,\omega)} \right] \frac{dp_2}{d\tau}\, d\tau, \tag{6.9}$$

$$\Lambda_s = \int_0^{-\alpha_s} \left\{ g_1(p_s) e^{ip_s(x+a)} + g_2[\mathrm{sgn}(x-a)p_s] e^{ip_s|x-a|} \right\} \times \left[\frac{n_2\xi_1(p_s) - n_1\xi_2(p_s)}{F(p_s,\omega)} - \frac{n_2\xi_1(p_1) - n_1\xi_2(p_s)}{F_s(p_s,\omega)} \right] \frac{dp_s}{d\tau}\, d\tau, \tag{6.10}$$

where the expressions for F_1, F_2, F_s are provided in (5.16), and the two residual terms are [$H(x)$ denotes the Heaviside function]

$$\mathrm{Res}_1 = \left\{ g_1(p_R) e^{ip_R(x+a)} + g_2[\mathrm{sgn}(x-a)p_R] e^{ip_R|x-a|} \right\} \frac{n_2\xi_1(p_R) - n_1\xi_2(p_R)}{F'(p_R)}, \tag{6.11}$$

$$\mathrm{Res}_2 = \frac{H(a-|x|)}{ia} \frac{n_2\xi_1(p_0) - n_1\xi_2(p_0)}{F(p_0)} \cos(p_0 x), \tag{6.12}$$

The main properties of the above wavetrain solution for the distributed source can be summarized as follows. The different character of the solution under the source $|x| < a$ and the solution away from the source $|x| > a$ can be clearly noted. Consider the factors in the expressions (6.8)–(6.10) and (6.11), where $i = 1, 2, s, R$,

$$g_1(p_i) e^{ip_i(x+a)} + g_2[\mathrm{sgn}(x-a)p_i] e^{ip_i|x-a|} = \begin{cases} 2g_1(p_i) e^{ipa} \cos(p_i x) & \text{if } |x| < a \\ f(p) e^{ipx} & \text{if } |x| > a \end{cases} \tag{6.13}$$

Therefore, the inner solution (under the source) represents superposition of the standing waves while the outer solution (away from the source) consists of traveling waves. Secondly, it can be noted that this solution is in agreement with the previously obtained wavetrain solution for the line traction (5.11)–(5.16). Indeed, in the limiting case $p_0 = 0$ and $a \to 0$,

$$g_1(p_i) e^{ip_i(x+a)} + g_2[\mathrm{sgn}(x-a)p_i] e^{ip_i|x-a|} = f(p) e^{ipx} \to 2a \exp(ip_i x), \quad i = 1, 2, s, R \tag{6.14}$$

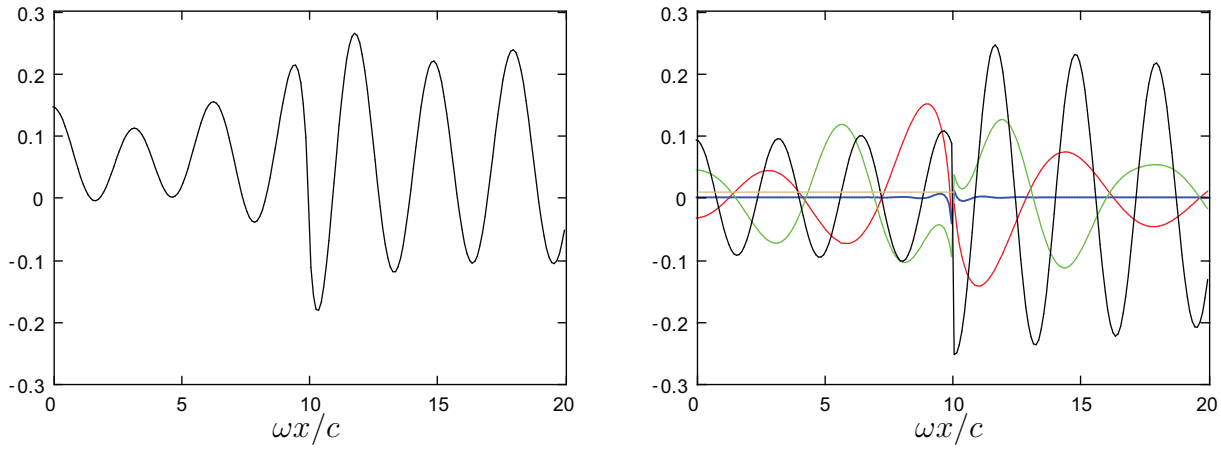

Figure 6.2: General solution for the vertical solid displacement (left) and wavetrain decomposition (right): uniform distributed source (ii); $p_0 = 0$, $a = 10$, $f = f_c$. P1-wavetrain (red), P2-wavetrain (blue), S-wavetrain (green), Rayleigh wave (black), standing wave (brown).

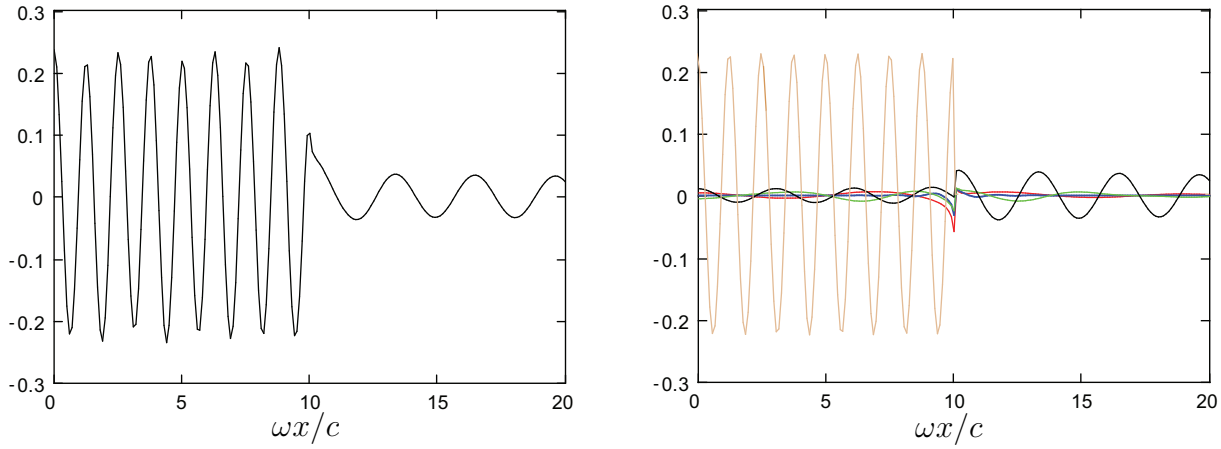

Figure 6.3: General solution for the vertical solid displacement (left) and wavetrain decomposition (right): distributed source (iii); $p_0 = 5$, $a = 10$, $f = f_c$. P1-wavetrain (red), P2-wavetrain (blue), S-wavetrain (green), Rayleigh wave (black), standing wave (brown).

and the second residual term (6.12) vanishes in the limiting case of the line source.

Finally, compared to the line source solution one should account for an additional residual term (6.11) apart from that due to the Rayleigh wave contribution (6.12). The additional residual term describes the standing wave which is only apparent under the area $|x| < a$ which is directly driven by the source. The standing wave has a flat profile in the case of uniform load (ii) $p_0 = 0$, and a harmonic profile when $p_0 \neq 0$, as in the case of distributed load (iii). From an energetic point of view, in analogy with the driven damped harmonic oscillator, this standing wave corresponds to the fractional power supply from the source into the half-space which is constantly absorbed by viscous dissipation. Thus, the corresponding power is further referred to as power absorption. The wavetrain decomposition is illustrated with a numerical example in Figures 6.2, 6.3.

In conclusion, a certain part of the energy supplied by the distributed harmonic source is constantly absorbed due to the intrinsic dissipation in the medium, while the remaining part is transferred away from the source by means of the corresponding P1, P2, S-wavetrains and the Rayleigh wave. The total energy supplied by the source and the relative energy partition among the wavetrains and the Rayleigh wave is discussed in the following.

6.2 Total power radiated by distributed source

According to (6.2) the total average power $\langle W \rangle$ supplied by the source is given by the following expression

$$\langle W \rangle = cP \int_0^a f(x) \mathrm{Im} u_z(x,0) dx, \tag{6.15}$$

where the factor $e^{i\omega t}$ is omitted in the expression (6.3), a and x are nondimensional quantities. The wavetrain solution for $\mathrm{Im}u_z(x,0)$ (6.7)–(6.12) can be used to decompose the expression for the total power (6.15) as follows,

$$\langle W \rangle = \langle W_{p1} \rangle + \langle W_{p2} \rangle + \langle W_{sh} \rangle + \langle W_{R} \rangle + \langle W_a \rangle \,, \tag{6.16}$$

where $\langle W_{p1} \rangle$, $\langle W_{p2} \rangle$, $\langle W_{sh} \rangle$, $\langle W_{R} \rangle$ quantify the fractional powers transported by the wavetrains and the Rayleigh wave, respectively, and $\langle W_a \rangle$ is the power absorption.

According to (6.15), (6.7)–(6.12), with the use of the following integrals,

$$\int_0^a \cos(p_i x)\cos(p_0 x) dx = \begin{cases} \frac{1}{2}a\left[\frac{\sin a(p_i+p_0)}{a(p_i+p_0)} + \frac{\sin a(p_i-p_0)}{a(p_i-p_0)}\right] = \frac{1}{2}f(p_i) & \text{if } p_i \neq p_0 \\ \frac{1}{2}a\left(1 + \frac{\sin 2ap_0}{2ap_0}\right) & \text{if } p_i = p_0 \end{cases} \tag{6.17}$$

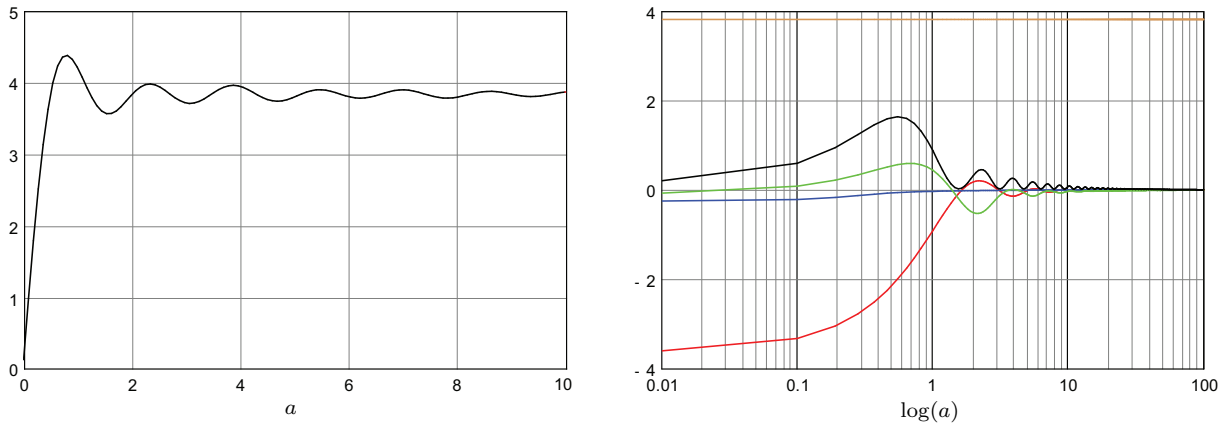

Figure 6.4: Total input power (left) and power decomposition (right) uniform distributed source (ii); $p_0 = 0$, $f = f_c$. P1-wavetrain (red), P2-wavetrain (blue), S-wavetrain (green), Rayleigh wave (black), standing wave (brown).

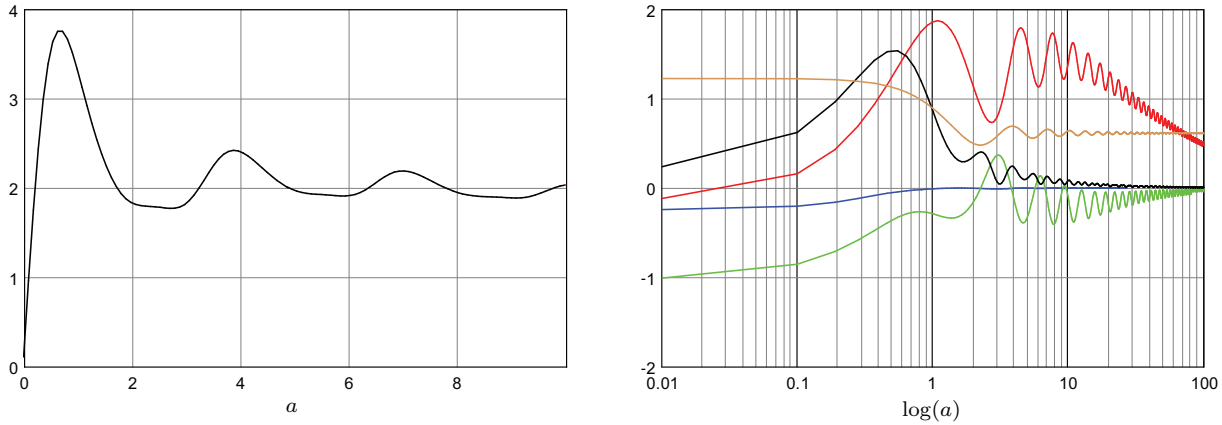

Figure 6.5: Total input power (left) and power decomposition (right): distributed source (iii); $p_0 = Re(p_1)$, $f = f_c$. P1-wavetrain (red), P2-wavetrain (blue), S-wavetrain (green), Rayleigh wave (black), standing wave (brown).

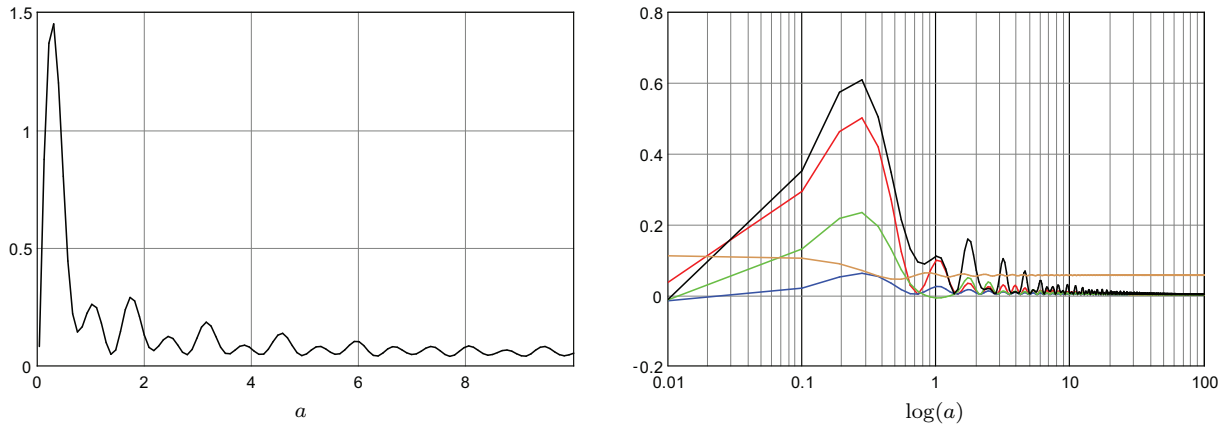

Figure 6.6: Total input power (left) and power decomposition (right): distributed source (iii); $p_0 = Re(p_2)$, $f = f_c$. P1-wavetrain (red), P2-wavetrain (blue), S-wavetrain (green), Rayleigh wave (black), standing wave (brown).

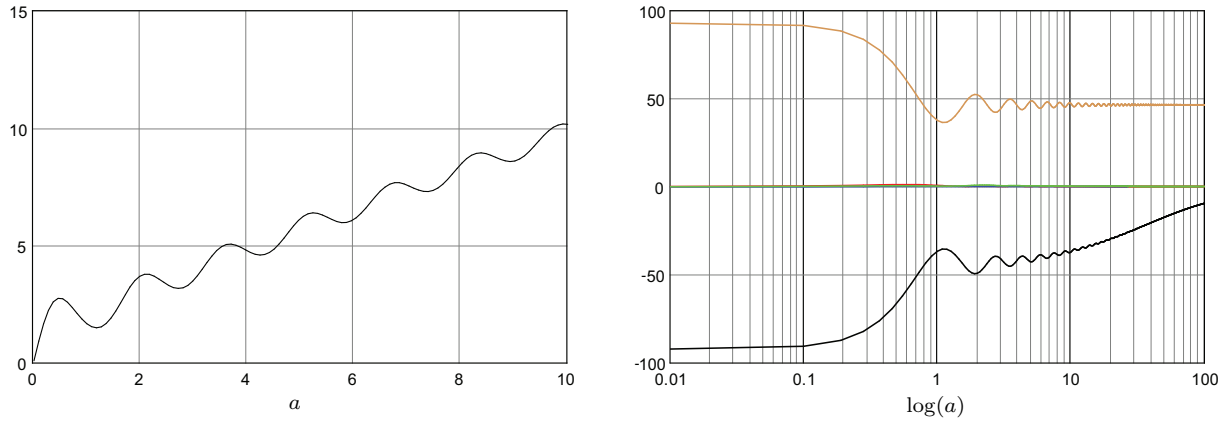

Figure 6.7: Total input power (left) and power decomposition (right): distributed source (iii); $p_0 = Re(p_R)$, $f = f_c$. P1-wavetrain (red), P2-wavetrain (blue), S-wavetrain (green), Rayleigh wave (black), standing wave (brown).

the components in the decomposition (6.16) can be evaluated as follows,

$$\langle W_{p1}\rangle = -\frac{P^2c^2}{4\pi\mu\omega}\mathrm{Im}\left\{p_s^2\int_0^{-\alpha_1} ag_1(p_1)f(p_1)e^{ip_1a}\times\right. \tag{6.18}$$

$$\left.\left[\frac{n_2\xi_1(p_1)-n_1\xi_2(p_1)}{F(p_1,\omega)}+\frac{n_2\xi_1(p_1)+n_1\xi_2(p_1)}{F_1(p_1,\omega)}\right]\frac{dp_1}{d\tau}\,d\tau\right\}, \tag{6.19}$$

$$\langle W_{p2}\rangle = -\frac{P^2c^2}{4\pi\mu\omega}\mathrm{Im}\left\{p_s^2\int_0^{-\alpha_2} ag_1(p_2)f(p_2)e^{ip_2a}\times\right.$$

$$\left.\left[\frac{n_2\xi_1(p_2)-n_1\xi_2(p_2)}{F(p_2,\omega)}-\frac{n_2\xi_1(p_2)+n_1\xi_2(p_2)}{F_2(p_2,\omega)}\right]\frac{dp_2}{d\tau}\,d\tau\right\}, \tag{6.20}$$

$$\langle W_{sh}\rangle = -\frac{P^2c^2}{4\pi\mu\omega}\mathrm{Im}\left\{p_s^2\int_0^{-\alpha_s} ag_1(p_s)f(p_s)e^{ip_sa}\times\right.$$

$$\left.\left[\frac{n_2\xi_1(p_s)-n_1\xi_2(p_s)}{F(p_s,\omega)}-\frac{n_2\xi_1(p_1)-n_1\xi_2(p_s)}{F_s(p_s,\omega)}\right]\frac{dp_s}{d\tau}\,d\tau\right\}, \tag{6.21}$$

$$\langle W_{R}\rangle = -\frac{P^2c^2}{4\pi\mu\omega}\mathrm{Im}\left\{2\pi iap_s^2g_1(p_R)f(p_R)e^{ip_Ra}\frac{n_2\xi_1(p_R)-n_1\xi_2(p_R)}{F'(p_R)}\right\}, \tag{6.22}$$

$$\langle W_{a}\rangle = -\frac{P^2c^2}{4\pi\mu\omega}\mathrm{Im}\left\{\pi p_s^2\left(1+\frac{\sin 2ap_0}{2ap_0}\right)\frac{n_2\xi_1(p_0)-n_1\xi_2(p_0)}{F(p_0)}\right\}. \tag{6.23}$$

While the total power $\langle W\rangle$ and power absorption $\langle W_a\rangle$ are always positive quantities, the remaining contributing powers (6.18)–(6.23) can possibly be negative for certain a values. Indeed, due to the phase shift between the source and velocities of the standing waves these negative values, when they occur, imply that negative values of the Poynting vector associated with the corresponding standing wave prevail in the area beneath the source. In this particular situation, the corresponding standing waves do work against the source. This could not occur for the case of a line source.

The results for the power decomposition (units $P^2c^2/4\pi\mu\omega$) according to (6.16), (6.18)–(6.23) are illustrated in Figures 6.4–6.7 for various configurations of the source. Poromechanical parameters used in calculations are provided in Table 5.1. The main properties of the solution (6.16) can be summarized as follows. The numerical results indicate that the total input power is inversely proportional to frequency ω, so that the results presented for nondimensional total power in Figures 6.4–6.7 do not depend on ω, unlike those for the constituent powers. It can also be noted that the results for the total power under different

loads closely resemble the results for the total specific power in the case of no dissipation in all cases shown. As expected, the total power in all cases tends to some constant values as $a \to \infty$ due to the intrinsic dissipation in the media, whereas in the non-dissipative media the total power grows unbounded. This includes the case of resonant excitation of the Rayleigh oscillations (Figure 6.7).

6.3 Energy partition

As was mentioned above, the approach to the problem of energy partition in the general dissipative case is different from that in the case of no dissipation. While in the case of no dissipation all of the energy supplied by the source is radiated away to infinity (2.30), in the general dissipative case all of the source energy is dissipated (2.29), hence the energy can only be transferred over certain distance away from the source. The input power decomposition (6.16) may serve as the foundation for the energy analysis in which case the problem can be formulated as follows: which fraction of the total energy is transferred (and is dissipated) in the particular wavetrain, associated with P1, P2, S-modes and the Rayleigh wave. The results for the power decomposition may seem somewhat artificial provided the presence of the negative power constituents. These negative power constituents (caused mainly by the geometry of the problem) introduce complications to the energy analysis. However, this difficulty can be overcame by considering sufficiently short wavelengths generated by the source. Numerical results suggest that indeed as the value of the parameter p_0 increases the source generates shorter waves and one may observe predominantly positive power constituents associated with the wavetrains, e.g. the results for sufficiently short wavelength $p_0 = \mathrm{Re}(p_2)$ in Figure 6.6 (further increase of p_0 provides similar results). The data for the power decomposition is found to be in agreement with the actual power distribution among the wavetrains as illustrated by the following case study.

Consider the distributed source which generates a standing wave with the profile $\cos(p_0 x)$, $|x| < a$, where $p_0 = \mathrm{Re}(p_2)$, so that the value of the parameter p_0 is chosen to be large enough to obtain positive power constituents (Figure 6.6). The total power and the power spent in generation of the wavetrains as well as the relative power contributions (measured in percentage of the power spent in generation of the wavetrains) due to three wavetrains and the Rayleigh wave is presented in Figure 6.8. It can be noted that the P2-wavetrain power exhibits peaks at $a = 2\pi/p_0$, $4\pi/p_0$, $6\pi/p_0$..., and consecutive minimums at $a = 5\pi/2p_0$, $9\pi/2p_0$, $13\pi/2p_0$.... The corresponding wavetrain solution presented in Figure 6.9 is obtained for the two different distribution radii $a = 2\pi/p_0$ and $a = 5\pi/2p_0$ which correspond to the peak and local minimum respectively. These values of a are also notable in the total power curve in Figure 6.7 (left), where they correspond to the local

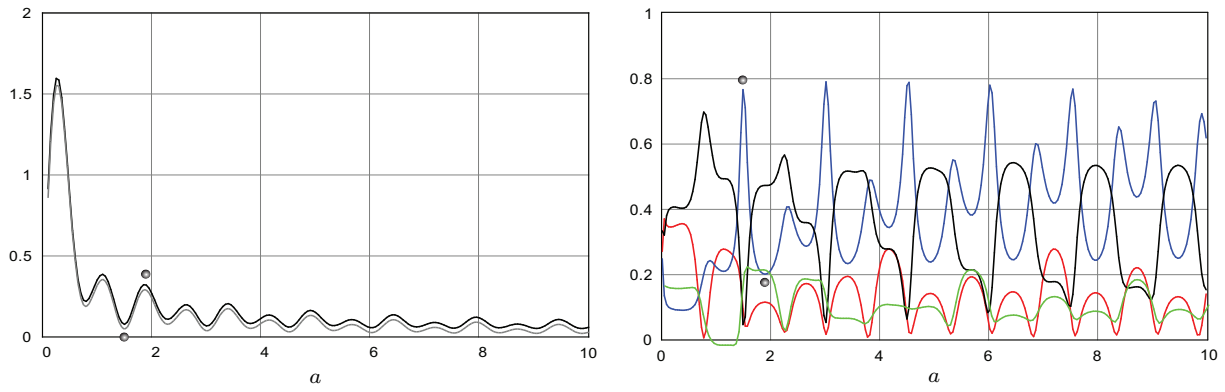

Figure 6.8: Total power and the power spent in generation of the wavetrains (left); relative (per unit total power) power decomposition (right). Distributed source (iii); $p_0 = Re(p_2)$, $f = 100 f_c$. P1-wavetrain (red), P2-wavetrain (blue), S-wavetrain (green), Rayleigh wave (black). Dots indicate the locations of local minimum and maximum under consideration.

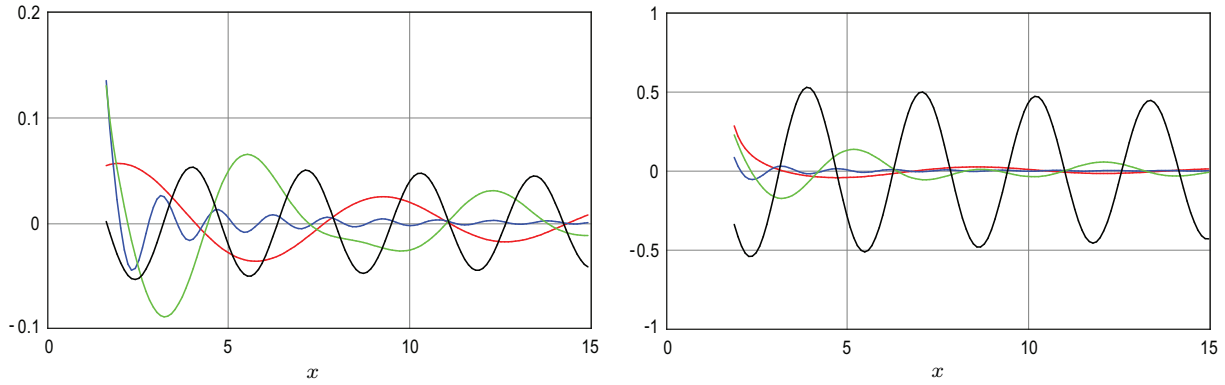

Figure 6.9: Wavetrain solution for $x > a$: distributed source (iii); $p_0 = Re(p_2)$, $f = 100 f_c$, $a = 2\pi/p_0 \approx 1.513$ (left), $a = 5\pi/2p_0 \approx 1.892$ (right). P1-wavetrain (red), P2-wavetrain (blue), S-wavetrain (green), Rayleigh wave (black).

minimum and maximum. As predicted by the result for the relative power decomposition (Figure 6.8) the P2-wavetrain is indeed more pronounced when the radius corresponds to the peak value, whereas the total power radiated by the source diminishes.

6.3.1 Energy redistribution between the Rayleigh and P2-wave

The Rayleigh wave corresponds to the free oscillations of the elastic and porous half-space. Unlike the case of a perfectly elastic solid, the Rayleigh wave mode is not always present for a non-dissipative porous half-space [39, 87]. As was discussed in Section 4 for the case of no dissipation, in the absence of the Rayleigh wave, the power spent in generation of the P2-wave significantly increases to compensate for the "missing" energy. In the general dissipative case the situation when the Rayleigh wave mode is not present also occurs. An upper cut-off frequency for the Rayleigh wave can be found for many realistic parameter sets. For instance, for the set of parameters provided in Table 5.1 the upper cut-off frequency can be found numerically to equal approximately $2449.5 f_c$ (see Table 5.2). Beyond this critical value of frequency the Rayleigh wave mode does not exist. At the same time the transition through the cut-off frequency does not introduce any significant changes to the results for the total power supply. It is thus instructive to investigate this situation from an energetic point of view.

The results for the general case in the absence of the Rayleigh wave demonstrate the energy redistribution pattern between the Rayleigh and P2-wave similar to that in the case of no dissipation. This implies that in the absence of the Rayleigh wave the energy spent in generating the P2-wave notably increases. Moreover, as the result of this energy redistribution, the displacements associated with the P2-wave often dominate in the near field.

Consider as an example the action of the uniform load at two different frequencies $f_c = 2440$ and $f_c = 2450$, so that the Rayleigh wave is excited at $f_c = 2440$ and unexcited at $f_c = 2450$. The result for the total power supply in nondimensional form is presented above in Figure 6.4 and applies to both cases. The results for the power decomposition (Figure 6.10) and corresponding wavetrain solutions (Figure 6.11) illustrate the remarkable property of the energy redistribution: the results for the Rayleigh wave and P2-wavetrain are almost identical in the near field. Such energy redistribution takes place in all cases including the case of resonant excitation of the Rayleigh wave, as shown in Figures 6.12, 6.13. Although the Rayleigh wave is unexcited beyond the cut-off frequency, again one may observe the increase of amplitude in the P2-wavetrain so that it essentially reproduces the pattern due to the absent Rayleigh wave.

From mathematical point of view this can be explained as follows. Consider the de-

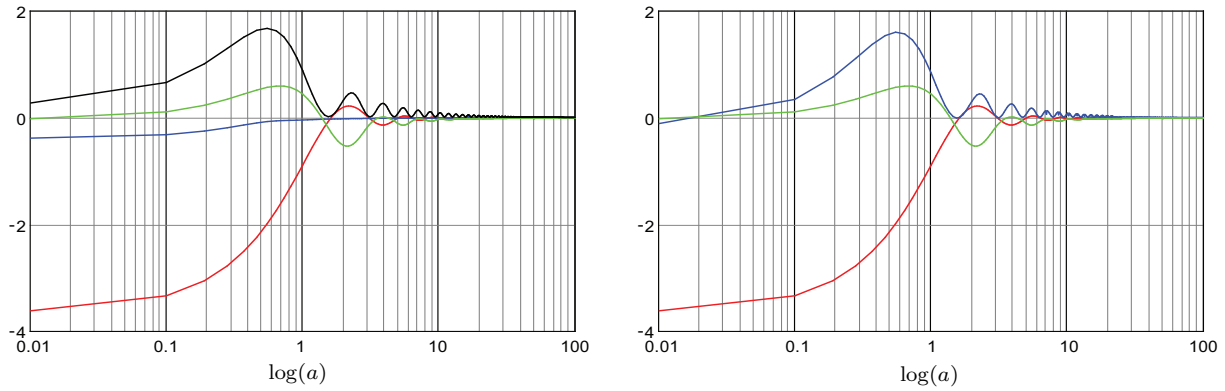

Figure 6.10: Uniform distributed load (ii): power decomposition $f = 2440 f_c$ (left), $f = 2450 f_c$ (right). P1-wavetrain (red), P2-wavetrain (blue), S-wavetrain (green), Rayleigh wave (black).

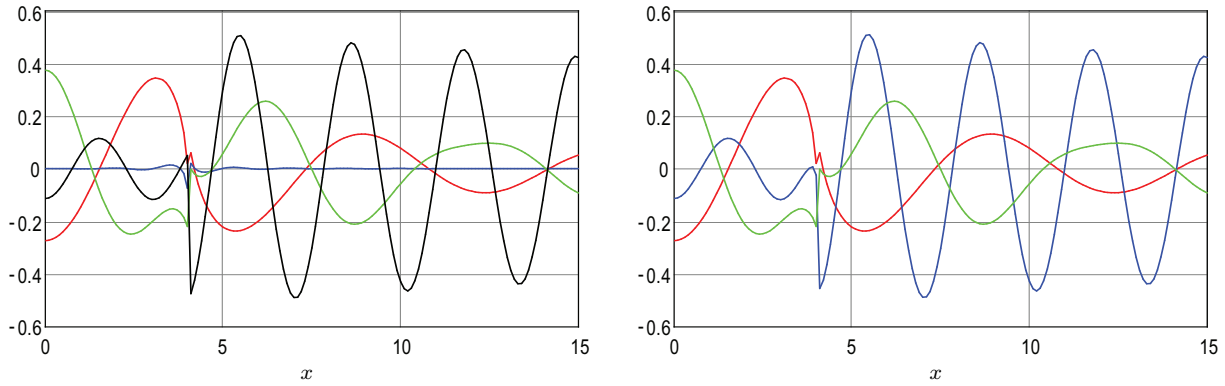

Figure 6.11: Uniform distributed load (ii): wavetrain solutions $a = 4$, $f = 2440 f_c$ (left); $a = 4$, $f = 2450 f_c$ (right). P1-wavetrain (red), P2-wavetrain (blue), S-wavetrain (green), Rayleigh wave (black)

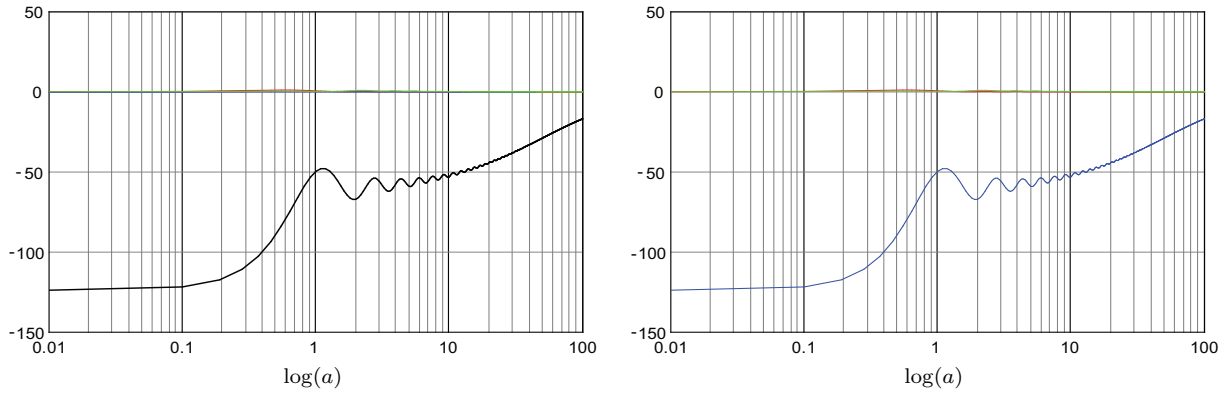

Figure 6.12: Uniform distributed load (ii): power decomposition $f = 2440 f_c$ (left), $f = 2450 f_c$ (right). P1-wavetrain (red), P2-wavetrain (blue), S-wavetrain (green), Rayleigh wave (black).

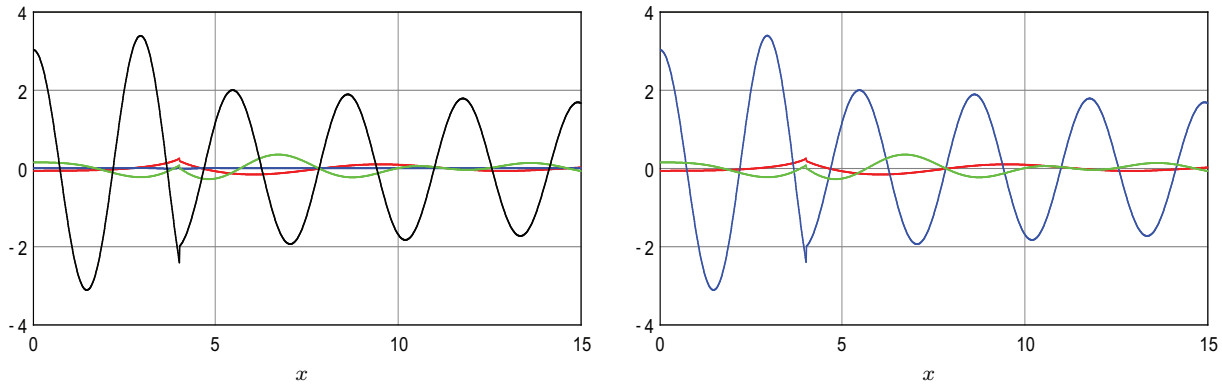

Figure 6.13: Distributed load (iii) with $p_0 = \mathrm{Re}(p_R)$ (corresponds to $f = 2440 f_c$): wavetrain solutions $a = 4$, $f = 2440 f_c$ (left); $a = 4$, $f = 2450 f_c$ (right). P1-wavetrain (red), P2-wavetrain (blue), S-wavetrain (green), Rayleigh wave (black)

nominators in the expression for the integral representation for the P2-wavetrain (6.9),

$$F(p,\omega) = \left(2p^2 - p_s^2\right)\left[n_1\left(p^2 - m_2\right) - n_2(p^2 - m_1)\right] + 2p^2\xi_s\left(n_2\xi_1 - n_1\xi_2\right), \quad (6.24)$$

$$F_2(p,\omega) = \left(2p^2 - p_s^2\right)\left[n_1\left(p^2 - m_2\right) - n_2(p^2 - m_1)\right] + 2p^2\xi_s\left(n_2\xi_1 + n_1\xi_2\right), \quad (6.25)$$

where the first expression represents the dispersion relation of the Rayleigh waves (3.23), while the second expression represents the same equation evaluated along the corresponding hyperbolic branch cut (Figure 6.1). The investigation of the roots of the above equation suggests that beyond the cut-off frequency the second equation has a root which is approximately equal to the root of the Rayleigh equation before the cut-off frequency. The location of this root does not change significantly with further increase of frequency, whereas the location of the P2 branch cut on the complex p-plane approaches this location. As a result the value of the integral rapidly increases.

6.4 Chapter Summary

The main results obtained in this chapter can be summarized as follows. The wavetrain solution is obtained in a more general form so that it includes the action of a distributed source. The character of the solution reveals that the inner solution (under the source) represents the superposition of the standing waves while the outer solution (away from the source) consists of traveling waves. The total power supplied by the distributed source is found to be inversely proportional to frequency.

The analysis of the energy partition is complicated due the presence of possible negative power constituents caused by the geometry of the driving configuration. However, even in the presence of negative constituents the results for the power decomposition can be informative, for instance, in the case of a uniform load (Figure 6.4) the power spent in generation of the Rayleigh wave can be maximized / minimized accordingly by changing the values of the source radius, a. Moreover, the consideration of the shorter driving wavelength yields positive power constituents, in which case the energy partition can be analyzed. Indeed, in this case the results for the energy partition agree with the actual solid displacement amplitude. In particular, these results suggest that changes in distribution radii may cause significant changes in amplitudes of the displacements.

The energy redistribution between the Rayleigh wave and P2-wavetrain has been investigated for materials which may not allow for the propagation of the Rayleigh wave beyond a certain cut-off frequency. In the absence of the Rayleigh wave, its virtual energy is compensated for by an increase in the energy of the P2 oscillations. The mechanism of such redistribution is explained by the presence of the leaky Rayleigh mode situated on the "unphysical" Riemann sheet. As long as this leaky mode is located in the vicinity of

the P2 branch cut it radiates its energy to the P2-wavetrain causing significant increase of amplitude.

Chapter 7

Complex group velocity and energy transport in absorbing media

Complex group velocity is common in absorbing and active media, yet its precise physical meaning is unclear. While in the case of a non-dissipative medium the group velocity of propagating waves $C_g = d\omega/dk$ is exactly equal to the observable energy velocity (defined as the ratio between the energy flux and the total energy density) $C_g = \bar{F}/\bar{E}$, in a dissipative medium $C_g = d\omega/dk$ is in general a complex quantity which can not be associated with the velocity of energy transport. Nevertheless, we find that the complex group velocity may contain information about the energy transport as well as the energy dissipated in the medium. The presented analysis is intended to expound the connection between the complex group velocity and energy transport characteristics for a class of hyperbolic, dissipative dynamical systems. Dissipation mechanisms considered herein include viscous and viscoelastic types of damping. Both cases of spatial and temporal decay are discussed. The presented approach stems from the Lagrangian formulation, and is illustrated with identities that relate the complex group velocity and energy transport characteristics for the damped Klein-Gordon equation; Maxwell's equations, governing electromagnetic waves in partially conducting media; and Biot's theory, governing acoustic wave propagation in porous solids.

The equivalence of the group velocity and the velocity of energy transport is known to be a classical result in the case of conservative dispersive media [25, 26, 13, 120, 76]. In this case, the group velocity C_g equals the energy velocity C_e, and thus, can be defined both kinematically, $C_g = \partial\omega/\partial k$, and from energy principles, as the ratio between the average energy flux $\bar{F}$ and the average mechanical energy $\bar{E}$. According to Whitham's average variational principle [120] and Lighthill's theorem [76], the relation

$$C_g = C_e = \frac{\bar{F}}{\bar{E}}, \tag{7.1}$$

is valid in the very general case of dispersive, uniform, lossless media. In the case of nonuniform and anisotropic media, with some restrictions of a geometric nature, the principle of eigenvalue perturbations, suggested by Biot [13], proves the identity. The latter heuristic approach does not prove (7.1) in general, but rather establishes the validity of the procedure in a wide variety of cases.

In the case of absorbing media, the energy velocity is defined similarly to conservative systems as the ratio between the average energy flux and average total mechanical energy [25, 26, 78, 20, 117, 35], however, the kinematically defined group velocity is in general complex and obviously can no longer be associated with the velocity of energy transport,

$$C_g \neq C_e = \frac{\bar{F}}{\bar{E}}. \tag{7.2}$$

Unlike conservative systems, the interpretation of the complex group velocity from energy principles is not established. The physical meaning of the complex group velocity thus remains obscure, so that it is sometimes referred to as a quantity with only an abstract mathematical meaning [109, 35].

On the other hand, from a kinematic point of view, the real and imaginary parts of the complex group velocity $C_g = \partial\omega/\partial k$ play an important role in the description of the behavior of a spatially localized Gaussian wave packet traveling in absorbing media [89, 109]. According to the saddle point approximation, the central wavenumber k_c is in general not conserved, but experiences a drift which is directly proportional to the imaginary part of the group velocity [89],

$$x_M = \mathrm{Re}\left(\left.\frac{d\omega}{dk}\right|_{k_M}\right) t, \tag{7.3}$$

$$k_M = k_c + \Delta^2 \mathrm{Im}\left(\left.\frac{d\omega}{dk}\right|_{k_M}\right) t, \tag{7.4}$$

where Δ corresponds to the width of the Gaussian. If a medium is dissipation free, then $\mathrm{Im}(d\omega/dk) = 0$, and the spatial maximum of the wave packet moves with the group velocity evaluated at the central wavenumber k_c, $x_M = C_g(k_c)t$ [120, 89]. As will be discussed in the following, examples of dissipative media with purely real group velocities are possible, in which case the central wavenumber k_c is conserved, and the location of the spatial maximum x_M can be found similarly to conservative systems.

The present analysis is intended to investigate the possibility of extrapolation of the energetic definition (7.1) of the complex group velocity to the case of absorbing media, and examples of dynamical systems whose group velocities allow energetic interpretations are presented.

The general analysis is limited to coupled hyperbolic nonconservative Lagrangian dynamical systems with viscous type dissipation. The Lagrangian densities are described by corresponding quadratic forms and the dissipation is included by the corresponding Rayleigh pseudopotential. The resulting governing equations represent a system of coupled linear Klein-Gordon equations with damping (KGD), and yield the conservation form

$$\frac{\partial E}{\partial t} + \frac{\partial F}{\partial x} + 2D = 0, \tag{7.5}$$

where D denotes viscous dissipation function.

In general, equipartition of energy does not hold in absorbing media. The modewise energy balance equations are derived to establish the connection between the kinetic energy, potential energy and energy losses. These relations replace the equipartition of energy principle and provide the foundation for further analysis.

The development, which to some extent follows Biot's approach for conservative systems [13], allows one to interpret complex group velocities of spatially damped waves in terms of the following average quantities: energy flux $\bar{F}$, kinetic energy $\bar{T}$ and energy losses $\bar{\mathcal{E}}$. In the case of temporally damped waves, group velocities are directly related to the velocities of energy transport. For example, in the case of single one-dimensional KGD equation group velocities of the spatially and temporally damped waves admit the following energetic interpretations, respectively,

$$C_g = \frac{\bar{F} + ic_\phi \bar{\mathcal{E}}}{2\bar{T} + i\bar{\mathcal{E}}}, \quad C_g = \frac{|\omega|^2}{\omega_R^2} C_e. \tag{7.6}$$

where $c_\phi = \omega/k_R$ denotes the phase velocity. It is important to stress that in the limiting case of no dissipation both resulting expressions (7.6) recover the energetic definition (7.1) for conservative systems. In the very general case of coupled KGD equations energetic representations (7.6) only hold approximately (modewise). The validity of approximations is subsequently discussed and illustrated.

Section 7.1 provides the necessary preliminaries and establishes the relations necessary for further development. In Section 7.2 modewise energy balance equations are derived to characterize the partition between the kinetic energy, potential energy and energy losses. Section 7.3 is dedicated to the interpretation of the complex group velocity from energy principles. The results are presented for both spatially and temporally damped waves. The following sections contain case studies. The identities are established for the three-dimensional version of the Klein-Gordon equation with damping in Section 7.4, and for electromagnetic waves in a partially conducting medium in Section 7.5. The results for a multiphase poroelastic continuum in the framework of Biot's theory, including the high frequency range theory, are given detailed consideration in Section 7.6. The conclusions are summarized in Section 7.7.

7.1 Wave motion and Lagrangian formalism

Consider the one-dimensional Lagrange equation [59],

$$\frac{\partial}{\partial t}\frac{\partial \mathcal{L}}{\partial \dot{q}_k} + \frac{\partial}{\partial x}\frac{\partial \mathcal{L}}{\partial q_{k,x}} - \frac{\partial \mathcal{L}}{\partial q_k} + \frac{\partial D}{\partial \dot{q}_k} = 0, \tag{7.7}$$

where $\mathcal{L} = \mathcal{L}(q, \dot{q}_k, q_{k,x}, x, t)$ is the volumetric Lagrangian density, D is the Rayleigh dissipation pseudopotential. Let the dynamical system with N degrees of freedom be governed by the following positive definite quadratic forms with corresponding symmetric matrices, so that kinetic and potential energies, T and V, dissipation pseudopotential D (possibly positive-semidefinite), are given by,

$$2T = \rho_{ij}\dot{q}_i\dot{q}_j, \tag{7.8}$$
$$2V = \alpha_{ij}q_{i,x}q_{j,x} + \beta_{ij}q_iq_j, \tag{7.9}$$
$$2D = b_{ij}\dot{q}_i\dot{q}_j. \tag{7.10}$$

Here and henceforth the summation over repeated indices is implied, unless otherwise specified. With these definitions the Lagrange equation reads,

$$\frac{\partial}{\partial t}\frac{\partial T}{\partial \dot{q}_k} - \frac{\partial}{\partial x}\frac{\partial V}{\partial q_{k,x}} + \frac{\partial V}{\partial q_k} + \frac{\partial D}{\partial \dot{q}_k} = 0, \quad (k = 1..N) \tag{7.11}$$

and, for instance, in terms of continuum theories, provides a single governing equation for single phase media, $N = 1$; two equations in the case of two-phase media, $N = 2$; three equations for three-phase media, $N = 3$ *etc.*

According to (7.8)–(7.11) the governing equations represent the following hyperbolic system of partial differential equations,

$$\rho_{ij}\ddot{q}_j - \alpha_{ij}q_{j,xx} + \beta_{ij}q_j + b_{ij}\dot{q}_j = 0, \quad (i = 1..N) \tag{7.12}$$

with corresponding energy conservation form (7.5),

$$\frac{\partial}{\partial t}\left(\frac{1}{2}\rho_{ij}\dot{q}_i\dot{q}_j + \frac{1}{2}\alpha_{ij}q_{i,x}q_{j,x} + \frac{1}{2}\beta_{ij}q_iq_j\right) + \\ + \frac{\partial}{\partial x}\left(-\alpha_{ij}\dot{q}_iq_{j,x}\right) + b_{ij}\dot{q}_i\dot{q}_j = 0. \tag{7.13}$$

which provides the expression for the energy flux F in terms of generalized coordinates,

$$F = -\alpha_{ij}\dot{q}_iq_{j,x}. \tag{7.14}$$

In the case of harmonic wave motion

$$q_j \sim A \exp\left[i(kx \pm \omega t)\right], \quad (j = 1..N)$$

the Lagrange equation (7.11) can be recast in the form analogous to [13],

$$-\omega^2 \frac{\partial T'}{\partial q_k} + \frac{\partial V'}{\partial q_k} \pm i\omega \frac{\partial D'}{\partial q_k} = 0, \quad (k = 1..N) \tag{7.15}$$

where $2T' = \rho_{ij} q_i q_j$, $2V' = (\alpha_{ij} k^2 + \beta_{ij}) q_i q_j$, $2D' = b_{ij} q_i q_j$, and provides the governing equations (7.12) in frequency-wavenumber space

$$\left[-\omega^2 \rho_{ij} + a_{ij}(k) \pm i\omega b_{ij}\right] q_j = 0, \quad (i = 1..N) \tag{7.16}$$

where $a_{ij}(k) = \alpha_{ij} k^2 + \beta_{ij}$.

Dissipation leads to complex dispersion relations restricting further analysis either to the case of spatially damped waves so that real circular frequencies are mapped into the complex space of wavenumbers $\omega \to k_R + ik_I$, or temporally damped waves, in which case real wavenumbers are mapped into complex frequency space $k \to \omega_R + i\omega_I$. Thus, in the case of spatially (temporally) damped waves, for a given real ω (real k) the system (7.16) represents one-parameter quadratic eigenvalue problem [114] for, in general, $2N$ complex eigenvalues k_n (eigenvalues ω_n) and up to $2N$ eigenvectors.

Multiplying the i^{th} equation (7.16) by $q_i^*/4$ one finds that in the case of spatially damped waves each of the eigenvalues k_n yields the following relation

$$-\frac{1}{4}\rho_{ij}\omega^2 q_i^n q_j^{n*} + \frac{1}{4} a_{ij}(k_n) q_i^n q_j^{n*} \pm i\frac{1}{4} b_{ij}\omega q_i^n q_j^{n*} = 0, \tag{7.17}$$

where q_i^n represents i^{th} component of the eigenmode associated with the n^{th} eigenvalue k_n,

$$q_i^n \quad = \quad A_i^n(\omega) \exp\left[i(k_n x \pm \omega t)\right]. \tag{7.18}$$

In the case of the temporally damped waves all eigenvalues ω_n yield similar relations

$$-\frac{1}{4}\rho_{ij}\omega_n^2 q_i^n q_j^{n*} + \frac{1}{4} a_{ij}(k) q_i^n q_j^{n*} \pm i\frac{1}{4} b_{ij}\omega_n q_i^n q_j^{n*} = 0, \tag{7.19}$$

where q_i^n represents i^{th} component of the eigenmode associated with the n^{th} eigenvalue ω_n,

$$q_i^n \quad = \quad A_i^n(k) \exp\left[i(kx \pm \omega_n t)\right]. \tag{7.20}$$

Equations (7.17) and (7.19) constitute the foundation for further analysis.

7.2 Modewise energy balance and energy partition

In the case of conservative systems ($b_{ij} = 0$) both eigenvalues and eigenvectors are real, the above considerations lead to

$$-\frac{1}{4}\rho_{ij}\omega_n^2 q_i^n q_j^n + \frac{1}{4}a_{ij}(k)q_i^n q_j^n = 0, \tag{7.21}$$

and equipartition of energy follows immediately for each mode [13],

$$\bar{T}_n = \bar{V}_n. \tag{7.22}$$

For nonconservative dynamical systems under consideration equipartition of energy does not hold for spatially attenuated modes, however, it is found to be the case for temporally damped modes.

7.2.1 Spatially damped waves

Consider the case of spatially damped waves in detail. The values of the period-average kinetic energy $\bar{T}_n$, potential energy $\bar{V}_n$ and viscous power dissipation $2\bar{D}_n$ associated with the n^{th} mode are provided in Appendix B.1. The expression for the modewise energy losses in one period is thus

$$2\bar{D}_n \times \frac{2\pi}{\omega} = \pi\omega b_{ij} q_i^n q_j^{n*}. \tag{7.23}$$

The following quantity, $\bar{\mathcal{E}}_n$, is introduced for further convenience to denote $1/4\pi$ fraction of viscous energy loss in one period,

$$\bar{\mathcal{E}}_n = \bar{D}_n/\omega = \frac{1}{4}\omega b_{ij} q_i^n q_j^{n*}. \tag{7.24}$$

According to the results of Appendix B.1 and (7.24) the expression (7.17) can be rewritten in the form of the modewise energy balance (no summation over repeated n's),

$$-\bar{T}_n + \Delta_n \bar{V}_n \pm i\bar{\mathcal{E}}_n = 0, \tag{7.25}$$

where the following complex, frequency dependent coefficient is introduced

$$\Delta_n = \frac{(\alpha_{ij}k_n^2 + \beta_{ij})\, q_i^n q_j^{n*}}{(\alpha_{ij}|k_n|^2 + \beta_{ij})\, q_i^n q_j^{n*}}. \tag{7.26}$$

The above relationship (7.25) replaces the energy equipartition principle for harmonic waves in conservative systems, $\bar{T} = \bar{V}$, which can be recovered from (7.25) in the limiting case of no dissipation ($\bar{\mathcal{E}}_n \to 0$, $\Delta_n \to 1$).

The modewise energy balance equation (7.25) can be applied to quantify the partition between the kinetic and potential energies. Taking the real and imaginary part of (7.25) one finds

$$\begin{cases} \bar{T}_n - \mathrm{Re}(\Delta_n)\bar{V}_n = 0, \\ \mathrm{Im}(\Delta_n)\bar{V}_n \pm \bar{\mathcal{E}}_n = 0. \end{cases} \tag{7.27}$$

Thus, the physical meaning of Δ_n is clear: $\mathrm{Re}(\Delta_n)$ represents the coefficient of energy partition between the kinetic and potential energies, while $\mathrm{Im}(\Delta_n)$ quantifies the proportion between viscous energy losses and the potential energy for the n'th mode, i.e.

$$\Delta_n = \frac{\bar{T}_n}{\bar{V}_n} \mp i\frac{\bar{\mathcal{E}}_n}{\bar{V}_n}. \tag{7.28}$$

In some particular cases, explicit expressions for Δ_n that do not involve the eigenvectors can be obtained. When β_{ij} vanishes,

$$\Delta_n = \frac{k_n^2}{|k_n|^2} = \frac{k_n}{k_n^*}, \tag{7.29}$$

and in the case of single degree of freedom

$$\Delta = \frac{\alpha k^2 + \beta}{\alpha |k|^2 + \beta}. \tag{7.30}$$

Thus, in certain cases, the information about the energy partition in nonconservative systems can be extracted directly from the dispersion relation. This includes the cases when the values of coefficients Δ_n are provided by either (7.29) or (7.30). In general, the eigenvectors are necessary to evaluate Δ_n according to definition (7.26).

Finally, it can be noted that for the dynamical systems under consideration, $Re(\Delta_n)$ is always less than unity, which indicates that in the case of spatially damped waves

$$\bar{T}_n < \bar{V}_n. \tag{7.31}$$

7.2.2 Temporally damped waves

The results for temporally damped waves can be recovered in a similar manner. According to (B.8) the expression for the energy losses in one wavelength is

$$2\bar{D}_n \times \frac{2\pi}{\omega_{nR}} = \pi \frac{|\omega_n|^2}{\omega_{nR}} b_{ij} q_i^n q_j^{n*}, \tag{7.32}$$

and again the following quantity, $\bar{\mathcal{E}}_n$, is introduced to denote $1/4\pi$ fraction of viscous energy loss in one wavelength,

$$\bar{\mathcal{E}}_n = \bar{D}_n/\omega_{nR} = \frac{1}{4}\frac{|\omega_n|^2}{\omega_{nR}} b_{ij} q_i^n q_j^{n*}. \tag{7.33}$$

According to the results for the wavelength-averaged quantities provided in Appendix B.2, (7.33) and (7.19) one may find (no summation over repeated n's)

$$-\omega_n^2 \bar{T}_n + |\omega_n|^2 \bar{V}_n \pm i\omega_n \omega_{nR} \bar{\mathcal{E}}_n = 0, \tag{7.34}$$

what represents the modewise energy balance in the case of temporally damped waves.

The real and imaginary parts of (7.34) are respectively,

$$\begin{cases} -(\omega_{nR}^2 - \omega_{nI}^2)\bar{T}_n + |\omega_n|^2 \bar{V}_n \mp \omega_{nR}\omega_{nI}\bar{\mathcal{E}}_n = 0, \\ -2\omega_{nI}\bar{T}_n \pm \omega_{nR}\bar{\mathcal{E}}_n = 0, \end{cases} \tag{7.35}$$

and equipartition of energy obviously follows from the above relations,

$$\bar{T}_n = \bar{V}_n. \tag{7.36}$$

7.3 Complex group velocity

This section investigates the possibility of extrapolation of the energetic definition (7.1) of the group velocity to the case of absorbing media. Both cases of spatial and temporal attenuation are examined.

7.3.1 Adiabatic approximation

In the following, the approximate expressions for the complex group velocities are sought based on the assumption that the corresponding eigenvectors A_i^n are sufficiently slowly varying functions of frequency (wavenumber) in the case of spatial (temporal) attenuation. The validity of the assumption is subsequently discussed.

In the case of spatially damped waves analysis stems from the equation (7.17) which can also be recast in the form,

$$\left[-\omega^2 \rho_{ij} + \alpha_{ij} k_n^2 + \beta_{ij} \pm i\omega b_{ij}\right] A_i^n(\omega) A_j^{n*}(\omega) = 0, \tag{7.37}$$

involving normalized eigenvectors $A_i^n(\omega)$.

Differentiating the equation (7.37) with respect to ω and neglecting the terms involving derivatives of eigenvectors one arrives at the following expression (no summation over repeated n's),

$$\left[-2\omega\rho_{ij} + 2\alpha_{ij}k_n\frac{dk_n}{d\omega} \pm ib_{ij}\right] A_i^n(\omega)A_j^{n*}(\omega) \approx 0, \tag{7.38}$$

which further allows the derivation of the approximate expression for the complex group velocity,

$$C_g^n \approx \frac{\left[2\alpha_{ij}k_{nR} + 2i\alpha_{ij}k_{nI}\right] A_i^n(\omega)A_j^{n*}(\omega)}{\left[2\omega\rho_{ij} \mp ib_{ij}\right] A_i^n(\omega)A_j^{n*}(\omega)}. \tag{7.39}$$

The identity obtained from the imaginary part of (7.37),

$$\left[2a_{ij}k_{nI} \pm \frac{\omega}{k_{nR}}b_{ij}\right] A_i^n(\omega)A_j^{n*}(\omega) = 0. \tag{7.40}$$

allows (7.39) to be rewritten as

$$C_g^n \approx \frac{\left[2\alpha_{ij}k_{nR} \mp i\omega b_{ij}/k_{nR}\right] A_i^n(\omega)A_j^{n*}(\omega)}{\left[2\omega\rho_{ij} \mp ib_{ij}\right] A_i^n(\omega)A_j^{n*}(\omega)}. \tag{7.41}$$

The energetic interpretation of the above expression is now straightforward. To proceed, we invoke the expressions for the period-average kinetic energy (B.1), energy flux (B.3) and power dissipation (B.4), so that it remains to multiply the numerator and denominator in (7.39) by $\omega\exp(-2k_Ix)/4$ to derive,

$$C_g^n \approx \frac{\bar{F}_n \pm ic_\phi^n\bar{\mathcal{E}}_n}{2\bar{T}_n \pm i\bar{\mathcal{E}}_n}, \tag{7.42}$$

where c_ϕ^n denotes the phase velocity and the plus (minus) sign is selected for the waves traveling in positive (negative) x direction.

The analysis for the temporally damped modes is completely analogous and follows from the equation (7.19),

$$\left[-\omega_n^2\rho_{ij} + \alpha_{ij}k^2 + \beta_{ij} \pm i\omega_n b_{ij}\right] A_i^n(k)A_j^{n*}(k) = 0. \tag{7.43}$$

Under the assumption of slowly varying eigenvectors, differentiation of the equation (7.43) with respect to k provides

$$\left[-2\rho_{ij}\omega_n\frac{d\omega_n}{dk} + 2\alpha_{ij}k \pm ib_{ij}\frac{d\omega_n}{dk}\right] A_i^n(k)A_j^{n*}(k) \approx 0, \tag{7.44}$$

and consequently, the expression for the group velocity is

$$C_g^n \approx \frac{2\alpha_{ij} k A_i^n(k) A_j^{n*}(k)}{\left[2\omega_n \rho_{ij} \mp i b_{ij}\right] A_i^n(k) A_j^{n*}(k)}. \tag{7.45}$$

With the use of the identity obtained by evaluation of the imaginary part of (7.43) this further simplifies to

$$C_g^n \approx \frac{\alpha_{ij} k A_i^n(k) A_j^{n*}(k)}{\omega_{nR} \rho_{ij} A_i^n(k) A_j^{n*}(k)}. \tag{7.46}$$

The energetic interpretation of (7.46) requires the expressions for the wavelength-averaged kinetic energy (B.5) and energy flux (B.7). For traveling modes ($\omega_{nR} \neq 0$), the following approximate relation can be obtained,

$$C_g^n \approx \frac{|\omega_n|^2}{\omega_{nR}^2} \frac{\bar{F}_n}{2\bar{T}_n}, \tag{7.47}$$

or alternatively, taking into account the equipartition of energy for temporally attenuated modes (7.36),

$$C_g^n \approx \frac{|\omega_n|^2}{\omega_{nR}^2} C_e^n, \tag{7.48}$$

where C_e^n denotes the energy velocity. Note, that the factor $|\omega_n|^2/\omega_{nR}^2$ in (7.48) may be neglected in the case of traveling waves with e-folding time greater than a period, however, should be preserved in the case of rapidly damped waves.

First of all, it is important to stress that the eigenvectors in (7.37) and (7.43), provided $b_{ij} \neq 0$, are parameter independent only in the case of weak coupling, so that the cross-coupling entries in (7.8)–(7.10) can be eliminated. Moreover, this appears to be the only case when (7.42) and (7.48) are in fact the exact energetic interpretations of the group velocities, i.e.

$$C_g^n = \frac{\bar{F}_n \pm i c_\phi^n \bar{\mathcal{E}}_n}{2\bar{T}_n \pm i\bar{\mathcal{E}}_n}, \quad C_g^n = \frac{|\omega_n|^2}{\omega_{nR}^2} C_e^n. \tag{7.49}$$

Thus, approximations (7.42) and (7.48) neglect coupling effect, and therefore, can be regarded as adiabatic approximations, in analogy with those known from quantum mechanics and acoustics. As a consequence, group velocities in the case of single degree of freedom dynamical system (7.8)–(7.10) (Klein-Gordon equation with damping, considered further in Section 7.4) yield,

$$C_g = \frac{\bar{F} \pm i c_\phi \bar{\mathcal{E}}}{2\bar{T} \pm i\bar{\mathcal{E}}}, \quad C_g = \frac{|\omega|^2}{\omega_R^2} C_e. \tag{7.50}$$

Secondly, adiabatic approximations may be accurate even with significant coupling, as for instance in the case of longitudinal modes in Biot's theory (considered further in Section 7.6).

Finally, it should be mentioned that the energetic interpretations (7.49) and (7.50) recover the energetic definition of the group velocity (7.1) in the limiting case of no dissipation.

7.3.2 Dissipation outflux

The adiabatic approximation in the case of spatially attenuated waves (7.42) can alternatively be written as

$$C_g \approx \frac{\bar{F} \pm i\bar{F}_{\mathcal{E}}}{2\bar{T} \pm i\bar{\mathcal{E}}} \tag{7.51}$$

where $\bar{F}_{\mathcal{E}} = c_\phi \bar{\mathcal{E}}$. The term $\bar{F}_{\mathcal{E}}$, the energy flux density on dimensional grounds is the product of the energy dissipated $\bar{\mathcal{E}}$ and the phase velocity $c_\phi = \omega/k_R$. It is important to stress that $\bar{F}_{\mathcal{E}}$ does not represent the energy flux in its usual sense as long as the energy generated by the viscous friction is immediately extracted from the system and does not propagate in a wave-like manner through the medium. This is generally true by virtue of idealization (e.g. in viscous fluid dynamics heat waves are neglected). Thus, in analogy with the mechanical energy flux $\bar{F}$, $\bar{F}_{\mathcal{E}}$ can be regarded as the energy dissipation outflux characterized by some energy dissipation velocity c_ϕ.

An analogous term is absent in the case of temporal damping (7.42). A more detailed discussion of dissipation outflux is provided in Section 8.5.

7.4 Klein-Gordon equation with damping

To illustrate the preceding considerations we consider the example of the damped Klein-Gordon equation (KGD) with constant coefficients [79],

$$\phi_{tt} - \alpha^2 \nabla^2 \phi + \beta^2 \phi + b\phi_t = 0, \tag{7.52}$$

where $\phi = \phi(\vec{x}, t)$, and extend the energetic interpretations (7.50) to more than one-dimension.

The energy conservation form (7.5) for the KGD equation reads,

$$\frac{\partial}{\partial t}\left(\frac{1}{2}\phi_t^2 + \frac{1}{2}\alpha^2 \phi_{x_i}^2 + \frac{1}{2}\beta^2 \phi^2\right) + \frac{\partial}{\partial x_i}\left(-\alpha^2 \phi_t \phi_{x_i}\right) + b\phi_t^2 = 0, \tag{7.53}$$

while the dispersion relation and the expression for the complex group velocity are, respectively,

$$-\omega^2 + \alpha^2 \vec{k}^2 + \beta^2 - ib\omega = 0, \tag{7.54}$$

$$\vec{C}_g = \frac{2\alpha^2 \vec{k}}{2\omega + ib}. \tag{7.55}$$

We first restrict our attention to the case of rightward propagating, spatially damped waves ($\omega_I = 0$, $\vec{k}_R \neq 0$, $\vec{k}_I \neq 0$) and consider a traveling damped wave solution of the form

$$\begin{aligned} \phi &\sim Ae^{-\vec{k}_I\vec{x}}\cos\left(\vec{k}_R\vec{x} - \omega t + \eta\right) \\ &= Ae^{-\psi(\vec{x})}\cos\left[\theta(\vec{x},t) + \eta\right], \end{aligned} \tag{7.56}$$

where θ denotes the phase, ψ corresponds to spatial attenuation and η is the phase shift,

$$\vec{k}_R = \frac{\partial\theta}{\partial\vec{x}}, \quad \vec{k}_I = \frac{\partial\psi}{\partial\vec{x}}, \quad \omega = -\frac{\partial\theta}{\partial t}. \tag{7.57}$$

The period-averaged kinetic energy is given by

$$\bar{T} = \frac{1}{2}\overline{A^2\omega^2 e^{-2\psi}\sin^2(\theta+\eta)} = \frac{1}{4}A^2\omega^2 e^{-2\psi}. \tag{7.58}$$

while the average power dissipation can be found as

$$2\bar{D} = \overline{A^2 b\omega^2 e^{-2\psi}\sin^2(\theta+\eta)} = \frac{1}{2}A^2 b\omega^2 e^{-2\psi}, \tag{7.59}$$

so that the expression for the average energy loss is

$$\bar{\mathcal{E}} = \bar{D}/\omega = \frac{1}{4}A^2 b\omega e^{-2\psi}. \tag{7.60}$$

According to (7.53) the expression for the average energy flux is now a vector quantity,

$$\vec{F} = -\overline{A^2\alpha^2 e^{-2\psi}\omega\sin(\theta+\eta)} \times \overline{\left[\vec{k}_I\cos(\theta+\eta) - \vec{k}_R\sin(\theta+\eta)\right]} = \frac{1}{2}A^2\alpha^2\omega\vec{k}_R e^{-2\psi}. \tag{7.61}$$

To establish the connection between the complex group velocity and energy transport characteristics we rearrange (7.55) as follows

$$\vec{C}_g = \frac{2\alpha^2\vec{k}_R + 2i\alpha^2\vec{k}_I}{2\omega + ib} = \frac{2\alpha^2\vec{k}_R\omega + 2i\alpha^2\vec{k}_I\omega}{2\omega^2 + ib\omega}, \tag{7.62}$$

and consider the imaginary part of the KGD dispersion relation (7.54),

$$2\alpha^2\vec{k}_R\cdot\vec{k}_I - b\omega = 0, \tag{7.63}$$

or alternatively,

$$2\alpha^2\vec{k}_R\cdot\vec{k}_I - b\omega\frac{\vec{k}_R\cdot\vec{k}_R}{|\vec{k}_R|^2} = 0, \tag{7.64}$$

so that,

$$2\alpha^2\vec{k}_I = b\frac{\omega\vec{k}_R}{|\vec{k}_R|^2} = b\vec{c}_\phi. \tag{7.65}$$

Finally, we rewrite (7.62) in the form,

$$\vec{C}_g = \frac{2\alpha^2\vec{k}_R\omega + i\vec{c}_\phi b\omega}{2\omega^2 + ib\omega}, \tag{7.66}$$

and multiply the numerator and denominator by $A^2e^{-2\psi}/4$ to obtain

$$\vec{C}_g = \frac{\vec{F} + i\vec{c}_\phi\bar{\mathcal{E}}}{2\bar{T} + i\bar{\mathcal{E}}} = \frac{\vec{F} + i\vec{F}_\mathcal{E}}{2\bar{T} + i\bar{\mathcal{E}}}, \tag{7.67}$$

which demonstrates the validity of the energetic interpretation (7.50) in more than one dimension.

Now consider the energetic interpretation of the group velocity in the case of temporally damped waves ($\omega_I \neq 0$, $\vec{k}_R \neq 0$, $\vec{k}_I = 0$). In this case the traveling damped wave solution is of the form (with $\omega_I < 0$ in the case of absorbing media)

$$\phi \;\sim\; Ae^{\omega_I t}\cos\left(\vec{k}\vec{x} - \omega_R t + \eta\right), \tag{7.68}$$

and one may recover the following expressions for the averaged over a wavelength kinetic energy and energy flux,

$$\bar{T} \;=\; \frac{1}{4}A^2|\omega|^2e^{2\omega_I t}, \tag{7.69}$$

$$\vec{F} \;=\; \frac{1}{2}\alpha^2A^2\omega_R\vec{k}e^{2\omega_I t}. \tag{7.70}$$

The expression for the group velocity (7.54) now simplifies to (with the use of the identity obtained by evaluation of the imaginary part of the dispersion relation (7.54))

$$\vec{C}_g = \frac{2\alpha^2\vec{k}}{2\omega_R + i(2\omega_I + b)} = \frac{\alpha^2\vec{k}}{\omega_R}. \tag{7.71}$$

It now suffices to compare (7.69), (7.70) and (7.71) to establish an exact representation,

$$\vec{C}_g = \frac{|\omega|^2}{\omega_R^2}\frac{\vec{F}}{2\bar{T}}, \tag{7.72}$$

and furthermore, taking into account the equipartition of energy, $\bar{T} = \bar{V}$ (which can be easily verified in the 3D case with the use of the identity $|\omega|^2 = \alpha^2\vec{k}^2 + \beta^2$, derived from the dispersion relation (7.54)),

$$\vec{C}_g = \frac{|\omega|^2}{\omega_R^2}\vec{C}_e. \tag{7.73}$$

Again, excluding rapidly damped waves in (7.73), the group velocity accurately approximates the energy velocity, $\vec{C}_g \approx \vec{C}_e$.

The result for temporally attenuated waves can be related to the behavior of a Gaussian wave packet. The one-dimensional version of (7.73), (7.3) and (7.4) suggests that the central wavenumber k_c is conserved, even though the position of the spatial maximum $x_M = C_g(k_c)t$ is always ahead of the location predicted by the energy velocity, $C_e t$.

7.5 Electromagnetic waves in a partially conducting medium. Maxwell's equations.

The physical interpretations of the group velocity in absorbing media developed in Section 7.3 were established for a special class of mechanical systems (7.8)–(7.10). Maxwell's equations for a partially conducting medium do not fit into this formalism. Nevertheless, completely analogous relations can be obtained.

Consider Maxwell's equations for a homogeneous, isotropic, linear, partially conducting medium in one dimension [77],

$$\frac{\partial^2 E_x}{\partial z^2} = \mu\epsilon\frac{\partial^2 E_x}{\partial t^2} + \mu\sigma\frac{\partial E_x}{\partial t}, \tag{7.74}$$

$$\frac{\partial^2 H_y}{\partial z^2} = \mu\epsilon\frac{\partial^2 H_y}{\partial t^2} + \mu\sigma\frac{\partial H_y}{\partial t}, \tag{7.75}$$

where μ, ϵ and σ denote permeability, permittivity and conductivity, respectively.

Assuming solutions in the form of traveling, spatially damped waves,

$$E_x = E_0 e^{i(kz-\omega t)}, \quad H_y = H_0 e^{i(kz-\omega t)}, \tag{7.76}$$

where $k = k_R + ik_I$, we note that from the equation

$$\nabla \times \mathbf{E} = -\mu\frac{\partial \mathbf{H}}{\partial t} \tag{7.77}$$

it follows that $ikE_0 = i\omega\mu H_0$.

The dispersion relation can be written down as

$$-k^2 + \mu\epsilon\omega^2 + i\mu\sigma\omega = 0, \tag{7.78}$$

or, in alternative form,

$$\begin{cases} -k_R^2 + k_I^2 + \mu\epsilon\omega^2 = 0, \\ 2k_R k_I - \mu\sigma\omega = 0, \end{cases} \tag{7.79}$$

and provides the following expression for the complex group velocity,

$$C_g = \frac{2k}{2\mu\epsilon\omega + i\mu\sigma}. \tag{7.80}$$

The expressions for the average electric and magnetic energy densities are, respectively,

$$\bar{W}_e = \frac{1}{2}\epsilon\mathbf{E}\mathbf{E}^* = \frac{1}{2}\epsilon E_x E_x^* = \frac{1}{2}\epsilon|E_0|^2 e^{-2k_I z}, \tag{7.81}$$

$$\bar{W}_m = \frac{1}{2}\mu\mathbf{H}\mathbf{H}^* = \frac{1}{2}\mu H_y H_y^* = \frac{1}{2}\frac{|k|^2}{\omega^2\mu}|E_0|^2 e^{-2k_I z}. \tag{7.82}$$

The average power flow per unit area equals the real part of the complex Poynting vector,

$$\bar{\mathbf{S}} = \mathrm{Re}\left(\mathbf{E}\times\mathbf{H}^*\right) = \mathrm{Re}\left(E_x H_y^*\right)\hat{\mathbf{z}}, \tag{7.83}$$

$$\bar{S}_z = \frac{k_R}{\omega\mu}|E_0|^2 e^{-2k_I z}. \tag{7.84}$$

The expression for the average dissipation power density can be found as

$$\bar{P}_d = \frac{1}{2}\mathbf{E}\cdot\mathbf{J}_c^* = \frac{1}{2}\sigma E_x E_x^* = \frac{1}{2}\sigma|E_0|^2 e^{-2k_I z}, \tag{7.85}$$

and again we define $1/4\pi$ fraction of the energy loss in one cycle $\bar{\mathcal{E}}$, so that

$$\bar{\mathcal{E}} = \bar{P}_d/\omega = \frac{\sigma}{2\omega}|E_0|^2 e^{-2k_I z}. \tag{7.86}$$

Using the second equation (7.79) we can rearrange (7.80) as follows,

$$C_g = \frac{k_R/\mu\omega + ic_\phi\sigma/2\omega}{\epsilon + i\sigma/2\omega}, \tag{7.87}$$

where $c_\phi = \omega/k_R$ is the phase velocity, so that finally,

$$C_g = \frac{\bar{S}_z + ic_\phi\bar{\mathcal{E}}}{2\bar{W}_e + i\bar{\mathcal{E}}} = \frac{\bar{S}_z + i\bar{F}_\mathcal{E}}{2\bar{W}_e + i\bar{\mathcal{E}}}, \tag{7.88}$$

where the quantity $\bar{F}_\mathcal{E} = c_\phi\bar{\mathcal{E}}$, in analogy with previous considerations, is recognized as the Joule dissipation outflux.

It can be easily verified that the energy partition coefficient Δ is given by

$$\Delta = \frac{k^2}{|k|^2} = \frac{\bar{W}_e}{\bar{W}_m} + i\frac{\bar{\mathcal{E}}}{\bar{W}_m}, \tag{7.89}$$

so that $\mathrm{Re}(\Delta)$ provides the ratio between the electric and magnetic energy densities, while $\mathrm{Im}(\Delta)$ quantifies the proportion between the energy loss in one period and magnetic density. In conducting media the magnetic energy density is known to be always larger than the electric energy density in the case of spatial attenuation [77] which also follows from equation (7.89).

One may also obtain the identity for the temporally damped waves. In this case the expression for the group velocity is

$$C_g = \frac{k}{\mu\epsilon\omega_R}. \tag{7.90}$$

The expressions for the energy densities and power flow averaged over a wavelength are

$$\bar{W}_e = \frac{1}{2}\epsilon|E_0|^2 e^{2\omega_I z}, \tag{7.91}$$

$$\bar{W}_m = \frac{1}{2}\frac{k^2}{|\omega|^2\mu}|E_0|^2 e^{2\omega_I z}, \tag{7.92}$$

$$\bar{S}_z = \frac{k\omega_R}{\mu|\omega|^2}|E_0|^2 e^{2\omega_I z}. \tag{7.93}$$

The equipartition of electric and magnetic energy densities, $\bar{W}_e = \bar{W}_m$, can be confirmed with the use of dispersion relation (7.78).

Consequently, one arrives at

$$C_g = \frac{|\omega|^2}{\omega_R^2}\frac{\bar{S}_z}{2\bar{W}_e} = \frac{|\omega|^2}{\omega_R^2}C_e. \tag{7.94}$$

7.6 Longitudinal waves in a multiphase continuum. Biot's theory.

The approach to the complex group velocity developed above applies to a multiphase continuum, in particular, to Biot's theory of wave propagation in an isotropic, homogeneous, porous solid [11, 12]. Biot's theory implies purely viscous solid-fluid interphase interactions in the low frequency range and viscoelastic interphase interactions in the higher frequency range. The governing equations in the low frequency range can be shown to satisfy the formalism (7.8)–(7.10) and approximate physical interpretations of the complex group velocities (7.42), (7.48) apply directly to both longitudinal modes. In the general, full frequency range theory it is necessary to include viscoelastic effects which introduce certain modifications to the earlier obtained result (7.42). Analysis is provided for the case

of spatially damped waves propagating in the negative x direction to maintain consistency with Biot's original work [11, 12].

According to low frequency Biot's theory

$$\begin{aligned} 2T &= \rho_{11}\dot{u}_i^2 + 2\rho_{12}\dot{u}_i\dot{U}_i + \rho_{22}\dot{U}_i^2, && (7.95)\\ 2V &= \sigma_{ij}e_{ij} + s\varepsilon, && (7.96)\\ 2D &= b(\dot{u}_i - \dot{U}_i)^2, && (7.97) \end{aligned}$$

where u and U are the displacements of the solid and fluid phases respectively, ρ_{ij} is the mass matrix whose diagonal (off-diagonal) components represent reference phase densities (added mass effects); $b = \phi^2\eta_f/K$, where ϕ, η_f and K denote porosity, viscosity and permeability, respectively.

The solid and fluid strains are defined as follows

$$e_{ij} = \frac{1}{2}\left(u_{i,j} + u_{j,i}\right),\ \varepsilon = U_{i,i} \tag{7.98}$$

and the constitutive equations thus read

$$\begin{aligned} \sigma_{ij} &= \lambda e_{kk}\delta_{ij} + 2\mu e_{ij} + Q\varepsilon\delta_{ij}, && (7.99)\\ s &= Qe_{kk} + R\varepsilon. && (7.100) \end{aligned}$$

Further analysis is provided for the 1D case and thus restricted to longitudinal waves. In this case we find the following expressions for the potential energy (7.96) in terms of generalized coordinates,

$$2V = (\lambda + 2\mu)u_x^2 + 2Qu_xU_x + RU_x^2, \tag{7.101}$$

which, along with (7.95) and (7.97), represent a particular case of the formalism (7.8)–(7.10). The poroacoustic Poynting vector

$$P_i = -\sigma_{ij}\dot{u}_j - s\dot{U}_i, \tag{7.102}$$

reduces to a scalar expression for the energy flux [consistent with the general expression (7.14)],

$$F = -\sigma\dot{u} - s\dot{U} = -(\lambda + 2\mu)u_x\dot{u} - 2Q(u_x\dot{U} + U_x\dot{u}) - RU_x\dot{U}. \tag{7.103}$$

To illustrate the steps in the approach for coupled systems we consider the quadratic forms

$$\begin{aligned} 2T' &= \rho_{11}u^2 + 2\rho_{12}uU + \rho_{22}U^2, && (7.104)\\ 2V' &= k^2\left[(\lambda + 2\mu)u^2 + 2QuU + RU^2\right], && (7.105)\\ 2D' &= b\left(u^2 - 2uU + U^2\right), && (7.106) \end{aligned}$$

and derive the governing equations in frequency-wavenumber space according to (7.15),

$$-\omega^2(\rho_{11}u + \rho_{12}U) + k^2\left[(\lambda + 2\mu)u + QU\right] + i\omega b\mathcal{F}(u - U) = 0, \tag{7.107}$$

$$-\omega^2(\rho_{12}u + \rho_{22}U) + k^2(Qu + RU) - i\omega b\mathcal{F}(u - U) = 0, \tag{7.108}$$

An ad hoc frequency dependent correction factor $\mathcal{F}$ [12] is introduced here in (7.107)–(7.107). Introduction of the complex viscosity $\mathcal{F}\eta_f$ includes viscoelastic effects and physically describes the lag between the filtration velocity and the shear stress exerted on the pore wall [12]. While the real part of the complex viscosity corresponds to the viscous interaction, the imaginary part takes into account the purely elastic response. By taking the viscoelastic interaction into account one can investigate a more general acoustic porous media model that is valid for both low and high frequency regimes. The more general results for the full frequency range problem must recover the results derived above for the low frequency theory in the limiting case $\mathcal{F} \to 1$.

The eigenvalue problem (7.107)–(7.108) for k^2, can be classified as a standard eigenvalue problem (or degenerate quadratic eigenvalue problem for k) and admits a simple analytic solution [12] (unlike the corresponding problem for ω, which is strongly nonlinear; this case of temporal attenuation is beyond the scope of the present analysis). Two possible longitudinal modes exist in Biot's theory, the so-called P1 and P2 waves, which we take to correspond to the eigenvalues k_1, k_2 and eigenvectors (u_1, U_1) and (u_2, U_2), respectively.

In this notation, the modewise, averaged over a period values of the kinetic energy, potential energy, energy flux and D_n are $(n = 1, 2)$,

$$\bar{T}_n = \frac{1}{4}\omega^2\left[\rho_{11}u_n u_n^* + \rho_{12}(u_n^* U_n + u_n U_n^*) + \rho_{22}U_n U_n^*\right], \tag{7.109}$$

$$\bar{V}_n = \frac{1}{4}|k_n|^2\left[(\lambda + 2\mu)u_n u_n^* + Q(u_n^* U_n + u_n U_n^*) + RU_n U_n^*\right], \tag{7.110}$$

$$\bar{F}_n = \frac{1}{2}\omega\mathrm{Re}(k_n)\left[(\lambda + 2\mu)u_n u_n^* + Q(u_n^* U_n + u_n U_n^*) + RU_n U_n^*\right], \tag{7.111}$$

$$2\bar{D}_n = \frac{1}{2}\omega^2 b\mathcal{F}(u_n u_n^* - u_n^* U_n - u_n U_n^* + U_n U_n^*). \tag{7.112}$$

Viscoelastic interaction implies elastic energy storage during each cycle as well as viscous energy losses [115]. Upon introduction of the frequency correction factor in (C.4) the average quantity $2\bar{D}_n$ becomes complex. It is now the real part of $2\bar{D}_n$ that corresponds to the viscous power dissipation, while the imaginary part of $2\bar{D}_n$ serves to quantify the elastic energy stored (see Chapter 8 for detailed explanation).

7.6.1 Complex group velocity

The approximate energetic interpretations of the complex group velocities for the longitudinal waves are sought in the following, and these now include an additional term due to

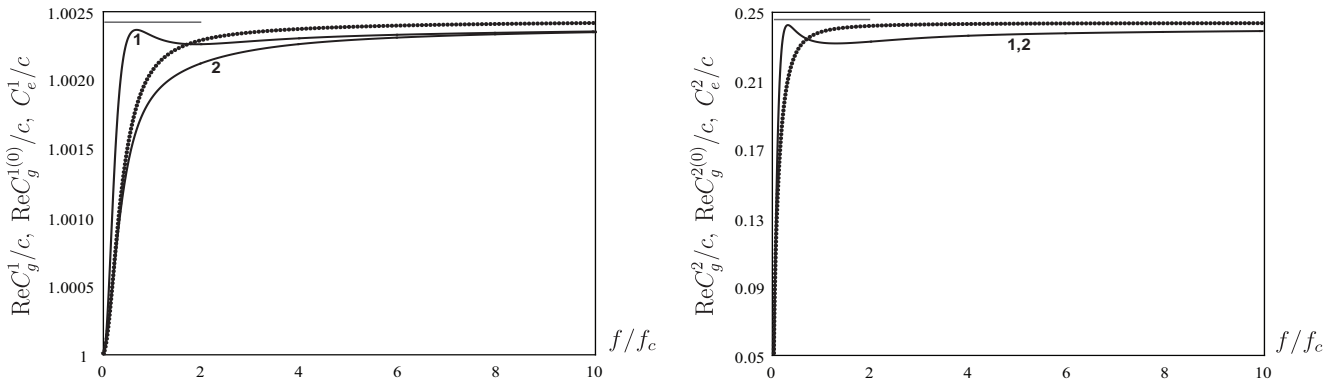

Figure 7.1: Group velocities and corresponding adiabatic approximations (real parts) versus frequency (curves labeled 1 and 2, respectively). Energy velocities versus frequency (dotted line). Horizontal lines indicate limiting wavefront velocities V_{p1}^{∞} and V_{p2}^{∞} (Table 5.1). P1-wave results (left), P2-wave results (right).

elastic energy stored.

As was mentioned above, Biot's theory admits two possible longitudinal modes. Each characteristic solution ($n = 1, 2$) must satisfy (7.17), which is now obtained by multiplication of (7.107) and (7.108) by u^* and U^*, respectively, and adding the two equations,

$$\begin{aligned} -\omega^2 \left[\rho_{11} u_n u_n^* + \rho_{12}(u_n^* U_n + u_n U_n^*) + \rho_{22} U_n U_n^*\right] + \\ +k_n^2 \left[(\lambda + 2\mu) u_n u_n^* + Q(u_n^* U_n + u_n U_n^*) + R U_n U_n^*\right] + \\ +i\omega b \mathcal{F}(u_n u_n^* - u_n^* U_n - u_n U_n^* + U_n U_n^*) = 0. \end{aligned} \tag{7.113}$$

In the form of the modewise energy balance (7.25) this reads

$$-\bar{T}_n + \Delta_n \bar{V}_n + i\bar{\mathcal{E}}_n' - \bar{\mathcal{E}}_n'' = 0, \quad \Delta_n = k_n^2/|k_n|^2 \tag{7.114}$$

where $\bar{\mathcal{E}}_n'$, $\bar{\mathcal{E}}_n''$,

$$\begin{pmatrix} \bar{\mathcal{E}}_n' \\ \bar{\mathcal{E}}_n'' \end{pmatrix} = \frac{1}{4}\omega b \begin{pmatrix} \mathcal{F}_R \\ \mathcal{F}_I \end{pmatrix} (u_n u_n^* - u_n^* U_n - u_n U_n^* + U_n U_n^*), \tag{7.115}$$

are, respectively, $1/4\pi$ fraction of the energy loss due to the viscous dissipation and half the maximum elastic energy stored in one cycle modewise. In particular, according to (7.114) and (7.115), the energy partition between the kinetic and potential energy, and the energy losses and potential energy can be quantified as follows,

$$\frac{\bar{T}_n}{\bar{V}_n} = \mathrm{Re}(\Delta_n) + \frac{\mathcal{F}_I}{\mathcal{F}_R}\mathrm{Im}(\Delta_n), \quad \frac{\bar{\mathcal{E}}_n'}{\bar{V}_n} = -\mathrm{Im}(\Delta_n). \tag{7.116}$$

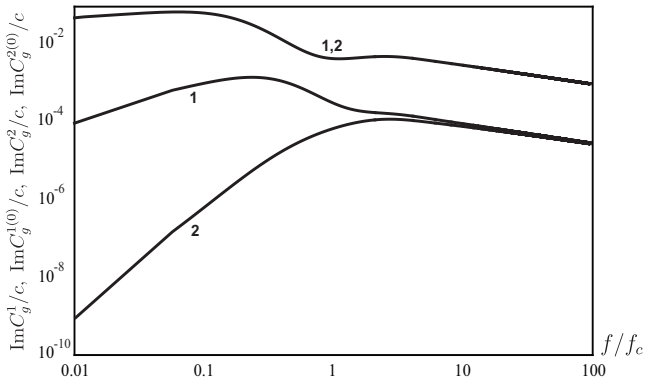

Figure 7.2: Group velocities and corresponding adiabatic approximations (imaginary parts) versus frequency (curves labeled 1 and 2, respectively). P1-wave results (lower curves), P2-wave results (upper curves).

With the above remarks the derivation for the group velocity interpretation can be recovered in the same manner as in Section 7.3. In this case, for leftward propagating waves, we obtain the following adiabatic approximations

$$\begin{aligned} C_g^n &\approx \frac{\bar{F}_n - ic_\phi^n \bar{\mathcal{E}}_n'}{2\bar{T}_n + \Psi''\bar{\mathcal{E}}_n'' - i\Psi'\bar{\mathcal{E}}_n'}, \\ \Psi' &= 1 + \frac{\omega}{\mathcal{F}_R}\frac{d\mathcal{F}_R}{d\omega},\ \Psi'' = 1 + \frac{\omega}{\mathcal{F}_I}\frac{d\mathcal{F}_I}{d\omega}. \end{aligned} \tag{7.117}$$

The physical interpretation of the above statement is clear. The term $\bar{F}_{\mathcal{E}n} = c_\phi^n \bar{\mathcal{E}}_n'$ represents the dissipation outflux due to the viscous interphase interactions as before, while $\bar{\mathcal{E}}_n'$ and $\bar{\mathcal{E}}_n''$ denote viscous energy losses and half of the maximum of the elastic energy stored (see Chapter 8 for detailed explanation), respectively. Ψ'' and Ψ' are nondimensional coefficients expressed in terms of the frequency correction factor. The results for the low frequency Biot's theory (7.42) can be recovered from (7.117) in the limiting case $\mathcal{F} \to 1$.

Moreover, in this particular case the adiabatic approximation (7.117) is also a leading order approximation for both the real and imaginary parts of the complex group velocity. In the high frequency range the small parameter in the eigenvalue problem (7.107), (7.108) is $\mathcal{F}/\omega$. As long as $\mathrm{Re}\mathcal{F} = O(\omega^{\frac{1}{2}})$ and $\mathrm{Im}\mathcal{F} = O(\omega^{\frac{1}{2}})$ [12], the perturbation is of order $O(\omega^{-\frac{1}{2}}) + iO(\omega^{-\frac{1}{2}})$. Thus, k_n and C_g^n can be expanded in powers $\omega^{\frac{1}{2}}$,

$$\begin{aligned} k_n/\omega &= \lambda_{n0} + i\lambda_{n1}/\omega^{\frac{1}{2}} + \lambda_{n2}/\omega^{\frac{1}{2}} + i\lambda_{n3}/\omega + \ldots, \\ C_g^n &= C_g^{n0} + C_g^{n1}/\omega^{\frac{1}{2}} + iC_g^{n2}/\omega^{\frac{1}{2}} + C_g^{n3}/\omega + \ldots. \end{aligned} \tag{7.118}$$

Further considerations suggest that

$$C_g^n = \frac{\bar{F}_n - ic_\phi^n \bar{\mathcal{E}}_n'}{2\bar{T}_n + \Psi''\bar{\mathcal{E}}_n'' - i\Psi'\bar{\mathcal{E}}_n'} + O\left(\frac{1}{\omega}\right) + iO\left(\frac{1}{\omega}\right), \tag{7.119}$$

where the first summand contains leading $O(1)$, $O(\omega^{-\frac{1}{2}})$ and $iO(\omega^{-\frac{1}{2}})$ terms.

The validity of the adiabatic approximation (7.119) is discussed further in Section 7.6.2 and illustrated with sample parameters for water saturated Berea sandstone.

7.6.2 Numerical results

Numerical results are obtained for water saturated Berea sandstone with the physical properties provided in Table 5.1. Generalized poroelastic parameters λ, Q, and R are related to the porosity, the solid and fluid bulk moduli, the bulk modulus of the porous drained matrix and the shear modulus via Gedanken experiments [16]; reference phase densities ρ_{ij} are related to porosity, tortuosity, grain and saturating fluid densities [11] (see Appendix D).

The dispersion relation for the longitudinal modes has the form [12]

$$(q_{11}q_{22} - q_{12}^2)z^2 - (q_{22}\gamma_{11} + q_{11}\gamma_{22} - 2q_{12}\gamma_{12})z + (\gamma_{11}\gamma_{22} - \gamma_{12}^2) + \frac{ib}{2\pi\rho f}\mathcal{F}(\kappa)(z-1) = 0, \tag{7.120}$$

where q_{ij} and γ_{ij} are normalized Biot's parameters and normalized reference densities, respectively, $\rho = \rho_{11} + 2\rho_{12} + \rho_{22}$, $z = (ck_n/\omega)^2$, $n = 1, 2$ (c is the characteristic velocity), $\kappa = \delta(f/f_c)^{1/2}$ with characteristic frequency f_c defined as

$$f_c = \frac{b}{2\pi\rho(\gamma_{12} + \gamma_{22})}. \tag{7.121}$$

The expression for the frequency correction factor in terms of Bessel-Kelvin zero order functions is [12]

$$\mathcal{F}(\kappa) = \frac{1}{4}\left(\frac{\kappa T(\kappa)}{1 - \frac{2}{i\kappa}T(\kappa)}\right), \quad T(\kappa) = \frac{\mathrm{ber}'(\kappa) + i\mathrm{bei}'(\kappa)}{\mathrm{ber}(\kappa) + i\mathrm{bei}(\kappa)}. \tag{7.122}$$

Figures 7.1, 7.2 contain the results for the complex group velocities (real and imaginary parts respectively) calculated both exactly, with the direct use of the dispersion relation (7.120), and approximately, according to the adiabatic (also the leading order) approximation (7.119). The results for the energy velocity are also included in Figure 7.1. As was mentioned above, the validity of the group velocity approximation strongly depends

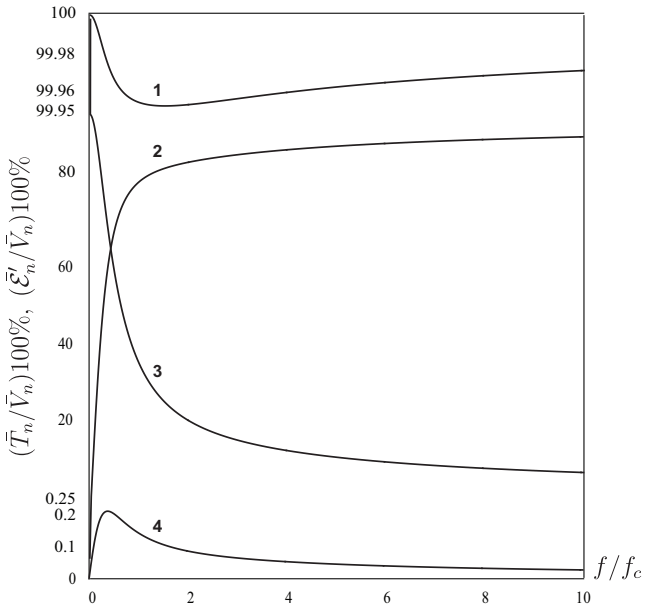

Figure 7.3: Kinetic energies, $\bar{T}_1$ (1) and $\bar{T}_2$ (2), and energy losses, $\bar{\mathcal{E}}'_1$ (4) and $\bar{\mathcal{E}}'_2$ (3), measured in percentage of the potential energies $\bar{V}_1$ and $\bar{V}_2$ respectively.

on certain properties of the eigenvectors. The solution of the eigenvalue problem (8.23), (8.24) indicates that eigenvectors indeed exhibit the desired property, not only in the high frequency range. Results for real and imaginary parts of the complex group velocities illustrate the relative error introduced by the truncation of the coupling terms. The approximation is much more accurate in the case of the P2 wave, so that the exact and approximate results are indistinguishable. This indicates that interphase coupling does not significantly affects the propagation of the highly damped P2 wave. In the case of the P1 wave the effect of interphase coupling is more pronounced, especially in the low frequency range. The approximation is more accurate in the higher frequency range, as was predicted theoretically. The energy velocity is found to be slower (faster) than the group velocity in the low (high) frequency range, however, never exceeds the values of the wavefront velocities, $C_e^1 < V_{p1}^\infty$, $C_e^2 < V_{p2}^\infty$, in accord with the causality principle.

Figure 7.3 contains the results for the modewise kinetic energy and energy losses in one period, due to viscous dissipation, $\bar{T}_n$ and $\bar{\mathcal{E}}'_n$, measured in percentage of the potential energies $\bar{V}_n$ in accordance with (7.116). For the P1 wave, equipartition of energy, $\bar{T}_1 \approx \bar{V}_1$, holds nearly exactly (with accuracy greater than 0.05%) at all frequencies. For the P2 wave similar results, $\bar{T}_2 \approx \bar{V}_2$, are only valid in the high frequency range. Significant energy losses are observed in the low frequency range, especially for the P2 wave, as expected. These results reconfirm, from an energetic point of view, the role of the P2 wave as the

main dissipation mechanism in porous solids. Moreover, this serves a vivid example of the application of the modewise energy balance equation, since the results for the energy partition were extracted directly from the dispersion relation (7.120).

7.7 Chapter Summary

In the case of conservative dynamical systems group velocity can be defined both kinematically and from energy principles. In the case of nonconservative systems, a general energetic definition, similar to that for conservative systems, does not exist. Nevertheless, in some exceptional cases, identities relating the complex group velocity and energy transport characteristics can be established for both the case of spatial and the case of temporal attenuation. The exact energetic interpretations have been presented for the KGD equation (7.67), (7.73) and Maxwell's equations (7.88), (7.94). In the latter case the complete analogy with mechanical systems is remarkable, since Maxwell's equations do not satisfy the formalism (7.8)–(7.10).

In the case of Biot's theory the results can be summarized as follows. The energetic interpretation in the form of the adiabatic approximation established for the complex group velocity (7.119) is a leading order approximation for both real and imaginary parts of the group velocity. Numerical results suggest a minuscule coupling effect on the propagation of the highly damped slow P2 mode.

All energetic interpretations of the complex group velocity in the case of spatial attenuation contain the dissipation outflux term representing the product of the phase velocity and energy dissipated. This quantity, although an energy flux on dimensional grounds, is not the energy flux in its usual sense as long as the energy generated by the internal friction is instantaneously extracted from the medium and does not propagate after it is generated. In all the cases considered, including low and higher frequency Biot's theory, the dissipation energy velocity is found to equal the phase velocity, as can be expected for cases in which dissipation is caused by friction. We believe this can be understood in terms of the following thought experiment. Imagine a chain of masses in a frictionless medium. The first mass begins to move with a constant velocity, hits the second mass, and transfers energy to this mass. The second mass, in turn, moves with a fixed velocity and hits the third mass, setting it in motion, and so on. Assume that the energy is only dissipated during inelastic collisions, which occur instantaneously, and each collision removes only a small fraction of the initial energy. In this simple example of a spatially damped longitudinal wave, heat waves are generated and extracted from the medium during collisions only, and hence, energy is dissipated with the velocity of the individual masses, or the phase velocity. An analogous thought experiment in the case of temporal attenuation assumes intrinsic friction of the medium and purely elastic collisions. In the latter case the energy

is extracted permanently, immediately after the first mass is set in motion. There is no characteristic velocity to be associated with the energy dissipated, therefore, the quantity $c_\phi \bar{\mathcal{E}}$ is physically meaningless, and the corresponding term is absent in the energetic interpretation of the group velocity.

Finally, it is important to stress that the analysis and the main conclusions presented herein apply to dynamical systems of a special type, namely those governed by second order hyperbolic partial differential equations with particular dissipation models (viscous and viscoelastic). Although this covers a variety of realistic physical systems, the question of whether or not the interpretation of the complex group velocity from energy principles can be established in general, or at least for a wider class of problems, remains open.

Chapter 8

Energy velocity and Q factor of poroelastic waves

The energy velocity and Q factor of poroelastic acoustic waves in the context of classical isotropic Biot's theory are revisited. Special attention is paid to the high frequency regime when interphase interaction is viscoelastic. The analogy with viscoelastic behavior is emphasized in derivation of the energy balance equations which relate kinetic energy, potential energy, viscous power dissipation and elastic energy stored associated with each wave. These lead to exact closed form expressions for the energy velocity and Q factor for both longitudinal and shear waves from energy principles. Most notably, the analysis of the resulting expressions reveals that the energy velocity of both longitudinal and shear waves equals (exceeds) the corresponding phase velocity in the case of the low (full) frequency range theory, and that the exact expression for the Q factor contains an additive correction due to viscoelastic interphase interaction.

In dissipative media the group velocity $C_g = d\omega/dk$ ceases to provide a clear physical meaning, whereas the energy velocity C_e can be defined similarly to conservative systems as the ratio between the average energy flux and average mechanical energy[25, 26],

$$C_g \neq C_e = \frac{\bar{F}}{\bar{E}}. \tag{8.1}$$

In the case of homogeneous plane waves the equality between the velocity of energy transport and the phase velocity $C_e = c_\phi$ is commonly observed in dissipative media what includes both electromagnetic [117, 78, 79, 35, 77] and mechanical wave propagation [22, 20, 78, 31]. However, in general this equality does not hold [79, 80].

As in regards the waves propagating in porous media the energy velocity has been discussed in [29, 30, 31, 104], where the results were established for the very general anisotropic

formulation. In anisotropic media the energy velocity vector does not necessarily coincide with the wave vector [8], nevertheless, the relation between the energy velocity and the phase velocity can also be established. The equality between the projection of the energy velocity vector onto the propagation direction and the magnitude of the phase velocity

$$\vec{C}_e \cdot \frac{\vec{k}}{|\vec{k}|} = \frac{\omega}{|\vec{k}|}, \tag{8.2}$$

has been verified for the waves propagating in anisotropic elastic media[8], anisotropic viscoelastic media [28, 31], anisotropic poro-viscoelastic media in the low frequency range [30], and anisotropic poro-viscoelastic media in the full frequency range [31]. Numerical studies of the energy velocity for the waves in anisotropic porous and poro-viscoelastic media can be found in [29, 104].

In the framework of Biot's isotropic full frequency range formulation [12] the expression for the energy velocity derived herein for the waves traveling in the negative x direction can be represented as follows,

$$C_e^n = \frac{\omega \mathcal{F}_{_R}}{\mathrm{Re}(k_n)\mathcal{F}_{_R} + \mathrm{Im}(k_n)\mathcal{F}_{_I}}, \quad n = 1, 2, s, \tag{8.3}$$

where $k_n = k_n(\omega)$ denote complex wavenumbers of P1, P2 and S-waves respectively, and $\mathcal{F} = \mathcal{F}_{_R} + i\mathcal{F}_{_I}$ is the frequency correction factor [12]. According to (8.3) the energy velocity equals the phase velocity when interphase interaction is purely viscous ($\mathcal{F} \equiv 1$), and exceeds the phase velocity when interphase interaction is viscoelastic ($\mathcal{F}_{_I} \neq 0$). On the other hand, the very general result for poro-viscoelastic waves in anisotropic media [31] indicates the equality between the energy velocity and the phase velocity for the plane homogeneous waves propagating in isotropic poroelastic continuum as must be recovered in the appropriate limiting case. The disagreement between the two results outlined above is subsequently addressed.

Apart from the energy velocity an important energy transport characteristic of absorbing media is the Q factor (quality factor) which serves to estimate the number of cycles required for the mechanical energy to fall off significantly. In the case of dissipative mechanical systems it can be formally defined as [2, 50]

$$Q^{-1} = -\frac{\Delta \bar{E}}{2\pi \bar{E}}, \tag{8.4}$$

where $\bar{E}$ is the average mechanical energy in the volume while $-\Delta\bar{E}$ is the average energy loss in one cycle. It is important to stress that a variety of other definitions are currently in use, e.g. [20, 30, 31, 104].

The general definition (8.4) is rarely of direct use and it is common to use simple approximate expressions instead. Assuming weak dissipation $Q \gg 1$, so that successive peaks have almost the same energy one arrives at the following approximation [50]

$$Q \approx -\frac{\mathrm{Re}(k)}{2\mathrm{Im}(k)}. \tag{8.5}$$

The kinematic, or high Q approximation (8.5) is widely used in the theory of viscoelastic media [22, 20] as well as in acoustics of porous media [53, 5, 124, 116, 103]. In the low frequency range Biot's theory [11] the interphase interaction is of purely viscous nature and it can be easily verified that the result (8.5) holds exactly. For instance, such an equality also known for homogeneous plane waves in the case of isotropic viscoelastic media [22, 31].

In the higher frequency range Biot's theory [12] when interphase interaction is viscoelastic the result $Q = -k_{R}/2k_{I}$ is no longer valid exactly. As derived in the following, the general exact result in accord with the definition (8.4) valid in the full frequency range reads as follows,

$$Q_n = -\frac{\mathrm{Re}(k_n)}{2\mathrm{Im}(k_n)} - \frac{\mathcal{F}_{I}}{2\mathcal{F}_{R}}, \quad n = 1, 2, s \tag{8.6}$$

and now contains the additive correction due to high frequency viscoelastic effects.

The derivation of the expressions for the energy velocity follows the modewise energy balance equation, originally presented in [56] for the longitudinal waves and developed herein for the shear wave. Using this approach the energy balance equation relates kinetic energy, potential energy, viscous power dissipation and elastic energy stored in one cycle associated with each wave.

The chapter is organized as follows. Section 8.1 contains the necessary preliminaries including the energy conservation forms related to the propagation of both longitudinal and shear waves. Special attention is paid to the direct analogy with viscoelastic behavior (summarily discussed above in Chapters 2, 7). These results are further used in the derivation of a modewise energy balance equation [56] which relates the average over one cycle kinetic energy, potential energy, viscous energy losses and elastic energy stored. These equations provide the necessary foundation for the derivation of the expressions for the energy velocity in Section 8.2, and for the Q factor in Section 8.3. Numerical results for the energy velocity and Q factor are presented for the set of parameters for water saturated Berea sandstone in Section 7.6.2. The conclusions are summarized in Section 8.5.

8.1 Viscoelastic behavior analogy and energy conservation forms

In the governing equations [12]

$$(\lambda+\mu)\,\nabla\nabla\cdot\mathbf{u}+\mu\vec{\nabla}^2\mathbf{u}+Q\nabla\nabla\cdot\mathbf{U}=\rho_{11}\ddot{\mathbf{u}}+\rho_{12}\ddot{\mathbf{U}}+b\mathcal{F}\left(\dot{\mathbf{u}}-\dot{\mathbf{U}}\right), \tag{8.7}$$

$$Q\nabla\nabla\cdot\mathbf{u}+R\nabla\nabla\cdot\mathbf{U}=\rho_{12}\ddot{\mathbf{u}}+\rho_{22}\ddot{\mathbf{U}}-b\mathcal{F}\left(\dot{\mathbf{u}}-\dot{\mathbf{U}}\right) \tag{8.8}$$

the frequency dependent correction factor $\mathcal{F}$ is included to take into account the deviation of the pore fluid motion from the Poiseuille flow in the higher frequency range. The complex viscosity $\mathcal{F}\eta_f$ introduced via frequency correction factor [12] (and via viscodynamic operator in subsequent formulation [14]) results from the analysis of the shear stress and shear stain rate at the pore wall.

Complex viscosity $\eta^*=\eta'-i\eta''$ defined as the ratio between the shear stress and shear strain rate, i.e. $\sigma=\eta^*\dot{\epsilon}$, is commonly used to describe viscoelastic liquids [17, 47]. The real (imaginary) components of complex viscosity are associated with the components of shear stress which are in phase (out of phase) with the strain rate. The stress-strain relation $\sigma=\eta^*\dot{\epsilon}$ is equivalent to a Kelvin-Voigt model $\sigma=E\epsilon+\eta\dot{\epsilon}$ characterized by the elastic energy storage $\mathcal{E}=\frac{1}{2}E\epsilon^2$ and dissipation rate $2D=\eta\dot{\epsilon}^2$ [17]. In terms of complex viscosity these quantities can be expressed as $\mathcal{E}=1/2\eta''\omega\epsilon^2$ and $2D=\eta'\dot{\epsilon}^2$ accordingly.

A direct analogy with the complex viscosity encountered in Biot's theory can be pointed out. Similarly to the case of a viscoelastic material the real and imaginary parts of the complex viscosity quantify viscous dissipation and elastic energy storage during interphase interaction, respectively. The energy conservation form established for the low frequency range theory [in which case $\mathcal{F}$ is set to equal unity in (8.7), (8.8)] reads [39]

$$\dot{E}+\nabla\cdot\mathbf{F}=-2D, \tag{8.9}$$

where E denotes the total mechanical energy density $E=T+V$, and $F_i=-\sigma_{ij}\dot{u}_j-s\dot{U}_j\delta_{ij}$ is the Poynting vector. As it is subsequently demonstrated, in the higher frequency range [provided $\mathrm{Im}(\mathcal{F})>1$, $\mathrm{Im}(\mathcal{F})>0$] the energy conservation form contains an additional term 2Ω in the right hand side due to the elastic energy stored,

$$\dot{E}+\nabla\cdot\mathbf{F}=-2D+2\Omega, \tag{8.10}$$

so that the result for the low frequency theory (8.9) can be recovered from (8.10) in the limiting case $\mathcal{F}\to 1$.

8.1.1 Longitudinal waves

Consider the one dimensional version of Eqs.(8.7),(8.8). Assuming $\mathbf{u} = (u(x), 0, 0)$ and $\mathbf{U} = (U(x), 0, 0)$ one arrives at the equations governing the propagation of longitudinal waves (P1 and P2-waves),

$$\begin{aligned} (\lambda + 2\mu)\, u_{xx} + QU_{xx} &= \rho_{11}\ddot{u} + \rho_{12}\ddot{U} + b\mathcal{F}\left(\dot{u} - \dot{U}\right), \\ Qu_{xx} + RU_{xx} &= \rho_{12}\ddot{u} + \rho_{22}\ddot{U} - b\mathcal{F}\left(\dot{u} - \dot{U}\right). \end{aligned} \tag{8.11}$$

Due to the presence of the complex coefficient these equations can only be satisfied with complex form solutions $u = u_R + iu_I$, $U = U_R + iU_I$. Consequently, Eqs. (8.11) can be recast in the form

$$(\lambda + 2\mu)\, u_{Rxx} + QU_{Rxx} = \rho_{11}\ddot{u}_R + \rho_{12}\ddot{U}_R + b\mathcal{F}_R\left(\dot{u}_R - \dot{U}_R\right) - b\mathcal{F}_I\left(\dot{u}_I - \dot{U}_I\right), \tag{8.12}$$

$$Qu_{Rxx} + RU_{Rxx} = \rho_{12}\ddot{u}_R + \rho_{22}\ddot{U}_R - b\mathcal{F}_R\left(\dot{u}_R - \dot{U}_R\right) + b\mathcal{F}_I\left(\dot{u}_I - \dot{U}_I\right). \tag{8.13}$$

The characteristic feature of the above representation is the explicit separation of the forces acting on solid by fluid (and similarly on fluid by solid) into the contribution of the viscous force which is out of phase with relative solid velocity $(\dot{u}_R - \dot{U}_R)$, and the contribution of the elastic shear force which is in phase with the relative solid displacement $(u_R - U_R)$. Indeed, noting an obvious identity $\dot{u}_I = \omega u_R$, these are recognized in the last two terms of the momentum equation (8.12) respectively,

$$-b\mathcal{F}_R\left(\dot{u}_R - \dot{U}_R\right) + b\omega\mathcal{F}_I\left(u_R - U_R\right). \tag{8.14}$$

Multiplying Eqs. (8.12) and (8.13) by $\dot{u}_R$ and $\dot{U}_R$ respectively, and adding them together one arrives at one-dimensional version of the conservation form (8.10) with

$$2T = \rho_{11}\dot{u}_R^2 + 2\rho_{12}\dot{u}_R\dot{U}_R + \rho_{22}\dot{U}_R^2, \tag{8.15}$$

$$2V = (\lambda + 2\mu)u_{Rx}^2 + 2Qu_{Rx}U_{Rx} + RU_{Rx}^2, \tag{8.16}$$

$$F = -(\lambda + 2\mu)u_{Rx}\dot{u}_R - Q(u_{Rx}\dot{U}_R + U_{Rx}\dot{u}_R) - RU_{Rx}\dot{U}_R, \tag{8.17}$$

$$2D = b\mathcal{F}_R(\dot{u}_R - \dot{U}_R)^2, \tag{8.18}$$

$$2\Omega = b\omega\mathcal{F}_I(u_R - U_R)(\dot{u}_R - \dot{U}_R). \tag{8.19}$$

Here F denotes the energy flux (as in agreement with the general expression for poroacoustic Poynting vector $P_i = -\sigma_{ij}\dot{u}_j - s\dot{U}_i$), while the terms $2D$, 2Ω represent power dissipation per unit volume, and the rate of change of the elastic stored energy per unit volume, respectively.

As was discussed above, viscoelastic interphase interaction implies elastic energy storage during each cycle in addition to the viscous energy losses as reflected by the presence of the two different terms in the right hand side of Eq. (8.10), 2Ω and $2D$, respectively. Averaging over a period one finds that $\bar{\Omega} = 0$, while in general $\bar{D} > 0$.

Viscous power dissipation $-2\bar{D}$ (8.18) is given by the product of the viscous force [first summand in (8.14)] and the relative solid velocity. Alternatively, viscous dissipation can also be characterized by the following average quantity $2\bar{D} \cdot 2\pi/\omega$, which represents viscous energy losses in one cycle.

The elastic stored energy $\mathcal{E}$ can be expressed as half the product the elastic shear force component [second summand in (8.14)] times relative solid displacement,

$$\mathcal{E} = \frac{1}{2} b\omega \mathcal{F}_{I} \left(u_{R} - U_{R}\right)^{2}, \tag{8.20}$$

in direct analogy with the elastic potential energy in mechanical systems. Consequently, the average elastic energy stored in one cycle can be represented as follows,

$$\bar{\mathcal{E}} = \frac{1}{4} \omega b \mathcal{F}_{I} (u u^{*} - u^{*} U - u U^{*} + U U^{*}), \tag{8.21}$$

and therefore $2\bar{\mathcal{E}}$ provides the maximum elastic energy stored over one cycle. Finally, in the case of harmonic motion

$$\frac{d\mathcal{E}}{dt} = 2\Omega, \tag{8.22}$$

so that 2Ω provides the rate of change of the elastic stored energy. As long as the elastic energy stored $\mathcal{E}$ builds to a maximum followed by recovery over each cycle, the average quantity $2\bar{\Omega}$ is necessarily zero.

The governing equations (8.11) in frequency-wavenumber space can be written as follows,

$$-\omega^{2}(\rho_{11} u + \rho_{12} U) + k^{2} \left[(\lambda + 2\mu) u + Q U\right] + i\omega b \mathcal{F} (u - U) = 0, \tag{8.23}$$

$$-\omega^{2}(\rho_{12} u + \rho_{22} U) + k^{2} (Q u + R U) - i\omega b \mathcal{F} (u - U) = 0. \tag{8.24}$$

For a given set of parameters ω Eqs. (8.23), (8.24) represents a standard eigenvalue problem for k^2 (or degenerate quadratic eigenvalue problem for k) which admits a simple analytic solution [12]. Two possible longitudinal modes exist in Biot's theory, the so-called P1 and P2-waves, which we take to correspond to the eigenvalues k_1, k_2 and eigenvectors (u_1, U_1) and (u_2, U_2), respectively.

Each characteristic solution ($n = 1, 2$) must satisfy the following relations (obtained by multiplication of Eqs. (8.23) and (8.24) by u^* and U^*, respectively, and adding the two equations),

$$
\begin{aligned}
-\omega^2 \left[\rho_{11} u_n u_n^* + \rho_{12}(u_n^* U_n + u_n U_n^*) + \rho_{22} U_n U_n^*\right] + \\
+k_n^2 \left[(\lambda + 2\mu) u_n u_n^* + Q(u_n^* U_n + u_n U_n^*) + R U_n U_n^*\right] + \\
+i\omega b \mathcal{F}(u_n u_n^* - u_n^* U_n - u_n U_n^* + U_n U_n^*) = 0.
\end{aligned} \tag{8.25}
$$

In the form of the modewise energy balance this reads (see Appendix C.1)

$$
-\bar{T}_n + \Delta_n \bar{V}_n + i\bar{D}_n/\omega - \bar{\mathcal{E}}_n = 0, \quad \Delta_n = k_n^2/|k_n|^2, \tag{8.26}
$$

where $\bar{T}_n$, $\bar{V}_n$ are average kinetic and potential energies associated with longitudinal modes, $\bar{D}_n/\omega$ can be interpreted as the $1/4\pi$ fraction of the energy loss due to the viscous dissipation, and $\bar{\mathcal{E}}_n$ is one half the maximum elastic energy stored in one cycle. Equipartition of energy $\bar{T}_n = \bar{V}_n$ can be recovered from the Eq. (8.26) in the limiting case of no dissipation.

8.1.2 Shear wave

Assuming $\mathbf{u} = (0, u(x), 0)$ and $\mathbf{U} = (0, U(x), 0)$ in Eqs. (8.7), (8.8) one arrives at the equations governing the propagation of the shear wave (S-wave),

$$
\begin{aligned}
\mu u_{xx} &= \rho_{11}\ddot{u} + \rho_{12}\ddot{U} + b\mathcal{F}\left(\dot{u} - \dot{U}\right), \\
0 &= \rho_{12}\ddot{u} + \rho_{22}\ddot{U} - b\mathcal{F}\left(\dot{u} - \dot{U}\right).
\end{aligned} \tag{8.27}
$$

In analogy with Eqs. (8.12), (8.13) one arrives at

$$
\mu u_{Rxx} = \rho_{11}\ddot{u}_R + \rho_{12}\ddot{U}_R + b\mathcal{F}_R\left(\dot{u}_R - \dot{U}_R\right) - b\mathcal{F}_I\left(\dot{u}_I - \dot{U}_I\right), \tag{8.28}
$$

$$
0 = \rho_{12}\ddot{u}_R + \rho_{22}\ddot{U}_R - b\mathcal{F}_R\left(\dot{u}_R - \dot{U}_R\right) + b\mathcal{F}_I\left(\dot{u}_I - \dot{U}_I\right). \tag{8.29}
$$

The corresponding energy conservation form (8.10) is now satisfied with

$$
\begin{aligned}
2T &= \rho_{11}\dot{u}_R^2 + 2\rho_{12}\dot{u}_R\dot{U}_R + \rho_{22}\dot{U}_R^2, && (8.30)\\
2V &= \mu u_{Rx}^2, && (8.31)\\
F &= -\mu u_{Rx}\dot{u}_R, && (8.32)\\
2D &= b\mathcal{F}_R(\dot{u}_R - \dot{U}_R)^2, && (8.33)\\
2\Omega &= b\omega\mathcal{F}_I(u_R - U_R)(\dot{u}_R - \dot{U}_R), && (8.34)
\end{aligned}
$$

so that the expressions for T, D and Ω are completely analogous to those in the case of longitudinal waves.

In the case of the shear wave the governing equations (8.27) in the frequency-wavenumber space read as follows

$$-\omega^2(\rho_{11}u + \rho_{12}U) + k^2\mu u + i\omega b\mathcal{F}(u - U) = 0, \tag{8.35}$$

$$-\omega^2(\rho_{12}u + \rho_{22}U) - i\omega b\mathcal{F}(u - U) = 0. \tag{8.36}$$

Unlike the case of longitudinal waves for a given ω (8.35) and (8.36) are uncoupled equations for u and U. The dispersion relation for the shear wave $k_s = k_s(\omega)$ can thus be easily derived. For a given ω (8.35) and (8.36) can be satisfied with a corresponding value of k_s and arbitrary amplitudes u_s and U_s related via Eq. (8.36).

Multiplying (8.35), (8.36) by u^* and U^*, respectively, and adding the two equations one arrives at

$$\begin{aligned}-\omega^2 \left[\rho_{11}u_s u_s^* + \rho_{12}(u_s^* U_s + u_s U_s^*) + \rho_{22}U_s U_s^*\right] + \\ +\mu k_s^2 u_s u_s^* + i\omega b\mathcal{F}(u_s u_s^* - u_s^* U_s - u_s U_s^* + U_s U_s^*) = 0.\end{aligned} \tag{8.37}$$

In the form of the modewise energy balance this reads (see Appendix C.2)

$$-\bar{T}_s + \Delta_s \bar{V}_s + i\bar{D}_s/\omega - \bar{\mathcal{E}}_s = 0, \quad \Delta_s = k_s^2/|k_s|^2, \tag{8.38}$$

and admits the same physical interpretation as in the above-mentioned longitudinal waves case.

The modewise energy balance equations (8.26) and (8.38) provide a necessary foundation for further analysis.

8.2 Energy velocity

The expression for the energy velocities of both longitudinal modes in the full frequency Biot's theory can be derived with the use of the modewise energy balance equations (8.26) and (8.38). As long as the form of the modewise energy balance equations for longitudinal waves and shear wave is identical, the general analysis can include both cases. Derivations, results and conclusions in this and the following section thus apply to both longitudinal waves, as well as the shear wave.

Without loss of generality consider the energy balance equation,

$$-\bar{T}_n + \Delta_n \bar{V}_n + i\bar{D}_n/\omega - \bar{\mathcal{E}}_n = 0, \quad \Delta_n = k_n^2/|k_n|^2 \tag{8.39}$$

where $n = 1, 2, s$ in the cases of P1, P2 and S-wave respectively. Taking the real and imaginary part of (8.39) one finds

$$\begin{cases} -\bar{T}_n + \mathrm{Re}(\Delta_n)\bar{V}_n - \bar{\mathcal{E}}_n = 0, \\ \quad \mathrm{Im}(\Delta_n)\bar{V}_n + \bar{D}_n/\omega = 0. \end{cases} \tag{8.40}$$

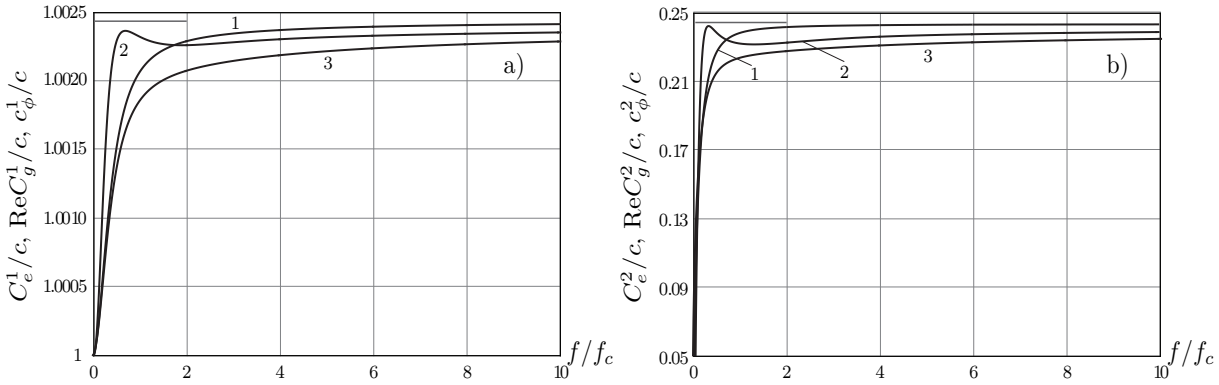

Figure 8.1: a) P1-wave, b) P2-wave; energy velocities C_e^n/c (1), group velocities $\mathrm{Re}C_g^n/c$ (2) and phase velocities c_ϕ^n/c (3) versus frequency f/f_c. Horizontal lines indicate wavefront velocities V_{p1}^∞ and V_{p2}^∞ (Table 5.1).

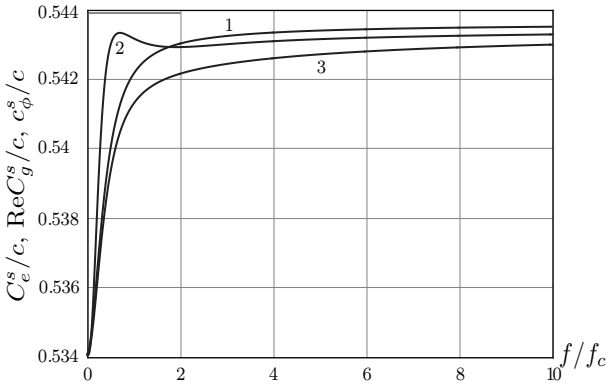

Figure 8.2: S-wave; energy velocity C_e^s/c (1), group velocity $\mathrm{Re}C_g^s/c$ (2) and phase velocity c_ϕ^s/c (3) versus frequency f/f_c. Horizontal line indicates wavefront velocity V_s^∞ (Table 5.1).

As follows from (7.16) and the obvious identity $\bar{D}_n/\bar{\mathcal{E}}_n = \omega\mathcal{F}_R/\mathcal{F}_I$, the modewise energy partition between the kinetic and potential energy can be quantified as follows

$$\frac{\bar{T}_n}{\bar{V}_n} = \mathrm{Re}(\Delta_n) + \frac{\mathcal{F}_I}{\mathcal{F}_R}\mathrm{Im}(\Delta_n), \quad n = 1, 2, s. \tag{8.41}$$

Moreover, according to (C.2), (C.3), (C.6) and (C.7) the following identity holds for all three waves

$$\frac{\bar{F}_n}{\bar{V}_n} = \frac{2\omega\mathrm{Re}(k_n)}{|k_n|^2}, \quad n = 1, 2, s. \tag{8.42}$$

Note that the right hand sides of Eqs. (8.41) and (8.42) only require the solution of the corresponding dispersion relations $k_n = k_n(\omega)$, $n = 1, 2, s$.

Following the definition of the energy velocity (8.1), and taking into account the identities (8.41) and (8.42) we derive for the energy velocities ($\bar{E}_n = \bar{T}_n + \bar{V}_n$),

$$C_e^n = \frac{\bar{F}_n}{\bar{E}_n} = \frac{2\omega\mathrm{Re}(k_n)}{|k_n|^2\left[1 + \mathrm{Re}(\Delta_n) + \mathrm{Im}(\Delta_n)\mathcal{F}_I/\mathcal{F}_R\right]},$$

which finally simplifies to

$$C_e^n = \frac{\omega\mathcal{F}_R}{\mathrm{Re}(k_n)\mathcal{F}_R + \mathrm{Im}(k_n)\mathcal{F}_I}. \tag{8.43}$$

In the low frequency range theory [11] the frequency correction factor can be neglected ($\mathcal{F} \equiv 1$), and consequently, for both longitudinal and shear waves

$$C_e^n = c_\phi^n, \tag{8.44}$$

so that the velocities of energy transport equal the corresponding phase velocities. This result is in agreement with the more general result reported for anisotropic poro-viscoelastic media reported in [30].

In contrast, in a full frequency range theory [12], when the frequency correction factor $\mathcal{F}$ is included, we find that the energy velocity always exceeds the corresponding phase velocity. From the expression (8.43) with $\mathrm{Im}(k_n) < 0$ for the waves traveling in negative x direction it follows that

$$C_e^n > c_\phi^n. \tag{8.45}$$

Therefore, in a full frequency range, the energy velocity of poroelastic acoustic waves exceeds the corresponding phase velocity of the waves. The latter is at odds with the result for the energy velocity in anisotropic poro-viscoelastic media (8.2) reported in [31], which implies the equality between the two for homogeneous waves in the full frequency range (see Section 8.5 for discussion).

Finally, we note that the energy velocity (8.43) must never exceed the corresponding high frequency limiting values of the phase velocity V_n^∞ (Table 5.1),

$$c_\phi^n < C_e^n < V_n^\infty, \tag{8.46}$$

in accord with the causality principle.

8.3 Q factor and energy damping length

The expression for the Q factor can be derived with the use of the identities (8.41) and

$$\frac{\bar{D}_n}{\bar{V}_n} = -\omega \mathrm{Im}(\Delta_\mathrm{n}), \tag{8.47}$$

which both follow the modewise energy balance (8.39). According to (8.4), (8.41) and (8.47),

$$Q_n = \frac{\omega \bar{E}_n}{2\bar{D}_n} = -\frac{[1 + \mathrm{Re}(\Delta_n) + \mathrm{Im}(\Delta_n)\mathcal{F}_I/\mathcal{F}_R]}{2\mathrm{Im}(\Delta_n)} = -\frac{\mathrm{Re}(k_n)}{2\mathrm{Im}(k_n)} - \frac{\mathcal{F}_I}{2\mathcal{F}_R}. \tag{8.48}$$

In the low frequency range the correction term vanishes, and the above expression takes the familiar form [53, 20]

$$Q_n = -\frac{\mathrm{Re}(k_n)}{2\mathrm{Im}(k_n)}. \tag{8.49}$$

As long as both the Q factor and the distance traveled by the wave in one period vary with frequency it is also convenient to introduce the energy damping length in order to estimate the distance over which a significant portion of the wave energy dissipates. The energy damping length D_δ can be defined as the product of the Q factor and the wavelength λ,

$$D_\delta = Q\lambda = \frac{2\pi Q}{k_R} = -\pi \frac{k_R \mathcal{F}_R + k_I \mathcal{F}_I}{k_R k_I \mathcal{F}_R}. \tag{8.50}$$

Unlike the Q factor the energy damping length decreases with frequency in the high frequency range. As $\omega \to \infty$ the small parameter in the eigenvalue problem (8.23), (8.24) and in the system (8.35), (8.36) is $\mathcal{F}/\omega = O(\omega^{-1/2})$, since $\mathcal{F}_R = O(\omega^{1/2})$, $\mathcal{F}_I = O(\omega^{1/2})$ [12]. Thus, k_n $(n = 1, 2, s)$ can be expanded in inverse powers of $\omega^{1/2}$ as follows,

$$k_n/\omega = \lambda_{n0} + i\lambda_{n1}\omega^{-\frac{1}{2}} + \lambda_{n2}\omega^{-\frac{1}{2}} + i\lambda_{n3}/\omega^{-1} + \ldots,$$

and consequently as $\omega \to \infty$, according to (8.50) $D_\delta^n = O(\omega^{-1/2})$, while according to (8.48) $Q_n = O(\omega^{1/2})$.

These considerations are illustrated with an example in the following section.

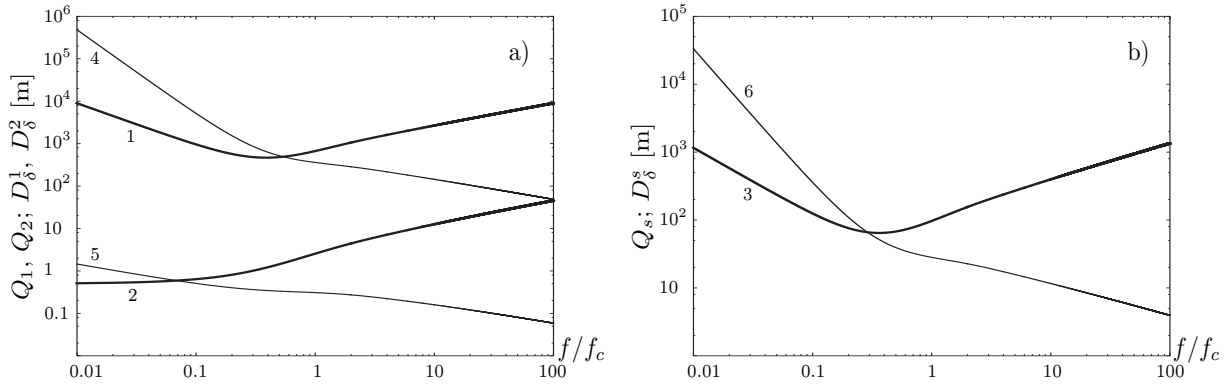

Figure 8.3: a) P1 and P2-wave, b) S-wave; Q factors Q_1 (1), Q_2 (2), Q_s (3), and energy damping lengths D^1_δ (3), D^2_δ (4), D^s_δ (5) versus frequency f/f_c.

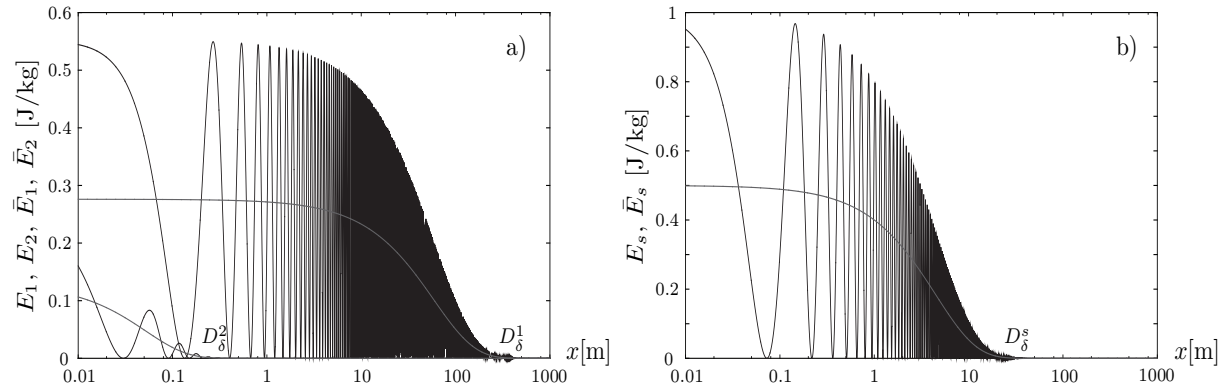

Figure 8.4: a) P1 and P2-wave, b) S-wave; mechanical energy densities E_1, E_2, E_s (at fixed time t, and $f/f_c = 1$) and corresponding average over a period quantities $\bar{E}_1$, $\bar{E}_2$, $\bar{E}_s$ versus x. Energy damping lengths D^1_δ, D^2_δ, D^s_δ are indicated.

8.4 Numerical results

Numerical results are obtained for water saturated Berea sandstone with the physical properties provided in Table 5.1. Generalized poroelastic parameters λ, Q, and R are related to the porosity, the solid and fluid bulk moduli, the bulk modulus of the porous drained matrix and the shear modulus via Gedanken experiments [16]; reference phase densities ρ_{ij} are related to porosity, tortuosity, grain and saturating fluid densities [16] (see Appendix D).

The dispersion relation for the longitudinal modes has the form [12]

$$(q_{11}q_{22} - q_{12}^2)z^2 - (q_{22}\gamma_{11} + q_{11}\gamma_{22} - 2q_{12}\gamma_{12})z + (\gamma_{11}\gamma_{22} - \gamma_{12}^2) + \frac{ib\mathcal{F}(\kappa)}{\rho\omega}(z-1) = 0, \quad (8.51)$$

where $z_{1,2} = (ck_{1,2}/\omega)^2$, c and ρ are characteristic density and velocity, q_{ij} and γ_{ij} are normalized Biot's parameters and normalized reference densities, $\kappa = \delta(f/f_c)^{1/2}$ and characteristic frequency f_c defined as [12]

$$f_c = \frac{b}{2\pi\rho(\gamma_{12} + \gamma_{22})}. \quad (8.52)$$

In the case of the shear wave the dispersion relation is

$$z_s^2 = \frac{H}{\mu}\left[\gamma_{11} + \gamma_{12}M_s - \frac{ib\mathcal{F}(\kappa)}{\rho\omega}(1 - M_s)\right], \quad M_s = -\frac{\gamma_{12} + ib\mathcal{F}(\kappa)/\rho\omega}{\gamma_{22} - ib\mathcal{F}(\kappa)/\rho\omega}, \quad (8.53)$$

where $z_s = (ck_s/\omega)^2$. The frequency correction factor used in the calculations is represented in terms of the Bessel-Kelvin zero order functions [12]

$$\mathcal{F}(\kappa) = \frac{1}{4}\left(\frac{\kappa T(\kappa)}{1 - \frac{2}{i\kappa}T(\kappa)}\right), \quad T(\kappa) = \frac{\mathrm{ber}'(\kappa) + i\mathrm{bei}'(\kappa)}{\mathrm{ber}(\kappa) + i\mathrm{bei}(\kappa)}.$$

Figures 8.1 and 8.2 represent the results for the energy velocity in accordance with (8.43). The results for the group and phase velocities are also included. The energy velocities are found to be slower (faster) than the group velocity in the low (high) frequency range, however, they never exceed the values of the wavefront velocities ($C_e^1 < V_{p1}^\infty$, $C_e^2 < V_{p2}^\infty$, $C_e^s < V_s^\infty$) in accord with the causality principle. The results of Figures 8.1 and 8.2 thus verify the theoretical predictions (8.44) and (8.45).

In particular, it can also be noted that group velocities are always greater than the corresponding phase velocities, $C_g^n > c_\phi^n$ $(n = 1, 2, s)$, which implies anomalous dispersion [80]. In analogy with electromagnetic waves one can think of $\sqrt{z_n} = ck_n/\omega$ $(n = 1, 2, s)$ as

the complex refractive index. Taking the real part $\mathrm{Re}\sqrt{z_n} = ck_{nR}/\omega$, and differentiating this relation with respect to ω one finds

$$\frac{d}{d\omega}\left(\mathrm{Re}\sqrt{z_n}\right) = \frac{c}{\omega}\left(\frac{1}{C_g^n} - \frac{1}{c_\phi^n}\right). \tag{8.54}$$

The nondimensional slowness $\mathrm{Re}\sqrt{z_n}$ is a decreasing function of ω [as long as the corresponding phase velocities increase with ω, e.g. [12]], and it thus follows from Eq. (8.54) that indeed $C_g^n > c_\phi^n$ $(n = 1, 2, s)$ for waves in a medium with physically meaningful mechanical parameters.

Figure 8.3 provides the results for the Q factors according to the expression (8.48), as well as for the energy damping lengths (8.50) versus frequency. The results for the Q factor suggest that in practice, the correction term $\mathcal{F}_I/2\mathcal{F}_R$ in expression (8.48) can be neglected. While this correction is definitely negligible in the case of the weakly damped P1-wave and S-wave as long as $Q \gg 1$, while $0 \leq \mathcal{F}_I/\mathcal{F}_R < 1$, we find this correction to be insignificant even in the case of the P2-wave, with comparatively low values of the Q factor. Indeed, in the low frequency range the P2-wave is overdamped, $Q \approx 1/2$ and the correction term is negligible as long as $\mathcal{F}_I \ll 1$. As frequency increases, the wave is no longer overdamped, the Q factor exceeds unity and increases as $Q \sim \omega^{\frac{1}{2}}$, while the value of the correction term always remains less than 1/2. These considerations justify the use of the approximation (8.5) as an accurate approximation valid in the full frequency Biot's theory. Note that $Q_2 \approx 1/2$ in the low frequency range in accordance with theoretical predictions [53], however, as frequency increases, Q_2 exceeds unity indicating the possibility of resonant excitation.

The numerical results indicate that the energy damping length decreases with frequency in accordance with the theoretical prediction. In particular, the maximum energy damping length $Q_2\lambda_2$ for the P2-wave achieved at low, seismic frequencies is on the order of one meter. This result theoretically reconfirms the near impossibility of detecting the P2-wave during field measurements [91] (on geophysical scales).

Figure 8.4 serves an illustration of the predictive power of the damping length estimated by Eq.(8.50). Mechanical energies (per unit reference mass) associated with P1, P2 and S-wave, and their corresponding average values are plotted versus x coordinate. These results for longitudinal waves require the solution of the eigenvalue problem (8.23), (8.24), while in the case of the shear wave the amplitudes are chosen arbitrarily to yield (8.36).

Finally, we note that in the case of longitudinal waves the results for the energy velocity (8.43) and Q factor (8.48), which depend only on the wavenumber, can be verified by comparing with values yielded by the definitions (7.2), (8.4), which require directly computed eigenvalues and eigenvectors of the eigenvalue problem (8.23), (8.24). Similar benchmark solutions can be established for the shear wave.

8.5 Chapter Summary

The main results can be summarized as follows. Exact closed form expressions which quantify the energy velocity (8.43) and Q factor (8.48) are derived following the very general definitions (7.2) and (8.4), and these only require the solutions of the dispersion relations. The main attention is paid to the full frequency range theory and as a consequence, to the treatise of the frequency correction factor. Strictly speaking, in the higher frequency range the reference phase densities ρ_{ij} are no longer constants, these become frequency dependent due to the corresponding changes in the added mass [15, 14]. This additional refinement is left beyond the scope of the present derivation as long as it would neither affect the derivation and resulting expressions obtained herein nor change the main conclusions.

The relationship obtained for the energy velocity indicates that in the low frequency regime the energy velocity of P1, P2 and S-waves exactly equals (exceeds) the corresponding phase velocity in the case of low (full) frequency range Biot's theory. In other words, in both low and high frequency limits the equality between the energy velocity and the phase velocity is observed, whereas in the intermediate frequency range the energy velocity is found to exceed the corresponding phase velocity. In practice, the difference between the two is quantitatively subtle.

The inconsistency of the above conclusions with the result earlier obtained for a more general anisotropic formulation [31] can be explained as follows. The interpretation of the kinetic energy provided in [31] follows the mathematical derivation of the energy balance equation and leads to different expressions for the kinetic energy, one for the low frequency range [30], which is consistent with Biot's formulation for anisotropic media [15], and one for the high frequency range [31] which accounts for an additional term (containing viscosity) in the expression for the kinetic energy. Moreover, the elastic stored energy in the higher frequency range is not quantified explicitly, therefore it must be absorbed by other terms. Conversely, unlike the previous results for the energy balance equation [31, 36, 104], the derivation provided herein does not require any changes in the expression for the kinetic energy depending on whether purely viscous or viscoelastic interphase interaction is considered; the viscoelastic effects are reflected by an additional term in the energy balance equation which takes into account the elastic energy stored.

The exact expression for the Q factor valid in the full frequency range contains a correction term due to viscoelastic effects. In the low frequency range this correction vanishes in which case the kinematic approximation provides the exact values of the Q factor as in the case of isotropic viscoelastic media. In the higher frequency range this correction has to be included to obtain the exact value of the Q factor. However, in practice, we find this correction to be insignificant, what reconfirms the validity of the kinematic approximation $Q \approx -k_R/2k_I$ for poroelastic waves in the higher frequency range from energetic considerations.

Chapter 9

Conclusions

The main conclusions can be divided into two parts. While the first logical part of the thesis is dedicated to the quantitative analysis of energy partition among poroelastic waves, the second part investigates fundamental characteristics of the energy transport in absorbing media, namely, the velocity of energy transport and quality factor.

First of all, it is important to make several remarks on the energy balance equation (considered in detail in Chapter 2). In mathematical physics derivation of the energy balance equations is often a routine procedure. Thus, for example the energy balance equation for Biot's theory was derived by Deresiewicz [41] shortly after the fundamental theory had appeared, however, this result only applies to the low frequency range theory. In the higher frequency range one should include complex viscosity in the governing equations. The presence of the complex viscosity factor not only introduces additional difficulties in the derivation (since in this case the governing equations can be satisfied exactly only with complex solutions), but also requires a more general physical interpretation of the energy balance equation to account for viscoelastic interphase interaction. Recently, the energy balance equation in the form of a complex Poynting theorem for the very general case of anisotropic poro-viscoelastic media was obtained by Carcione (2007) [31], and these results include the treatise of the frequency correction factor. However, the presented approach can be disputed since the expression for the kinetic energy [formula (7.486) p.311 in Carcione (2007)] upon the introduction of the complex viscosity is at odds with the definition of the kinetic energy as it is provided in the fundamental paper by Biot (1962) [15], namely [formula (8.16) in Biot (1962)]. The definition of the kinetic energy introduced in Carcione (2007) [31] depends on both viscosity and permeability in the higher frequency range, and this is disputable from a physical point of view. Indeed, the kinetic energy is the energy of motion and can only be defined as a positive-definite quadratic form in the solid and fluid velocities and the reference phase masses, irregardless of the kind of dissipation (or no dissipation) being considered. Consequently, in the energy balance equation presented

herein, the expression for the kinetic energy is in accord with the classical definition of Biot, so that its form is independent on the type of interphase interaction. Moreover, the resulting energy balance equation contains an additional term which quantifies the elastic energy storage during viscoelastic interphase interaction in the higher frequency range. Thus, the rate of change of the mechanical energy equals to the viscous power dissipation and the rate of change of the elastic energy stored (the time average of the latter quantity is obviously zero).

Secondly, the structure of the wave field in Lamb's problem is investigated. In absorbing media waves exhibit exponential attenuation, therefore a clear interpretation of the wave processes in the near field is important. The study based on complex analysis methods leads to the wavetrain decomposition of the wave field. Each wavetrain represents the superposition of the spectrum components over a certain wavenumber range, so that it consists of the waves which travel faster and exhibit higher attenuation with respect to the corresponding bulk modes (P1, P2 and S). Thus, it is only at a certain distance from the source that one may observe the wavelengths and attenuations predicted by the dispersion relations for longitudinal and shear waves. The asymptotic solution established for these wavetrains traveling along the plane boundary reveals an additional geometric attenuation $x^{-3/2}$, quantitatively equivalent to that encountered in the case of perfectly elastic media. The wavetrain decomposition is subsequently applied to the energy partition analysis.

The results for energy partition are obtained for two separate cases. In the case of inviscid pore fluid dissipation can be ignored, consequently, the waves propagate without dispersion. In the general case of viscous pore fluid the interphase interaction is viscous (viscoelastic) in the low (high) frequency range, the waves are dispersive and attenuated which introduces certain complications into the analysis.

In the case of non-dissipative porous media the energy analysis stems from the classical approach by Miller & Pursey [84, 85] primarily established for waves in a perfectly elastic medium, and is generalized herein for waves in a non-dissipative, saturated porous medium. Two possible situations, in which the Rayleigh wave is excited or unexcited in non-dissipative porous media are considered. A refined phasewise distinction between the powers transported by the particular wave species is obtained. The quantitative analysis of the energy budget indicates strong dependence of the relative power contributions on the driving configuration. Thus for example, the surface Rayleigh wave (when excited) can be either energetically predominant, as in the case of resonant excitation, or conversely, virtually unexcited depending on the parameters of the source. In particular, as follows from the analysis of the energy flux through the cylindrical surface the traveling shear wave in the fluid phase does not transfer energy. This somewhat paradoxical situation is caused by the absence of shear stresses in the pore fluid, so that the corresponding energy flux component vanishes. In the special case of complete absence of the Rayleigh wave, a significant increase of the power transfered by the P2-wave compared to the underdamped case is

observed. Moreover, in this case the P2-wave exhibits resonant-like behavior. The reasons for the energy redistribution between the P2-wave and the Rayleigh wave are subsequently explained.

In the general case of porous media saturated with viscous fluid the energy transported by the waves is dissipated. The analysis therefore follows the interface wavetrain solution of the Lamb's problem. In the case of a distributed source the character of the solution under the applied load and away from the source is different. It is shown that the interface displacements within the contact area (away from the source) represent a superposition of the standing (traveling) waves. The obtained solution allows the decomposition of the total power supplied by the source into constituents related to particular wave types. These decomposition results are verified to agree with the actual displacement fields. Again, as in the case of no dissipation relative power contributions vary significantly depending on the driving configuration. Special attention is paid to the upper cut-off frequency of the Rayleigh wave. It is demonstrated that beyond the cut-off frequency when the Rayleigh wave is no longer excited its virtual energy is instantly redistributed into the P2 motion. Such energy redistribution is caused by the influence of the leaky Rayleigh mode. An additional root of the Rayleigh dispersion equation is found situated on the "unphysical" Riemann sheet. When passing through the cut-off frequency the true Rayleigh mode disappears while the leaky mode root abruptly changes its location, moving towards the vicinity of the P2 branch cut. In turn, the corresponding P2-wavetrain exhibits an abrupt increase of amplitude, and consequently, one observes the remarkable predominance of the P2 displacements.

The remaining results are dedicated to the investigation of the complex group velocity, energy velocity and Q factor of poroelastic waves. The precise physical meaning of the complex group velocity often encountered in absorbing media, and in particular in the case of a saturated porous solid, is still unclear. However, it is demonstrated that in some special cases of non-conservative dynamical systems the exact physical interpretations of the complex group velocity can be established in terms of kinetic energy, energy flux and energy losses. This includes the mechanical waves governed by the damped Klein-Gordon equation and electromagnetic waves in partially conducting media. The general analysis is based on the application of the Lagrangian formalism to the coupled system of the Klein-Gordon equations. Under a certain approximation Biot's theory fits this formal description, and indeed the derived adiabatic approximation for the complex group velocities applies to both longitudinal poroelastic waves. Moreover, the actual complex group velocity of the P2-wave and its adiabatic approximation are found to be virtually indistinguishable.

Finally, the energy velocity and Q factor of poroelastic acoustic waves in the context of classical isotropic Biot theory are revisited. The modewise energy balance equations derived herein relate kinetic energy, potential energy, viscous power dissipation and elastic energy stored in one cycle associated with each wave. These allow the derivation of exact

closed form expressions for the energy velocity and Q factor for both longitudinal and shear waves from energy principles. Most notably, the analysis of the resulting expressions reveals the following. The energy velocity of both longitudinal and shear waves equals (exceeds) the corresponding phase velocity in the case of the low (full) frequency range theory. The exact expression for the Q factor contains an additive correction due to viscoelastic interphase interaction.

APPENDICES

Appendix A

Stresses in polar coordinates

$$\sigma_{_R} = (\lambda+2\mu)\frac{\partial u_{_R}}{\partial R} + \lambda\left(\frac{u_{_R}}{R} + \frac{1}{R}\frac{\partial u_\theta}{\partial \theta}\right) + Q\left(\frac{U_{_R}}{R} + \frac{\partial U_{_R}}{\partial R} + \frac{1}{R}\frac{\partial U_\theta}{\partial \theta}\right), \tag{A.1}$$

$$\sigma_{_{R\theta}} = \mu\left(\frac{1}{R}\frac{\partial u_{_R}}{\partial \theta} + \frac{\partial u_\theta}{\partial R} - \frac{u_\theta}{R}\right), \tag{A.2}$$

$$\sigma_\theta = (\lambda+2\mu)\frac{\partial u_{_R}}{\partial R} + \lambda\left(\frac{\partial u_{_R}}{\partial R} + \frac{1}{R}\frac{\partial u_\theta}{\partial \theta}\right) + Q\left(\frac{U_{_R}}{R} + \frac{\partial U_{_R}}{\partial R} + \frac{1}{R}\frac{\partial U_\theta}{\partial \theta}\right), \tag{A.3}$$

$$s = Q\left(\frac{\partial u_{_R}}{\partial R} + \frac{\partial u_{_R}}{\partial R} + \frac{1}{R}\frac{\partial u_\theta}{\partial \theta}\right) + \mathcal{R}\left(\frac{\partial U_{_R}}{\partial R} + \frac{\partial U_{_R}}{\partial R} + \frac{1}{R}\frac{\partial U_\theta}{\partial \theta}\right). \tag{A.4}$$

Leading order terms in the far-field ($R >> 1$)

$$\sigma_{_R} \sim (\lambda+2\mu)\frac{\partial u_{_R}}{\partial R} + Q\frac{\partial U_{_R}}{\partial R}, \tag{A.5}$$

$$\sigma_{_{R\theta}} \sim \mu\frac{\partial u_\theta}{\partial R}, \tag{A.6}$$

$$\sigma_\theta \sim 2(\lambda+\mu)\frac{\partial u_{_R}}{\partial R} + Q\frac{\partial U_{_R}}{\partial R}, \tag{A.7}$$

$$s \sim Q\frac{\partial u_{_R}}{\partial R} + \mathcal{R}\frac{\partial U_{_R}}{\partial R}. \tag{A.8}$$

Appendix B

Averaged quantities

B.1 Spatially damped waves

$$\bar{T}_n = \frac{1}{2}\rho_{ij}\overline{\dot{q}^n_{iR}\dot{q}^n_{jR}} = \frac{1}{4}\omega^2\rho_{ij}q^n_i q^{n*}_j, \tag{B.1}$$

$$\bar{V}_n = \frac{1}{2}\alpha_{ij}\overline{q^n_{iR,x}q^n_{jR,x}} + \frac{1}{2}\beta_{ij}\overline{q^n_{iR}q^n_{jR}} = \frac{1}{4}\left(\alpha_{ij}|k_n|^2 + \beta_{ij}\right)q^n_i q^{n*}_j, \tag{B.2}$$

$$\bar{F}_n = -\alpha_{ij}\overline{\dot{q}^n_{iR}q^n_{jR,x}}\cdot\mathbf{n} = \frac{1}{2}\omega\mathrm{Re}(k_n)\alpha_{ij}q^n_i q^{n*}_j, \tag{B.3}$$

$$2\bar{D}_n = b_{ij}\overline{\dot{q}^n_{iR}\dot{q}^n_{jR}} = \frac{1}{2}\omega^2 b_{ij}q^n_i q^{n*}_j. \tag{B.4}$$

B.2 Temporally damped waves

$$\bar{T}_n = \frac{1}{2}\rho_{ij}\overline{\dot{q}^n_{iR}\dot{q}^n_{jR}} = \frac{1}{4}|\omega_n|^2\rho_{ij}q^n_i q^{n*}_j, \tag{B.5}$$

$$\bar{V}_n = \frac{1}{2}\alpha_{ij}\overline{q^n_{iR,x}q^n_{jR,x}} + \frac{1}{2}\beta_{ij}\overline{q^n_{iR}q^n_{jR}} = \frac{1}{4}\left(\alpha_{ij}k^2 + \beta_{ij}\right)q^n_i q^{n*}_j = \frac{1}{4}a_{ij}(k)q^n_i q^{n*}_j, \tag{B.6}$$

$$\bar{F}_n = -\alpha_{ij}\overline{\dot{q}^n_{iR}q^n_{jR,x}}\cdot\mathbf{n} = \frac{1}{2}\mathrm{Re}(\omega_n)k\alpha_{ij}q^n_i q^{n*}_j, \tag{B.7}$$

$$2\bar{D}_n = b_{ij}\overline{\dot{q}^n_{iR}\dot{q}^n_{jR}} = \frac{1}{2}|\omega_n|^2 b_{ij}q^n_i q^{n*}_j. \tag{B.8}$$

Appendix C

Averaged quantities

C.1 Longitudinal waves

$$\bar{T}_n = \frac{1}{4}\omega^2 \left[\rho_{11} u_n u_n^* + \rho_{12}(u_n^* U_n + u_n U_n^*) + \rho_{22} U_n U_n^*\right], \tag{C.1}$$

$$\bar{V}_n = \frac{1}{4}|k_n|^2 \left[(\lambda + 2\mu) u_n u_n^* + Q(u_n^* U_n + u_n U_n^*) + R U_n U_n^*\right], \tag{C.2}$$

$$\bar{F}_n = \frac{1}{2}\omega \mathrm{Re}(k_n) \left[(\lambda + 2\mu) u_n u_n^* + Q(u_n^* U_n + u_n U_n^*) + R U_n U_n^*\right], \tag{C.3}$$

$$2\bar{D}_n = \frac{1}{2}\omega^2 b \mathcal{F}_{R}(u_n u_n^* - u_n^* U_n - u_n U_n^* + U_n U_n^*). \tag{C.4}$$

C.2 Shear wave

$$\bar{T}_s = \frac{1}{4}\omega^2 \left[\rho_{11} u_s u_s^* + \rho_{12}(u_s^* U_s + u_s U_s^*) + \rho_{22} U_s U_s^*\right], \tag{C.5}$$

$$\bar{V}_s = \frac{1}{4}\mu |k_s|^2 u_s u_s^*, \tag{C.6}$$

$$\bar{F}_s = \frac{1}{2}\mu\omega \mathrm{Re}(k_s) u_s u_s^*, \tag{C.7}$$

$$2\bar{D}_s = \frac{1}{2}\omega^2 b \mathcal{F}_{R}(u_s u_s^* - u_s^* U_s - u_s U_s^* + U_s U_s^*). \tag{C.8}$$

Appendix D

Poroelastic mechanical parameters

Reference phase densities,

$$\begin{aligned} \rho_{11} &= (1-\phi)\rho_s + \phi\rho_f(a-1), \\ \rho_{12} &= \phi\rho_f(1-a), \\ \rho_{22} &= a\phi\rho_f. \end{aligned} \tag{D.1}$$

Generalized poroelastic mechanical parameters,

$$\begin{aligned} \lambda &= K_b - 2\mu/3 + K_f\left(1-\phi-K_b/K_s\right)^2/\phi_{\text{eff}}, \\ Q &= \phi K_f\left(1-\phi-K_b/K_s\right)/\phi_{\text{eff}}, \\ R &= \phi^2 K_f/\phi_{\text{eff}}, \\ \phi_{\text{eff}} &= \phi + K_f\left(1-\phi-K_b/K_s\right)/K_s. \end{aligned} \tag{D.2}$$

Characteristic quantities,

$$\begin{aligned} \rho &= \rho_{11} + 2\rho_{12} + \rho_{22}, \\ H &= \lambda + 2\mu + R + 2Q, \\ c &= \sqrt{H/\rho}. \end{aligned} \tag{D.3}$$

Nondimensional parameters,

$$\begin{aligned} \gamma_{11} = \rho_{11}/\rho, \quad \gamma_{12} = \rho_{12}/\rho, \quad \gamma_{22} = \rho_{22}/\rho, \\ q_{11} = (\lambda+2\mu)/H, \quad q_{12} = Q/H, \quad q_{22} = R/H. \end{aligned} \tag{D.4}$$

Bibliography

[1] M. Abramovich and I.A. Stegun. *Handbook of mathematical functions with formulas, graphs and mathematical tables*. Dover Publications, New York, 1974.

[2] K. Aki and P. Richards. *Quantitative Seismology (2nd Edition)*. University Science books, Sausalito, 2002.

[3] B. Albers. *Modelling of surface waves in poroelastic saturated materials by means of a two component continuum*. Lecture notes // WIAS-Preprint, 2004.

[4] B. Albers and K. Wilmanski. Monochromatic surface waves on impermeable boundaries in two-component poroelastic media. *Continuum Mech. Thermodyn.*, 17:269–285, 2005.

[5] D. Albert. A comparison between wave propagation in water-saturated and air-saturated porous materials. *J. Appl.Phys.*, 73:28–36, 1993.

[6] D.G. Albert. Observations of acoustic surface waves in outdoor sound propagation. *J. Acoust. Soc. Am.*, 113:2495–2500, 2003.

[7] J.F. Allard. *Sound propagation in porous media (modelling sound absorption materials)*. Chapman and Hall, London, 1993.

[8] B.A. Auld. *Acoustic fields and waves in solids*. John Wiley & Sons, New York, 1973.

[9] C.M. Bender and S.A. Orszag. *Advanced mathematical methods for scientists and engineers*. McGraw-Hill, New York, 1978.

[10] M.A. Biot. General theory of three-dimensional consolidation. *J. Appl. Phys.*, 12:155–164, 1941.

[11] M.A. Biot. The theory of propagation of elastic waves in fluid-saturated porous solid. I. Low frequency range. *J. Acous. Soc. Am.*, 28:168–178, 1956.

[12] M.A. Biot. The theory of propagation of elastic waves in fluid-saturated porous solid. II. High frequency range. *J. Acous. Soc. Am.*, 28:179–191, 1956.

[13] M.A. Biot. General theorems on the equivalence of group velocity and energy transport. *Phys. Rev.*, 105:1129, 1957.

[14] M.A. Biot. Generalized theory of acoustic propagation in porous dissipative media. *J. Acous. Soc. Am.*, 34:1254–1264, 1962.

[15] M.A. Biot. Mechanics of deformation and acoustic propagation in porous media. *J. Appl. Phys.*, 33:1482–1498, 1962.

[16] M.A. Biot and D.G. Willis. The elastic coefficients of the theory of consolidation. *J. Appl. Mech.*, 24:594–601, 1957.

[17] D.R. Bland. *The theory of linear viscoelasticity.* Pergamon press, New York, 1960.

[18] R. De Boer. *Theory of porous media. Highlights in historical development and current state.* Springer, Berlin, 2000.

[19] G. Bonnet and J.L. Auriault. *Dynamics of saturated and deformable porous media: homogenization theory and determination of the solid-liquid coupling coefficients. In: Physics of finely divided matter*, pages 306–316. Springer, 1985.

[20] R. Borcherdt. Energy and plane waves in linear viscoelastic media. *J. Geoph. Res.*, 78:2442–2453, 1973.

[21] R.D. Borcherdt. Energy and plane waves in linear viscoelastic media. *J. Geoph. Res.*, 78:2442–2453, 1973.

[22] R. Bouchen. Plane waves in linear viscoelastic media. *Geophys. J. R. Astr. Soc.*, 23:531–542, 2001.

[23] T. Bourbie, O. Coussy, and B. Zinszner. *Acoustics of porous media.* Gulf publishing company, Paris, 1987.

[24] Y. Bouzidi and D. Schmitt. Measurement of the speed and attenuation of the biot slow wave using a large ultrasonic transmitter. *J. Geoph. Res.*, 114:B08201, 1990.

[25] L. Brillouin. *Wave Propagation in Periodic Structures: Electric Filters and Crystal Lattices.* McGraw-Hill, Dover, 1953.

[26] L. Brillouin. *Wave propagation and group velocity.* Academic press, New York and London, 1960.

[27] J. Carcione and F. Cavallini. Attenuation and quality factor surfaces in anisotropic-viscoelastic media. *Mech. Mater.*, 19:311–327, 1995.

[28] J.M. Carcione. Energy balance and fundamental relations in anisotropic-viscoelastic media. *Wave motion*, 18:11–20, 1993.

[29] J.M. Carcione. Wave propagation in anisotropic, saturated porous media: plane-wave theory and numerical simulation. *J. Acous. Soc. Am.*, 99:2655–2666, 1996.

[30] J.M. Carcione. Energy balance and fundamental relations in dynamic anisotropic poro-viscoelasticity. *Proc. Roy. Soc. Lond. A*, 457:331–348, 2001.

[31] J.M. Carcione. *Wave Fields in Real Media: Wave Propagation in Anisotropic, Anelastic, Porous and Electromagnetic Media (2nd Edition).* Elsevier, Amsterdam, 2007.

[32] G. Chao, D. M. J. Smeulders, and M. E. H. van Dongen. Dispersive surface waves along partially saturated porous media. *J. Acoust. Soc. Am.*, 119:1347–1355, 2006.

[33] O. Coussy. *Poromechanics.* John Wiley & Sons, New York, 2004.

[34] Zhi-Jun Dai, Zhen-Bang Kuang, and She-Xu Zhao. Reflection and transmission of elastic waves from the interface of a fluid-saturated porous solid and a double porosity solid. *Transp.Por.Media.*, 65:237–264, 2006.

[35] M.V. Davidovich. Electromagnetic energy density and velocity in a medium with anomalous positive dispersion. *Tech. Phys. Lett.*, 32:982–986, 2006.

[36] O. Dazel, F. Sgard, F.-X. Becot, and N. Atalla. Expressions of dissipated powers and stored energies in poroelastic media modeled by {u,U} and {u,P} formulations. *J. Acoust. Soc. Am.*, 123:2054–2063, 2008.

[37] R. de Boer. *Trends in continuum mechanics of porous media.* Springer, Dordrecht, 2005.

[38] A.I.M. Denneman, G.G. Drijkoningen, D.M.J. Smeulders, and K. Wapenaar. Reflection and transmission of waves at a fluid/porous medium interface. *Geophys.*, 67:282–291, 2002.

[39] H. Deresiewicz. The effect of the boundaries on wave propagation in a liquid filed porous solid. IV. Surface waves in a half-space. *Bull. Seism. Soc. Amer.*, 52:627–638, 1962.

[40] H. Deresiewicz and J.T. Rice. The effect of the boundaries on wave propagation in a liquid filed porous solid. III. Reflection of plane waves at a free plane boundary (general case). *Bull. Seism. Soc. Amer.*, 52:595–625, 1962.

[41] H. Deresiewicz and R. Skalak. On uniqueness in dynamic poroelasticity. *Bull. Seism. Soc. Amer.*, 53:783–788, 1963.

[42] S. Dey and R.K. De. Stresses in fluid saturated porous half-space due to normal and tangential loadings. *Indian J. Pure Appl. Math.*, 15:1375–1397, 1984.

[43] M. Emerson and P.Foray. Laboratory P-wave measurements in dry and saturated sand. *Acta Geotech.*, 1:167–177, 2006.

[44] I. Fatt. The Bio-Willis coefficients for sandstone. *J. Appl. Mech.*, 2:296–297, 1959.

[45] S. Feng and D. L. Johnson. High-frequency acoustic properties of a fluid/porous solid interface. I. new surface mode. *J. Acoust. Soc. Am.*, 74:906–914, 1983.

[46] S. Feng and D. L. Johnson. High-frequency acoustic properties of a fluid/porous solid interface. II. The 2d reflection Green's function. *J. Acous. Soc. Amer.*, 74:915–924, 1983.

[47] J.D. Ferry. *Viscoelastic properties of polymers (3rd Edition).* John Wiley & Sons Inc., New'York, 1980.

[48] P. Fillunger. Der Auftrieb von Talsperren, Teil I–III. *Osterr. Wochenschrift fur den offentlicen Baudients*, 7:510–532, 1913.

[49] L. Forest, V. Gibiat, and T. Woignier. Biot's theory of acoustic propagation in porous media applied to aerogels and alcogels. *J. Non-Cryst. Solids*, 225:287–292, 1998.

[50] C.M.R. Fowler. *The Solid Earth: An Introduction to Global Geophysics (2nd Edition).* Cambridge University Press, New York, 2005.

[51] Y. Frenkel. On the theory of seismic and seismoelectric phenomena in moist soil. *J. Phys.*, 8:230–241, 1944.

[52] F. Gassmann. Elastic waves through a parking of spheres. *Geophys.*, 16:673–685, 1951.

[53] J. Geertsma and D. Smit. Some aspects of elastic wave propagation in fluid-saturated porous solids. *Geophysics*, 26:169–181, 1961.

[54] V. Gerasik and M. Stastna. Poroelastic acoustic wave trains excited by harmonic line tractions. *Proc. Roy. Soc. Lond. A*, 464:491–511, 2008.

[55] V. Gerasik and M. Stastna. *The time-dependent response of a poroelastic half-space to line tractions. In: Integral Methods in Science and Engineering, Constanda, C.; Potapenko, S. (Eds.)*, pages 99–108. A Birkhauser Boston book, 2008.

[56] V. Gerasik and M. Stastna. Complex group velocity and energy transport in absorbing media. *Phys. Rev. E*, 81:056602, 2010.

[57] V. Gerasik and M. Stastna. Energy partition and resonant excitation of poroelastic waves (no dissipation case). *Wave motion*, (submitted), 2011.

[58] V. Gerasik and M. Stastna. Energy velocity and quality factor of poroelastic waves in isotropic media. *J. Acoust. Soc. Am.*, 129:(in press), 2011.

[59] H. Goldstein, C. Poole, and J. Safko. *Classical mechanics (3rd Edition)*. Addison-Wesley Publishing, San Francisco, 2002.

[60] A.M. Gomilko, O.A. Savitsky, and A.N. Trofimchuk. Asymptotic solution of a harmonic contact problem for a permeable stamp on a liquid saturated base. *Nonlinear Oscillations*, 74:1–19, 2002.

[61] N.S. Gorodetskaya. Waves reflected from the boundary of poroelastic saturated media [*in russian*]. *Akust. Vestn.*, 5:5–14, 2002.

[62] N.S. Gorodetskaya. Waves in the interface of poroelastic saturated media. i. free boundary [*in russian*]. *Akust. Vestn.*, 8:28–41, 2005.

[63] N.S. Gorodetskaya. Waves in poroelastic saturated media [*in russian*]. *Akust. Vestn.*, 10:43–63, 2007.

[64] K.F. Graff. *Wave motion in elastic solids*. Dover publications, New York, 1991.

[65] V.T. Grinchenko and V.V. Meleshko. *Vibrations and waves in elastic solids [in russian]*. Naukova dumka, Kiev, 1981.

[66] A.A. Gubaidullin, O.Y. Kuchugurina, D. M. J. Smeulders, and C. J. Wisse. Frequency-dependent acoustic properties of a fluid/porous solid interface. *J. Acoust. Soc. Am.*, 116:1474–1480, 2005.

[67] J. Haldorsen, D.L. Johnson, T. Plona, B. Sinha, H.P. Valero, and K. Winkler. Borehole acoustic waves. *Oilfield review*, 18:34–43, 2006.

[68] M. Halpern and P. Christiano. Response of poroelastic half-space to steady-state harmonic surface tractions. *Int. J. Numer. Anal. Geomech.*, 10:609–632, 1986.

[69] J. Johnes. Rayleigh Waves in a Porous, Elastic, Saturated Solid. *J. Acoust. Soc. Am.*, 7:959–962, 1961.

[70] D. L. Johnson, J. Koplik, and R. Dashen. Theory of dynamic permeability and tortuosity in fluid-saturated porous media. *J. Fluid Mech.*, 116:379–402, 1987.

[71] D.L. Johnson. Equaivalence between fourthsound in liquid he ii at low temperature and the biot slow wave in consolidated porous media. *Appl. Phys.Lett.*, 37:1065–1067, 1980.

[72] D.L. Johnson and T.J. Plona. Acoustic slow waves and the consolidation. *J. Acoust. Soc. Amer.*, 72:556–565, 1982.

[73] O. Kelder and D.M.J. Smeulders. Observation of the biot slow wave in water-saturated nivelsteiner sandstone. *Geophys.*, 62:17941796, 1997.

[74] M.S. King, J.R. Marsden, and J.W. Dennis. Biot dispersion for p- and s-wave velocities in partially and fully saturated sandstones. *Geophys. Resch.*, 48:10751089, 2000.

[75] H. Lamb. On the propagation of tremors over the surface of an elastic solid. *Phil. Tran. Roy. Soc. A*, 203:1–42, 1904.

[76] M.J. Lighthill. Group velocity. *J. Inst. Math. Appl.*, 1:1, 1964.

[77] P. Lorrain, D.R. Corson, and F. Lorrain. *Electromagnetic fields and waves (3rd Edition)*. W.H. Freeman and Company, New York, 1996.

[78] F. Mainardi. On energy velocity of viscoelastic waves. *Lettere al Nuovo Cimento*, 6:443449, 1973.

[79] F. Mainardi. Energy velocity for hyperbolic dispersive waves. *Wave motion*, 9:201–208, 1987.

[80] F. Mainardi. Energy propagation in linear hyperbolic systems. *Il Nuovo Cimento*, 104:487–496, 1989.

[81] D. Makarynska, B. Gurevich, J. Behura, and M.Batzle. Fluid substitution in rocks saturated with viscoelastic fluids. *Geophys.*, 75:E115E122, 2010.

[82] V.V. Meleshko. Energy analysis of wave motions in the lamb problem. *Int. Appl. Mech.*, 17:1105–1110, 1981.

[83] A. Mesgouez, G. Lefeuve-Mesgouez, and A.A. Chambarel. Transient mechanical wave propagation in semi-infinite porous media using a finite element approach. *Soil Dyn. and Earth. Eng.*, 25:421–430, 2005.

[84] G.F. Miller and H. Pursey. The field and radiation impedance of mechanical radiators on the free surface of a semi-infinite isotropic solid. *Proc. Roy. Soc. Lond. A*, 223:521–541, 1954.

[85] G.F. Miller and H. Pursey. Ton the partition of energy between elastic waves in a semi-infinite solid. *Proc. Roy. Soc. Lond. A*, 233:55–69, 1955.

[86] K. Mizuno, M. Matsukawa, T. Otani, P. Laugier, and F. Padilla. Propagation of two longitudinal waves in human cancellous bone: An in vitro study. *J. Acoust. Soc. Am.*, 125:3460–3466, 2009.

[87] L. A. Molotkov. Propagation of normal waves in an isolated porous fluid-saturated biot layer. *J. Math. Sci.*, 108:758–771, 2002.

[88] L. A. Molotkov. Sources acting on the free boundary of a porous biot medium and reflection on this boundary. *J. Math. Sci.*, 111:3750–3762, 2002.

[89] L. Muschietti and C.T. Dum. Real group velocity in a medium with dissipation. *Phys. Fluids*, 5:1383, 1993.

[90] P.B. Nagy. Slow wave propagation in air-filled permeable solids. *Acous. Soc. Am*, 1993:3224–3234, 1993.

[91] P.B. Nagy. *Acoustics and ultrasonics. In: Experimental Methods in the Physical Sciences*, pages 161–221. Academic Press, 1999.

[92] P.B. Nagy, L. Adler, and B.P. Bonnet. Slow wave propagation in air-filled porous materials and natural rocks. *Appl. Phys. Lett.*, 25:2504–2506, 1990.

[93] P.H.F. Nicholson and R. Strelitzkib. Ultrasonic slow waves in air-saturated cancellous bone. *Ultrasonics*, 37:445–449, 1999.

[94] V.N. Nikolaevskiy, K.S. Basniev, A.T. Gorbunov, and G.A. Zotov. *Mechanics of saturated porous media.* Nedra, Moscow, 1970.

[95] S. Paul. On the displacements produced in a porous elastic half-space by an impulsive line load (no dissipative case). *Pure and Appl. Geoph.*, 114:605–614, 1976.

[96] A. J. Philippacoupoulos. Lamb's problem for fluid saturated porous media. *Bull. Seism. Soc. Amer.*, 78:908–923, 1988.

[97] T.J. Plona. Observation of second bulk compressional wave in a porous medium at ultrasonic frequencies. *Appl. Phys. Lett.*, 36:556–565, 1980.

[98] A.P. Prudnikov, Yu.A. Brychkov, and O.I. Marichev. *Integrals and series*. Gordon and Breach Science Publishers, New York, 1986.

[99] D. Salin and W.M. Schon. Acoustics of water saturated packed glass spheres. *J. Phys. Lett.*, 42:477–480, 1981.

[100] M. Schanz and S. Diebels. A comparative study of biots theory and the linear theory of porous media for wave propagation problems. *Acta Mech.*, 161:213–235, 2003.

[101] M. Schanz and V. Struckmeier. Wave propagation in a simplified modelled poroelastic continuum: Fundamental solutions and a time domain boundary element formulation. *Int. J. Numer. Meth. Engng.*, 64:1816–1839, 2005.

[102] V.M. Seimov, A.N. Trofimchuk, and O.A. Savitsky. *Vibrations and waves in layered media [in russian]*. Naukova Dumka, Kiev, 1990.

[103] M.D. Sharma. Wave propagation in a general anisotropic poroelastic medium with anisotropic permeability: phase velocity and attenuation. *Int. J. Solids Structures*, 41:4587–4597, 2004.

[104] M.D. Sharma. Energy velocity and quality factor of plane harmonic inhomogeneous waves in anisotropic poro-viscoelastic media. *Geophys. J. Int.*, 180:1265–1273, 2010.

[105] R. Sidler, J.M.Carcione, and K.Holliger. Simulation of surface waves in porous media. *Geoph. J. Int.*, 183:820–832, 2010.

[106] D.B. Silin, V.A. Korneev, G.M. Goloshubin, and T.W. Patzek. Low frequency asymptotic analysis of seismic reflection from a fluid-saturated medium. *Transp.Por.Media.*, 62:283–305, 2006.

[107] G. Simmons, R. Wilkens, L. Caruso, T. Wissler, and F. Miller. Physical propertied and microstructures of a set of sandstones. *Ann. Rept. SchlumbergerDoll Resch. Center.*, VI-16, 1983.

[108] D.M.J. Smeulders. Experimental evidence for slow compressional waves. *J. Engng Mech.*, 9:908–917, 2005.

[109] E. Sonnenschein, I. Rutkevich, and D. Censor. Wave packets, rays, and the role of the real group velocity in absorbing media. *Phys. Rev. E*, 57:1005, 1998.

[110] R.D. Stoll. *Acoustic waves in saturated sediments. In: Physics of Sound in Marine Sediments.Acoustics and ultrasonics*, pages 19–39. Plenum, 1974.

[111] R.D. Stoll and T.K. Kan. Reflection of acoustic waves at water-sediment interface. *J. Acoust. Soc.Amer.*, 70:149156, 1981.

[112] M. Tajuddin. Rayleigh waves in a poroelastic halfspace. *J. Acoust. Soc. Am.*, 75(3):682–684, 1984.

[113] K. Von Terzaghi. Die berechnung der durchlassigkeit des tones aus dem verlauf der hydromechanischen spannungserscheinungen. *Sitzungsber. Akad.Wissensch. Math.-Naturwiss. Klasse.*, 132:125–128, 1923.

[114] F. Tisseur and K. Meerbergen. The quadratic eigenvalue problem. *SIAM Rev.*, 43:235–286, 2001.

[115] N.W. Tschoegl. *The Phenomenological Theory of Linear Viscoelastic Behavior: An Introduction*. Springer-Verlag, Berlin, 1989.

[116] A. Turgut. Approximate expressions for viscous attenuation in marine sediments: Relating biots critical and peak frequencies. *J. Acoust. Soc. Am.*, 108:513–518, 2000.

[117] L.A. Vainshtein. Group velocity of damped waves. *Soviet Phys. Techn. Phys.*, 2:2420–2428, 1957.

[118] S. Valiappan, J.Tabatabaie, and C.S. Zhao. Analytical solution for two-dimensional dynamic consolidation in frequency domain. *Int. J. Numer. Anal. Geomech.*, 19:663–682, 1995.

[119] K.N. van Dalen, G.G. Drijkoningen, and D.M.J. Smeulders. On wavemodes at the interface of a fluid and a fluid-saturated poroelastic solid. *J. Acoust. Soc. Am.*, 127(4):2240–2251, 2010.

[120] G.B. Whitham. *Linear and nonlinear waves*. Wiley & Sons, New York, 1974.

[121] K. Wilmanski. Porous media at finite strains. the new model with the balance equation for porosity. *Arch. Mech.*, 48:591–628, 1996.

[122] K. Wilmanski. A few remarks on biot's model and linear acoustics of poroelastic saturated materials. *Soil Dyn. Engrg.*, 26:509–536, 2006.

[123] K. Wu, Q. Xue, and L. Adler. Reflection and transmission of elastic waves from a fluid-saturated porous solid boundary. *J. Acoust. Soc. Am.*, 87:2349–2358, 1990.

[124] T. Yamamoto and A. Turgut. Acoustic wave propagation through porous media with arbitrary pore size distributions. *J. Acoust. Soc. Am.*, 83:1744–1751, 1988.